Aalborg University

Department of physics and nanotechnology

Master Thesis

# Multivalent nanoparticle interactions of membranes to design targeting systems for cells

*Author:*
Justas Svirelis

*Supervisors:*
Peter Fojan
Erik Reimhult

AALBORG UNIVERSITY
DENMARK


Universität für Bodenkultur Wien

AALBORG UNIVERSITY
DENMARK

**Department of Physics and Nanotechnology**
**The Faculty of Engineering and Science**
**Aalborg University**
Skjernvej 4a
9220 Aalborg Ø

**Title:**
Multivalent nanoparticle interactions of membranes to design targeting systems for cells

**Project period:**
September 2017 - June 2018

**Participants:**
Justas Svirelis

**Supervisors:**
Peter Fojan
Erik Reimhult

**Copies: 1**
**Total pages: 109**
**Appendices: 1**
**Finalized 06-06-2018**

**Abstract**:

The understanding of how nanoparticles (NPs) specifically bind to receptors in cell membranes is still lacking. In particular, a focus on decorating NPs with specifically binding ligand for target receptors have largely ignored the influence of nonspecific colloidal interactions on targeting affinity. Thus, model systems were established in order to set a basis for interpretation of the effect on the avidity of NPs. Silica NPs were coated with lipid bilayers by liposome fusion, using different composition liposomes that would modulate the interaction potential of the particles. A controlled density of biotin functional groups in the lipid membrane served as a model for specific interactions with avidin proteins. The quality of the coating was estimated by dynamic light scattering and zeta potential. An optimal coating procedure was developed. In addition, supported lipid bilayers and poly(ethylene glycol) surface coatings were self-assembled on silica sensor surfaces with different coverages of avidin proteins to mimic the cell membrane and used to investigate the specific and non-specific interactions with coated silica NPs via Quartz Crystal Microbalance with Dissipation monitoring.

# Prologue

The master thesis project is written in the period from September the $1^{st}$ 2017 to June the $10^{th}$ by Justas Svirelis, a student studying Nanobiotechnology at the department of Physics and Nanotechnology at Aalborg University with associate professor Peter Fojan (Aalborg University) acting as primary supervisor and professor Erik Reimhult (Institute of biologically inspired materials, BOKU, Vienna). Relevant theory and methodology regarding the project will be explained in the report as well as the results obtained will be presented and discussed.

The experiments were conducted in biochemistry and biophysics laboratories at and in collaboration with the institute of biologically inspired materials, University of Natural Resources and Life Sciences (BOKU), Vienna.

The references in this report will be placed before the dot if the reference relates the sentence, e.g.: "[number]." , and after the dot if the reference relates to the paragraph or several sentences in that paragraph e.g.: '.[number]'. Figures used in this report will be referenced as adopted if they are directly the same as the one cited to, or as adapted if it is inspired by the referenced publication. If there is no reference for the figure, it is unique for this report.

# Contents

# 1. Introduction

## 1.1 Motivation

Nowadays different kinds of nanoparticles (NPs) with various functional groups, moieties or ligands are vastly researched in biomedical investigations such as hyperthermia therapy, vaccine improvement, as contrast agents for imaging techniques and more efficient drug delivery than conventional methods. In addition, often nanoparticles are employed in order to purify and identify proteins, nucleic acids and cells as molecular marking systems. Moreover, NPs as targeting machines are redolent of biological identification of exosomes as well as viruses via receptors in the membrane, potentially serving as mimetic models for these significant mechanisms [1].

The binding avidity of targeted-NPs is the quantitative description of the strength of the binding to, e.g., a membrane, consisting of lipids. The former is dependent on the NP-membrane association constant, which quantitavely defines it. [2] Accordingly, it is crucial to address the question of how NPs's physico-chemical characteristics are related to the dissociation constant. Understanding the contributions of multivalency and nonspecific colloidal interactions to the avidity of targeted NPs is very important since the outcome of targeting will relate to this and not to the affinity of the specific molecular interaction. Effects of nonspecific interactions can be expected to be large for large colloids such as cells (membranes), drug delivery vehicles and viruses. The dominating nonspecific interactions for membrane systems are the Derjaguin-Landau-Verwey-Overbeek (DLVO) interactions, often referred to as Van der Waals and double-layer interactions. Also of interest is the ability of ligands to move laterally in a lipid (cell) membrane and therefore increase the ligand density and valency of an interaction occurring in an interaction zone. Even though, in this project mainly silicon oxide NP (z-average $\approx$ 130 nm) interaction between mimetic cell membrane (single lipid bilayer (SLB)) will be investigated, it was previously presented that with increasing nanoparticle diameter from roughly 20 nm to around 50 nm the cellular uptake of these targeting systems notably increases as well [3, 4, 5, 6, 7]. However, there is a possibility that this effect is probably relevant to selectivity by size in cellular uptake, being passive (receptor-mediated) [8, 9] and/or active (clathrin-dependent) [10, 11].

Being responsible for NP-attached ligands's relation to the lipid membrane's receptors, multivalent interaction, influences the detachment rate $k_{off}$ to be several orders of magnitude smaller than the monovalent interaction of the same origin. [4, 12, 13] It is known, that with the increasing NP dimensions the avidity of binding mechanism rises as well, results from the apparent geometry of NP itself, influencing the count of ligand-receptor connections made among the receptors of the lipid membrane and the NP (due

to increased areas of contact) [4, 13, 14]. However, it has generally been disregarded that the rate of specific binding (explained by the rate of binding constant, $k_{on}$) relates to the performance of targeted-NP function and the avidity in overall. With bond formation being the leading event, the exclusive focus on multivalency and dissociation might overlook a critical factor influencing recognition and downstream events in vivo. [1] A model of that may be presented as: due to the fact that the time of attachment of a targeted NP to an interface rises, [2, 15, 16, 17] as a result of the ligand-receptor interaction multivalency, the binding rate constant is usually higher for the ligand that is free rather than the binding related to the system of receptor-NP based. [15, 16, 17] Furthermore, the multivalent interaction has a tendency of being neglected on the equilibrium binding level by the avidity, being characterized as the $k_{on}$ and $k_{off}$ rate constant (low binding rates) ratio. In addition to that, when taking into account that the multivalent interaction effect is really substantial, and the targeted NP attachment to a substrate is relatively permanent, explained by large avidity, the initial event of binding itself might still be significantly slow, thus the targeting of the cell-membrane receptors by the NP can, in fact, be restricted by the specific binding rate ($k_{on}$). [1]

## 1.2 Scope of the thesis

In this project, I intend to investigate the interaction of multivalent NPs with membrane-type interfaces. The focus is on using supported lipid bilayers from liposomes coated on NPs and on solid supports to measure the effect on the avidity of targeted-NP by a) non-specific interactions, b) ligand density in relation to particle dimensions, and c) ligand mobility. The basic platform consists of monodisperse silicon oxide and iron oxide NPs functionalized with supported lipid membranes interacting with lipid and proteolipid membranes self-assembled on biosensor substrates. The use of lipid-coated NPs instead of liposomes makes it possible to have monodisperse lipid membranes of different compositions interacting with a cell membrane mimic, while liposomes cannot be formed monodisperse for thermodynamic reasons. The work includes both assembling the particle and sensor interfaces, however, not the particle synthesis, and investigating their interactions. The colloids are characterized by Dynamic Light Scattering (DLS) and electrophoretic measurements of the zeta potential. Binding of coated nanoparticles to supported proteolipid bilayers is investigated in real time by using Quartz Crystal Microbalance With Dissipation Monitoring (QCM-D). Due to its complexity and the high demands on the model system to achieve quantitative results, the major part of the thesis work was focused on developing a set of lipid membrane coated monodisperse silica particles, for which the DLVO interaction potential is varied in a controlled way. The results will be relevant for the understanding of specific and non-specific interactions in biology (e.g. of viruses) as well as for the design of cell-targeting medical NPs.

## 1.3 Liposomes

Being the most essential part of the biological membranes, phospholipids comprise of unsaturated or saturated fatty acids attached to a polar headgroup. For example, the most frequently observed glycerol phospholipids contain two fatty acids, which connect with the carbon atoms of the glycerol moiety. However, glycerol's third carbon atom is attached to a phosphate group, which consequently is bound to a neutral or charged moiety like glycerol (negatively charged) and choline (neutral; zwitterionic). In addition, the lipids are found to have various degrees of saturation, sizes of the head group, chain lengths and charges. It is also important to note that phospholipid headgroups, with positive charge, do not appear in nature. [18]

Around four decades ago, Alec Bangham observed that phospholipids dispersed in aqueous media may develop bilayered arrangements, having a closed form. These structures, called liposomes, are considered to be artificially produced microparticulate vesicles, which obtain spherical shape upon synthesis. These systems may be constructed from substances like non-toxic phospholipids or cholesterol. In addition, they are well known for gene delivery (cationic liposomes as transfecting vectors) and cancer therapy applications due to the fact that they have relatively small size, hydrophilic/hydrophobic properties and are biocompatible. However, these transport vehicles's characteristics strongly depend on their surface charge, method of preparation and the lipids that form them. For example, unsaturated phosphatidylcholine (PC) phospholipids produce bilayers that are less stable, rigid and permeable compared to saturated dipalmitoylphosphatidylcholine (DPPC) lipids. Furthermore, by including cholesterol into the structure, it is possible to reduce membrane fluidity (above the phase transition temperature) correlating with reduced permeability to aqueous solutes. The allowed inclusion of up to 50 mol %, observed *in vivo* and *in vitro*, also displays maximum stability increase for the bilayer. [19, 20, 21, 22]

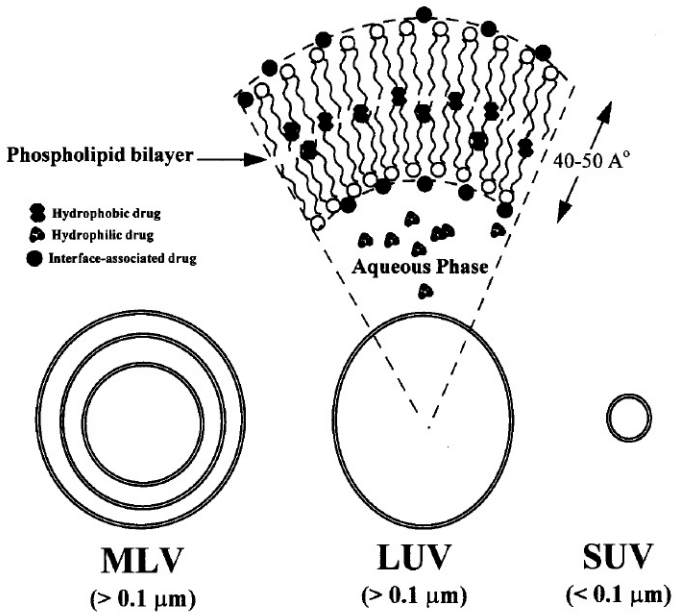


**Figure 1.1:** Different species of liposomes relying upon their number of lamellae and size. Taken from Amarnath Sharma et al. [23]

Lipid vesicles may have different sizes and consist of different number of layers, being multilamellar (MLV; great mechanical stability for long term storage, relatively easy to produce), large unimellar (LUV; is used for encapsulating hidrophilic molecules) or single unimellar (SUV; usually with high homogeneity, however, thermodynamically not stable, lenghty circulation time and sensitive to aggregation) (fig. 1.1). An important factor, on which liposome formation depends, is called the packing parameter or surfactant parameter expressed in eq. 1.1:

$$N_S = \frac{V_C}{L_C \sigma_A} \tag{1.1}$$

Where the lipid's/surfactant's hydrophobic part's volume is $V_C$, $L_C$ is the magnitude of the hydrocarbon chain and $\sigma_A$ refers to the specific effective area per single head group of the lipid/surfactant. When the packing parameter of the lipids is close to 1, they tend to achieve bilayer or vesicle forms. Knowing these basics and depending on the to be internalized substance's varying hydrophobicity or hydrophilicity, it can be enveloped either at liposome's bilayer interface, in the bilayer of the phospholipids itself or rather in the aqueous center of the vesicle. Another classification of these transport vehicles may be according to the type of drug delivery and the arrangement of the liposome as well. Several examples include: conventional liposomes (CL) usually containing phospholipids with cholesterol, which having no and/or negative charge (PC, phosphatidylserine (PS) or phosphatidylglycerol (PG)); cationic liposomes such as 1,2-Dioleoyl-sn-glycero-3-phosphoethanolamine (DOPE) or 1,2-dioleoyl-3-trimethylammonium-propane (DOTAP),

involving the possible induction of fusion with endosome or cell membranes and being employed to deliver negatively charged macromolecules (DNA, RNA); pH-sensitive liposomes such as mentioned above DOPE, being subject to coated-pit endocytosis due to the fact that the endosome has a lower pH than the vesicle. In addition, liposome size determines the circulation half-life in the organism as well as the quantity of the substance that can be encapsulated within. [19, 20, 23, 24].

In order to have a stable vesicle, one must consider several other parameters besides size, such as surface charge density, surface hydration and bilayer fluidity. Firstly, knowing that liposomes have a phase transition temperature denoted as $T_c$, it is note able that there are two physical states below and above this temperature. When temperature is lower than $T_c$, phospholipids experience an ordered structure, which is observed as a gel-like phase. On the other hand, lipids are in fluid phase when the temperature is above $T_c$. Secondly, the charge density and nature of lipids highly influences not just the mechanism, but also the degree of how well liposomes interact with other systems such as a cell. It is known that the negatively charged surface could increase the uptake of liposomes in cells, stimulate vesicle's plasma clearance upon systematic administration, reduce aggregation of vesicles and also increase their degree of encapsulation. In contrast, cationic liposomes are known to fuse with cell membranes in order to deliver the cargo inside. Lastly, surface hydration plays a significant role in vesicle stabilization. For example, by including a small amount (5-10 mol%) of molecules containing hydrophilic moieties (Polyethylene glycol (PEG) - slows down the recognition by molecules called opsonins; hydrogenated phosphatidylinositol (HPI)) into bilayers, it is possible to decrease the interaction with blood components or cells, making liposomes have higher circulation half-lives. [23, 25].

### 1.3.1 Liposome preparation methods

There are several liposome preparation methods, which will be listed in the later text, but the basic steps for the production usually involve: drying out the organic solvent of the lipid solution; resuspending the lipids in other aqueous media; the produced liposomes are purified and analyzed. However, in order to choose the most appropriate method for the preparation, one should think about the application of the resulting system. For the most common employement of liposomes, drug loading, there are three general loading techniques - passive and active - which include solvent dispersion, mechanical dispersion as well as detergent removal methods (where non-encapsulated material is removed) listed in the table [20]:

**Table 1.1:** Overview of the different liposome preparation methods. [20]

| |
|---|
| **Mechanical dispersion methods** |
| Sonication |
| French pressure cell: extrusion |
| Freeze-thawed liposomes |
| Lipid film hydration by hand shaking, non-hand shaking or freeze drying |
| Micro-emulsification |
| Membrane extrusion |
| Dried reconstituted vesicles |
| **Solvent dispersion** |
| Ether injection (solvent vaporization) |
| Ethanol injection |
| Double emulsion |
| Stable pluri lamellar vesicles |
| Reverse phase evaporation method |
| **Detergent removal method** |
| Dyalysis |
| Detergent (Alkyl glycoside) removal of mixed micelles (absorption) |
| Gel permeation chromatography |
| Dilution |
| Reconstituted sendai virus enveloped |

In this project there were mainly these methods applied: bath/tip sonication, membrane extrusion, freeze-thaw, solvent dispersion method (with THF) - therefore they will be explained more in detail. First of all, the sonication method is probably the most commonly applied method for the preparation of SUVs (15 - 50 nm in diameter). When the solution of MLVs are prepared, they are subjected to either a probe or bath sonicator at ambient atmosphere conditions. The probe sonication follows as: tip sonicator is directly immersed into the liposome aqueous media and due to high energy input in this method, quite significant amount of local heat is produced, thus, the glass/vial with the liposomes has to be submersed into ice or cold water. In addition, the main disadvantage of this method is that usually titanium particles and ions will polute the dispersion even though it supposedly can be removed by centrifugation. However, in contrast to probe, bath sonication is relatively smoother method in terms of temperature control and exclusion of unwanted material. Overall, sonication contains quite a few drawbacks, including MLV presence besides SUVs, possible metal contamination from tip, usually small internal volume/encapsulation effectiveness and a chance that the phospholipids along side with the future to be encapsulated molecules will degrade. Another mechanical dispersion method involves extrusion of MLVs through nanosized and monodispersed pores. Compared to sonication, extrusion offers high reproducibility, no induction of phospholipid breakdown is observed and it is possible to tune the average size of the liposomes by choosing the pore size of the track-etched membranes. Nevertheless, main limiting features of this procedure remain relatively small working volumes and some loss of material during the process.

The last method of mechanical dispersion for liposome production is freeze-thawed vesicles, which include SUV fusion to form LUVs by swiftly freezing and haltingly thawing. Finally, the solvent injection method includes a rapid injection of lipid solution in, for example, ethanol to a surplus amount of selected buffer. Consequently, vesicles are produced, being largely polydisperse (range from 30 to 110 nm in size). [20, 26, 27]

## 1.4 DLVO and other forces affecting the stability of colloids

Around six decades ago, Derjaguin, Landau, Verwey and Overbeek came up with a theory that quantitavely explains aggregation process of particles in aqueous environments. The approach is known as the DLVO theory [24, 28]. In it, the agglomeration between particles, that are dispersed, is described mainly by two acting DLVO (figure 1.2) and two non-DLVO forces: the repulsive force of the electric double layer, the attractive force of Van der Waals, the solvation force, when particles interact with solvent molecules and the steric force [29]. The former is responsible for dispersion stabilization and the Van der Waals results in the aggregation of the particles [24].

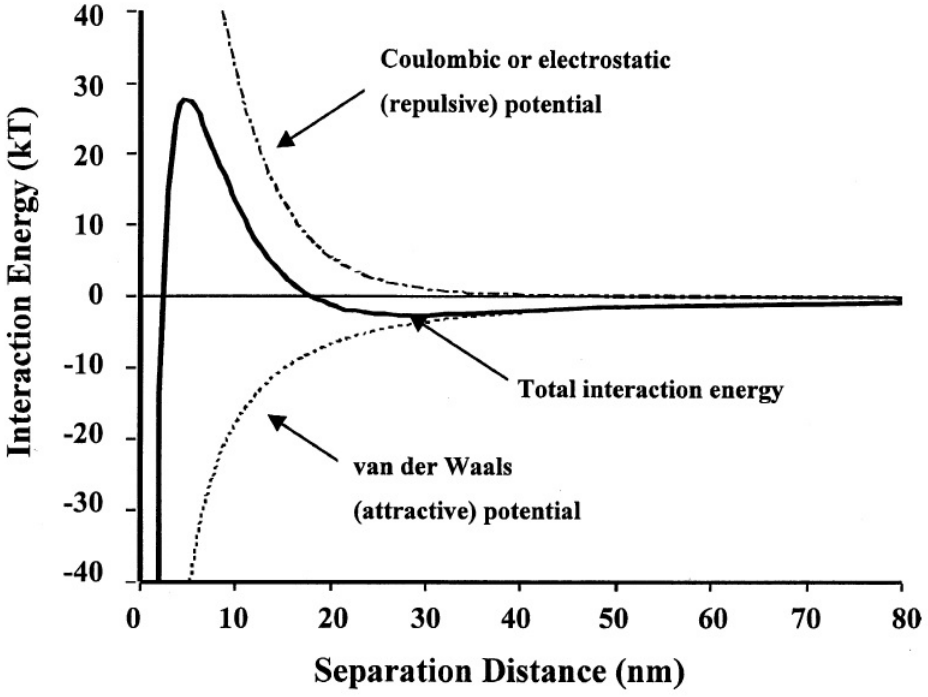


**Figure 1.2:** The contribution of Van der Waals and electrostatic potentials to the sum interaction energy [29]

The DLVO estimations are applied mostly for cases with rather low separations between surfaces of around 5 nm [29].

### 1.4.1 Van der Waals Forces

Van der Waals forces are always present between particles that are distinct among any environment - air, water or vacuum - and at relatively short distances, e.g. compared to gravity, (correspond to the intermolecular gaps of atoms/molecules by a factor of inverse power of seven) [29]. They arise from the relation between the fluctuation and rotation of dipoles of atoms or molecules in question and are mostly attractive [28, 29]. For example, the known Debye interaction includes the attraction of nonpolar molecules to polar molecules or vice versa. In addition, the Keesom relation belonging to the Van der Waals forces results when one dipole that is permanent interacts with another permanent dipole. Finally, the third class of the Van der Waals attraction forces is called the London dispersion forces, arising when atoms are interacting with each other and their electron density polarizes. [29] In most general case of such interaction it is possible to assume that:

$$W(D) = -\frac{A_{131}R}{12D} \tag{1.2}$$

or

$$W_{vdW}(h) = -\frac{H}{12\pi h^2} \tag{1.3}$$

where H or $A_{131}$ is the Hamaker constant and is influenced by the dielectric relative constants of the matter and it's atmosphere, h or D - surface separation between two particles and R is the particle's radius. [29, 28] Most commonly, the Hamaker constant corresponds to a range of $10^{-21}$ - $10^{-19}$ J. However, these characters may vary a bit due to addition of salt. These equations may be used accurately until separation is relatively small and for particles with smooth surfaces. On the other hand, when the separation reaches a certain length limit, the interaction between the particles will start decaying, because of particular retardation effects as well as the unevenness of the matter. [28]

When talking about the interaction Hamaker constant, e.g. $A_{121}$ (equation 1.4; vacuum environment) or $A_{132}$, which can also be calculated from the dielectric constants at imaginary and normal frequencies - $\epsilon$ and $\epsilon(iv)$ (equation 1.5:

$$A_{121} = [A_{11}^{1/2} - A_{22}^{1/2}]^2 \tag{1.4}$$

$$A_{132} \approx \frac{3}{4}kT\left(\frac{\epsilon_1 - \epsilon_3}{\epsilon_1 + \epsilon_3}\right)\left(\frac{\epsilon_2 - \epsilon_3}{\epsilon_2 + \epsilon_3}\right) + \frac{3h}{4\pi}\int_{v_1}^{\infty}\left(\frac{\epsilon_1(iv) - \epsilon_3(iv)}{\epsilon_1(iv) + \epsilon_3(iv)}\right)dv \tag{1.5}$$

In the latter relation, the first function is known as the zero frequency, including Debye and Keesom energy contributions, however, the second function, usually being dominant

over the first one, describes the London dispersion forces and any other polarizations, which may contribute to each frequency of the dipoles being induced for the atmosphere or matter in question. [29, 24] Furthermore, compared to the electrostatic forces term in the overall interaction energy, Van der Waals is independent of the ionic strength. It results in a negative state (eqn. 1.2) and is reversly proportional to the surface seperation parameter, in contrast to electrostatic force term. Thus, it is important to note that at relatively significant distances between particles, repulsive force dominates, however, when the kinetic energy corresponding from the thermal motion would be bigger than the fixed barrier of energy. [29]

A controversial fact may be considered that when the ionic strength is relatively large, the amplitude of Van der Waals force is bigger, thus, making the overall interaction energy attractive at long distances between particles in accordance with, when moderate distances between particles exist, an energy barrier that is repulsive will be generated. Consequently, a secondary minimum is created. Now that the barrier is rather low, the particles are able to surmount it more readily. Therefore, if we consider dispersions that are electrostatically stable, they still might be prone to clustering. As a result, this stabilization technique is rather used as a method of transient dispersion in the processing of ceramic powder. [29]

### 1.4.2 Electrostatic Forces

Firstly, it is important to note that the electrostatic forces only exist in the presence of polar media and charged particles. When compared to other common forces residing at surfaces, the previously mentioned one is the strongest and general act in longer distances. In addition, imagine having a system with charged particles surrounded by an electrolyte - it will be neutral in overall. Therefore, such charged surface of the particle is considered to be compensated, disregarding any origin it may have, through electrostatically arranging ions of the opposite charge, also known as counterions, and ions that are chemically attached in the vicinity of the *Stern layer*. The former ions come from the other side of the Stern interface to the preponderance of the solution, where the surface potential $\phi(x)$ is turning into zero (Figure 1.3). [29]

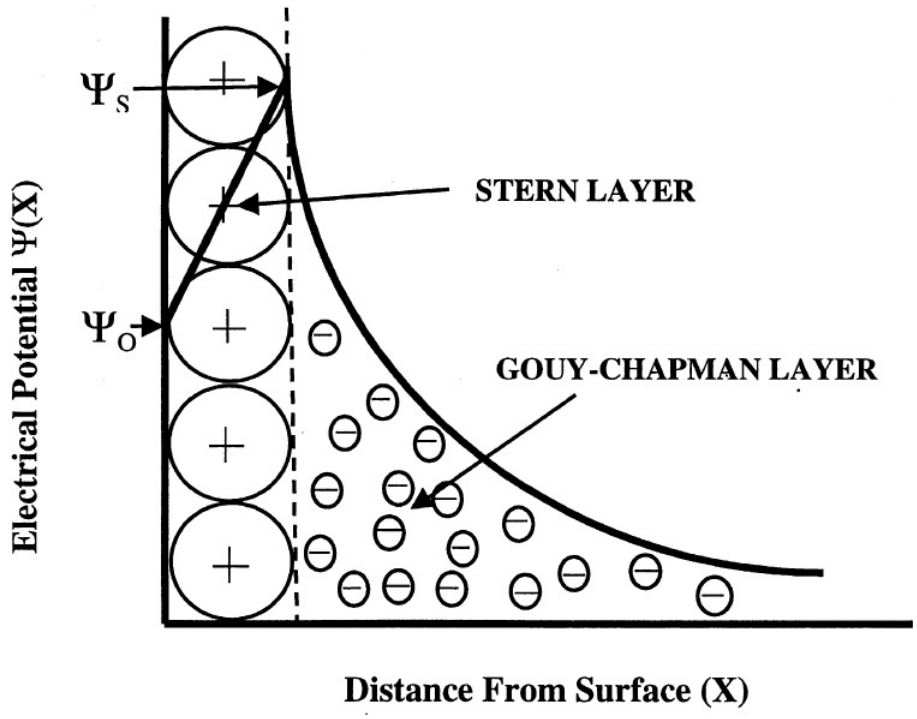


**Figure 1.3:** An electric double layer is shown at the figure. Stern layer consists of positively charged particles, residing at the surface. Potentials $\Phi_0$ and $\Phi_S$ are related to the surface and Stern layer, accordingly. [29]

The band that goes after the ions of the Stern interface is called the *Gouy-Chapman layer*. In order to have an electrically neutral system, as mentioned before, the interface of positively charged particles edict the amplitude of charge for the counterion layer. However, if the layers of counterions of two particles overlap, this will result in repulsion due to excess ions of the same species. [24, 29] This repulsion may be evaluated by the Poisson-Boltzmann equation. The interaction energy $W_{El(D)}$ among two spherical, identical and having low Stern potential ($\phi_S$) particles is expressed in a simplified version of the previously mentioned equation:

$$W_{El}(D) = 2\pi\epsilon\epsilon_0 R\phi_s^2 exp(-\kappa D) \tag{1.6}$$

Therefore $W_{El(D)}$ is decreasing in an exponential manner with the separation between the particles $D$. In addition, even though the counterion interface rather restricts the repulsion force, it cannot be absolutely distinguished from the potential at the Stern layer. For example, with the increasing salt concentration, the Gouy-Chapman interface will extend more into the main part of the solution. [29]

The electric double layer theory and fundamental mathematical estimations is continued in section **1.3.2** (zeta potential measurements) due to relevancy to zeta potential.

### 1.4.3 Steric Forces

The theory in this possible colloid stabilization method is not going to be looked at in detail, however, in short, it includes grafted polymers on colloid surfaces in order to stabilize their suspensions [29]. Most commonly, the interaction in question is called the *steric force* [24]. Polymers are known to have two main attributes for the activity with the particles in question - reactivity and solubility. One part of the acting polymer may anchor a certain molecule to the surface of the particle, whereas a polymer that is strongly solvated also induces an entropic barrier for other objects to approach the particle surface since the local chemical potential of the polymer segments then increase further to produce a barrier of sterical kind to counter agglomeration. [29]

### 1.4.4 The solvation force

The liquid structure at the vicinity of a certain interface is known to be distinctive from that, that is in the bulk solution. For a lot of aqueous solutions the density scope, that is considered adequate to a hard surface, fluctuates around the density of the bulk with a periodic factor of one molecular diameter, near to the surface. It is known that this area may expand to several molecular diameters. Within this limit, molecules arrange in layers. [24]

For example, in the event of these kind of two surfaces approaching one another, layers are pushed away from the gap that is about to be closed. The oscillations in density as well as some specific interactions result in exponentially reducing force that is periodic; the magnitude of periodicity is related to the width of every layer. These forces are known as *solvation forces* due to the aftermath of solvent molecules adsorbing on the surface of solids [30]. Such forces between enclosed fluids were firstly estimated by theoretical calculations and computer simulations [30, 31, 32, 33]. Consequently, the experimental evidence came only some years after by employing the surface force apparatus [34, 35]. The solvation force importance is involved not only in the stabilization of dispersion, but as well as in order to study the confined liquid structure [24].

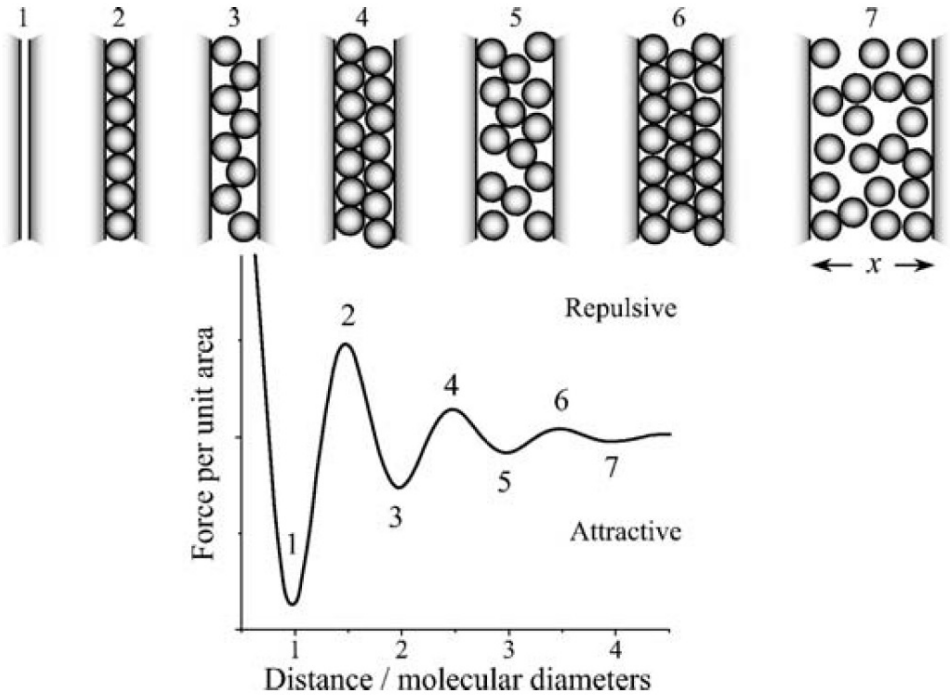


**Figure 1.4:** A picture, representing a liquid trapped between to adjacent surfaces. The periodic force arises from the drastic change of order that depends on the distance. [24]

Solvation forces are commonly explained by the following function:

$$f(x) = f_0 \cdot cos\left(\frac{2\pi x}{d_0}\right) \cdot e^{-\frac{x}{x_0}} \tag{1.7}$$

where f is denoted as the force per unit area, $f_0$ is the force that is extrapolated according to x = 0, $d_0$ is known as the width of the layer (equal to the diameter of the molecule in cases of simple liquids) and $x_0$ - characteristic decay length [24].

## 1.5 Dynamic light scattering

Dynamic light scattering (DLS; Photon correlation spectroscopy) is a well-known and dominant technique not only for the analysis of size distributions of particles such as polymers, liposomes, colloids, etc. In addition to that, the diffusion processes of molecules in suspension. In this section, only the basic theory about dynamic light scattering and size distribution measurement theory for spherical particles will be looked into more detail.

For an established scattered light angle towards the detector, conventional DLS instruments resolve the mean particle size in a certain size range. The common setup is shown in figure 1.5.

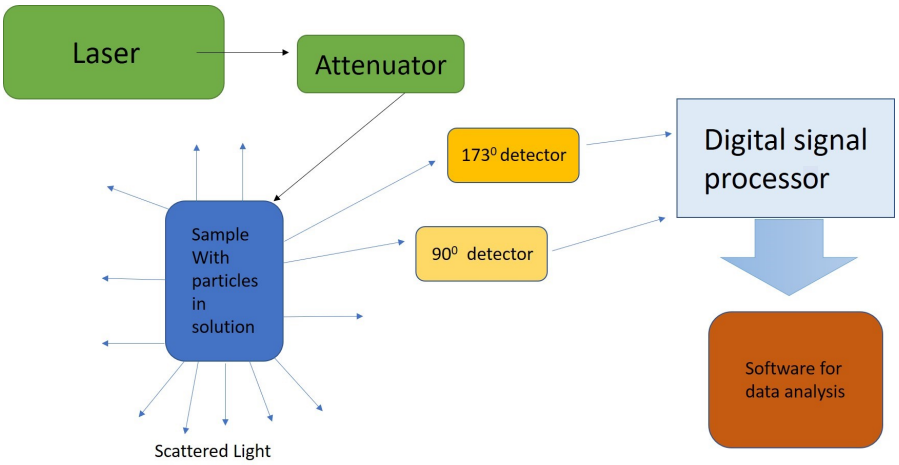


**Figure 1.5:** Conventional DLS method setup

The main characteristic analyzed by the DLS is the *Brownian motion* of the different size of the particles [36, 37, 38]. This movement is explained by the solvent molecules's colision into the particles of interest resulting in the random motion. If the particles are relatively big, they are subjected to a slower movement and vice versa. In addition, Brownian motion of the particles are greatly influenced by the viscosity of the liquid they are in, which in turn is related to its temperature [39]. A change in the latter may result in currents of convection leading to incorrect analysis of the particle size in question due to establishment of non-random particle movement. Furthermore, an attribute called translational diffusion coefficient, most commonly denoted as $D$, affects the level of the Brownian motion and will be explained in more detail in the next subsection [36].

In more practical and microscopic point of view, one can imagine the sample, containing the material of interest that is immobilized, illuminated with a laser light and a glass cover is applied to examine the sample. A conventional pattern of dots, which position and size do no change due to the fact that the whole sample is stationary, would be observed. The dots, marked in black, are representing an addition of two opposite phase electromagnetic waves (scattered light) being jointly destructive due to cancellation in respect to each other. The bright dots result from electromagnetic waves that interfere constructively, resulting in greater intensity. When particles undergo Brownian movement, this dotted arrangement is varying due to continual motion. This is explained by the fact that the positions at which the constructive and destructive interference occurs from light scattered from the same particles varies to produce novel patterns, due to particles's movement. Thus the diameter of the particles influences their velocity and thereby the speed at which the dot patterns fluctuate. [38]

Even though it is known how to measure the spectrum of different speed intensity fluctuations due to Brownian motion of the particles of interest straightforwardly, however, it is ineffective and therefore a machinery called digital signal processer/correlator was

developed. The instrument is made to analyze the extent at which two different signals are similar to each other or one, being analogous to itself, at shifting periods of time. Taking as an example that if signal's intensity is correlated to itself at a certain time point and one significantly later, then it is clear that there will be no correlation what so ever between these cases (fig. 1.6). Consider the case of diffusion - if it will be determined at initial time $t$, then this information cannot anyhow correlate to the diffusion of the particles at $t$ = infinity. On the contrary, if the signal's intensity at the initial time value is related to a relatively bigger increase of time next ($t + 2\delta t$), the affiliation will be high between those signals. [36]

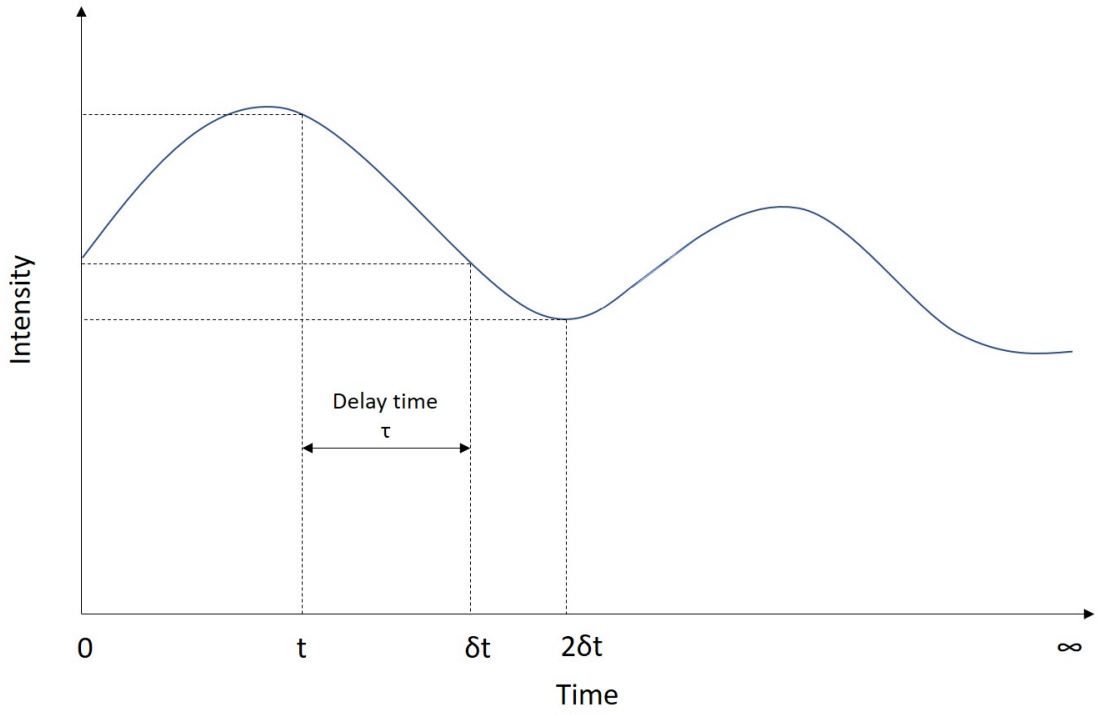


**Figure 1.6:** A dependency of the fluctuation of scattered light intensity compared to time

Taken Brownian motion of such example, the initial signal at time value $t$ will still be sufficiently acceptable related to time point $t + 2\delta t$, however, not as great as the first incline of time. Thus it is observed that this relation is declining in time. Furthermore, two more points are important to mention. Firstly, if there is a complete correlation between two signals, then it is identified as unity, yet, when correlation is non-existing, it will be observed as zero. Secondly, the correlation is highly dependent on particle size, thus for smaller particles the relation between signals at different points of time will decrease rather quicker than for substantial ones. [36]

The first-order correlation function mentioned in the previous paragraph is applied by the instrument in general form:

$$G(\tau) =< I(t)I(t+\tau) > \tag{1.8}$$

where $\tau$ is the difference in time between the correlated points [36]. If one considers a more vast number of monodisperse particles that are dispersed in Brownian motion, the beforehand mentioned equation becomes exponentially decaying of the time delay $\tau$ in the correlator/processer:

$$G(\tau) = B + Ae(-2q^2D\tau) \tag{1.9}$$

where B is denoted as correlation function's baseline, A - intercept, D - the translational diffusion coefficient and vector q is related as follows:

$$q = (4\pi\eta/\lambda_0)sin(\theta/2) \tag{1.10}$$

$\eta$ being the dispersant's refractive index, $\lambda_0$ - laser light's wavelength and $\theta$ - the angle, at which the light is scattered. [37, 40]

However, it is rather not that often that samples are monodisperse, therefore it is important to consider the polydispersity model as well:

$$g_1(\tau) = \sum_i A_i e(-\Gamma_i\tau) \tag{1.11}$$

where $\Gamma_i = q^2D_i$ is called the reciprocal decay time, $A_i$ is denoted as the coefficient proportional to a part of the intensity that is scattered by the certain particles of interest. Therefore, the latter equation includes a sum of exponentials that contribute the first order correlation function. [37]

### 1.5.1 Size distribution measurements

In DLS method, the size of a particle of interest is estimated from the translational diffusion coefficient defined in the Stokes-Einstein equation:

$$R_h = \frac{k_BT}{6\pi\eta D} \tag{1.12}$$

where $R_h$ is the hydrodynamic diameter, D = translational diffusion coefficient, $k_B$ = Boltzmann's constant, T = absolute temperature and $\eta$ = viscosity of solvent [40]. However, it is important to note, that the obtained hydrodynamic diameter is just referred to a hard sphere's diameter, which in fact has identical translational diffusion coefficient

as the particle of interest, therefore the size is significantly dependent on the shapes of the particles under investigation, type of ions existing in the medium and concentration [41].

Firstly, the type of ions in the solution as well as the overall concentration of the ions may influence the diffusion velocity of the particles due to change in the density of the Debye length, $\kappa^{-1}$, of the electric double layer [42]. Therefore, if low conductivity medium is achieved, it will result in a prolonged double layer of ions in the circumference of the particle, lowering the diffusion velocity and giving a bigger supposed hydrodynamic diameter. Secondly, another important point to mention that affects the diffusion velocity of the particle is its surface texture, resulting in varying hydrodynamic sizes [43, 44]. For example, if there is a polymer layer grafted onto the particle of interest and it's part is arranged in the solvent, it will lower the diffusion velocity, thus, leading in greater hydrodynamic size compared to a flatly grafted polymer layer. Furthermore, polymer's nature itself and the overall ionic concentration may influence the conformation of the polymer, which sequentially varies the size by a few nanometers.

Generally, the instrument obtains the size of the particles by employing different algorithms on the correlation function [44]. However, there are mainly two methods that may be applied:

1. Fitting of an individual exponential in the correlation function in order to attain z-average diameter (or mean size of the particle) and polydispersity index (PDI - distribution's width parameter), which shows how dispersed the sample is in terms of size (Cumulant method; PDI = 1 = highly polydispersed and PDI = 0 = greatly monodisperse) [44].

2. Fitting several exponentials in the correlation function in order to achieve a profile of particle sizes (The CONTIN algorithm) [44].

Therefore, the attained plot is related to the relative probability of a certain particle size to be found and noted as the intensity size distribution [44].

## 1.6 Zeta potential measurements

The theory about zeta potential (ZP) is included in this chapter due to the fact that the ZP measurements were done with the zetasizer machinery in accordance with the size distribution measurements.

The zeta potential is commonly known as the electrokinetic potential, arising at the shear/sliping plane of a particle of interest that is subjected to an electric field. However, generally speaking, the work, required to be achieved in order to move an individual positive charge from the infinity plane to the surface in question without applying additional acceleration is called the electric potential [44]. By knowing these terms, one can note that the zeta potential is a parameter that is necessary to indicate the difference

in potentials between the electrophoretically migrant particles belonging to the electric double layer as well as the dispersant's layer in the vicinity of the particles at the slipping plane's location. [44]

If we imagine a dispersed charged particle, it is known that an electric double layer will form on its surface [45] (fig. 1.7). In the electric double layer, an inner composite of such, called the *Stern layer*, mostly contains molecules or ions, having a reverse charge compared to the particle of interest. In addition, the electrostatic effects arising from the particle's surface charge decrease by a value of 1/e as stated by the *Debye's law* with the distance of each Debye length [46].

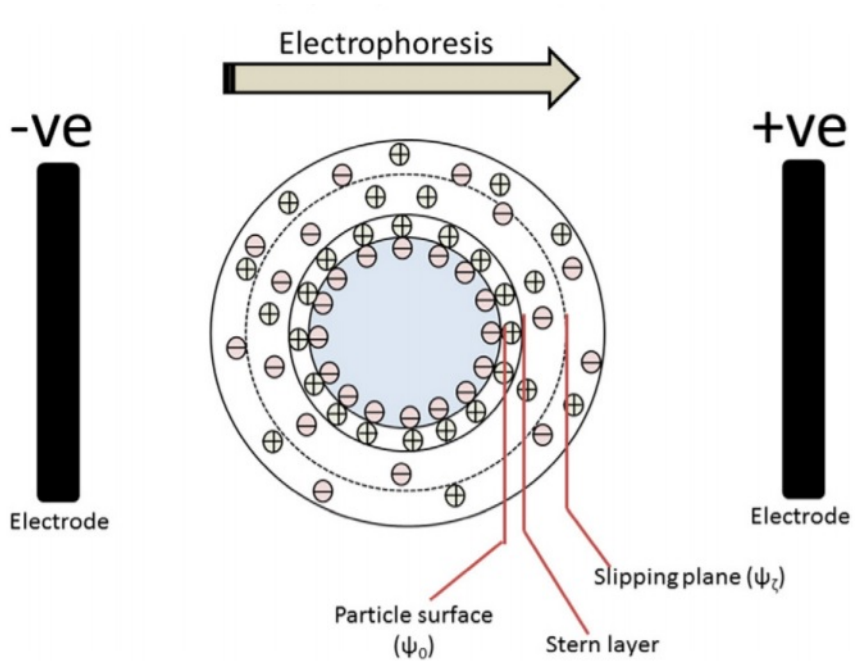


**Figure 1.7:** In the figure it is seen how the negatively charged particle, enveloped by an electric double layer, is moving to the positive electrode when the electric field is applied. Electric double layer is shown to contain a Stern layer and a Slipping plane, being a transition location among the particle and the solvent. The potential at the slipping plane interface is referred to as the zeta potential. [44]

Even though it is known that theoretically this electrostatic event continues until infinity, experiments show that it is negligible beyond a few nm outside of particle surface for solutions with typical ionic strengths. The electric double layer also contains a *diffuse layer*, which is located after the *Stern layer* and contains ions of both positive and negative charges, but with an average and exponentially decaying higher concentration of the counterions. There are a few factors that affect the beforehand mentioned layer - ionic strength, concentration, pH, etc. A process called *electrophoresis* arises from such a distribution when an electric field is administered. In addition, a hypothetical plane exists, acting as the interface among mobile particles and the solvent layer around it (during electrophoresis), in the diffusion layer. The potential at this liquid-particle interface is

called the zeta potential $\zeta$ as well as the plane itself is refered as the *slipping/shear* plane. Unfortunately, particle's potential, commonly noted as the *Nernst potential* $\phi_0$, cannot be estimated experimentally. [44, 47]

As previously mentioned, the electrostatic effect is decreasing with the range away from the particle's surface as seen in the equation:

$$\phi = \phi_d e^{-\kappa x} \tag{1.13}$$

where $\phi$ is the potential at a certain range x from the stern layer, $\phi_d$ is the surface potential at the vicinity of the stern layer and $\kappa$ is known as the Debye-Hückel factor. [44]

If one can imagine that the slipping plane is approximately at the same location as the stern layer, then it is accepted that $\phi_d$ is $\approx \zeta$, thus, the equation 1.13 can be edited to:

$$\phi = \zeta e^{-\kappa x} \tag{1.14}$$

The Debye-Hückel factor $\kappa$ is influenced by ionic strenght, therefore if the later is increased, the double layer is subjected to compression and the zeta potential declines. [44] This factor can be expressed as:

$$\kappa^{-1} = \left( \frac{\epsilon \epsilon_0 kT}{e^2 \sum_i c_i z_i^2} \right)^{1/2} = \left( \frac{\epsilon \epsilon_0 kT}{2e^2 I} \right)^{1/2} \tag{1.15}$$

where e is denoted as the charge of the electron, $\epsilon_0$ and $\epsilon$ are permitivity and the dielectric constants, respectively, and c is the ion concentration having the valence z. The reverse square root of the denominator determines the size of the Debye-Hückel factor. Therefore, the interaction length or the electrostatic force range are highly influenced by the ion valency and concentration existing in the dispersion. [29, 34]

Due to the fact that zeta potential cannot be estimated straightforwardly, it needs to be calculated from the electrophoretic mobility $\mu_e$ (1.16) of particles with certain charge when electrostatic effect takes place. [44]

$$\mu_e = \frac{V}{E} \tag{1.16}$$

where V is the velocity of the particles ($\mu$m/s) and E is the strength of the applied electric field (V/cm) [44]. Consequently, when $\mu_e$ is known, it is possible to calculate the zeta potential from *Henry's equation*:

$$\mu_e = \frac{2\epsilon_r \epsilon_0 \zeta f(Ka)}{3\eta} \tag{1.17}$$

where $\epsilon_r$ is the dielectric constant, $\epsilon_0$ - vacuum's permitivity, f(Ka) - Henry's function as well as $\eta$ is the viscosity at an exact temperature of the experiment. If one considers a width of the electric double layer that is significantly smaller than the radius of the particle, the Henry's function is considered as value of 1.5, hence, is also updated to *Helmholtz-Smoluchowski* equation [44]:

$$\mu_e = \frac{\epsilon_r \epsilon_0 \zeta}{\eta} \tag{1.18}$$

In contrast, when the width of the electric double layer is significantly larger than the radius of the particle, then the Henry's function is taken as 1 and the equation 1.17 can be updated to (Hückel equation) [44]:

$$\mu_e = \frac{2\epsilon_r \epsilon_0 \zeta}{3\eta} \tag{1.19}$$

In this thesis, the electrophoretic mobility, from which zeta potential is calculated, was measured by *electrophoretic light scattering* method. During this approach, the scattered electromagnetic waves have contrasting frequencies compared to the laser light when the particles are moving as well as the shift in frequency is related to the velocity of these particles. Generally, the instrumentation applies a laser beam, which is divided into two - one being the reference and other illuminates the sample. When the laser light is scattered by the particles in the sample, it is joined with the reference beam to evaluate the *Doppler shift*. Consequently, the amplitude of the particles's speed (V) is calculated from this shift and then the zeta potential is estimated through the equations 1.16 - 1.19. [44]

As mentioned before, zeta potential is influenced by additional factors beside the ionic strength such as particle concentration and pH. First of all, the former is known as the most important factor towards zeta potential in aqueous environments. If pH is negative, zeta potential is positive and vice versa [48], depending on the isoelectric point and the pKa of the surfaces and molecules involved. Due to this fact, most commonly a pH curve is estimated from which isoelectric point, also known as point of zero charge in aqueous environments [49] (zeta potential = 0), is determined [50]. Furthermore, the concentration of the particles influence on the zeta potential is often complicated and conventionally estimated through the eletric double layer effect and the surface adsorption [44]. When an exact threshold of concentration is reached, the electric double layer effect becomes dominant over the latter one, controversially declining the zeta potential value and destabilizing the dispersion [51].

As a last point in this chapter, it is relatively significant to mention that nanoparticles's surface charge may rely upon distinctive phases within the particle. According to the *Cohen's rule*, if solvent and solute are both insulating substances, then the substance with a higher $\epsilon_r$ will be positive at the vicinity of the interface. Therefore, if one considers silica

nanoparticles ($\epsilon_r = 3.9$), at room temperature, they will have a negative surface charge in water ($\epsilon_r = 80$), however, positive surface charge in benzene ($\epsilon_r = 2.27$). [44]

## 1.7 Quartz crystal microbalance with dissipation monitoring

Quartz Crystal Microbalance (QCM) or Quartz Crystal Microbalance with Dissipation monitoring (QCM-D) has been emerging as a profoundly resourceful tool for analyzing solvated interfaces (e.g., interface between bulk liquid and solid surface) due to the fact that it presents data not only about changes in mass with nanogram sensitivity, but in film, made out, possibly, of proteins, phospholipid vesicles or virus particles structure/height due to solvation as well. Some of the applications for this technique include: food processing, marine technologies and biosensors. In addition, a few of the biggest QCM-D advantages over other systems is that it contains the ability of measuring the molecule organization in real time, the change in organization in accordance with external stimuli (physical or chemical) and the method itself is quantitative. [52, 53] The basic setup and components of a QCM-D system can been seen in figures 1.8 and 1.9. 1 - is the q-sense analyzer, 2 - chamber, containining 4 cells with sensors (this enables high throughput of the system and the ability to simultaneously compare the measurement parameters) and 3 - peristaltic pump.

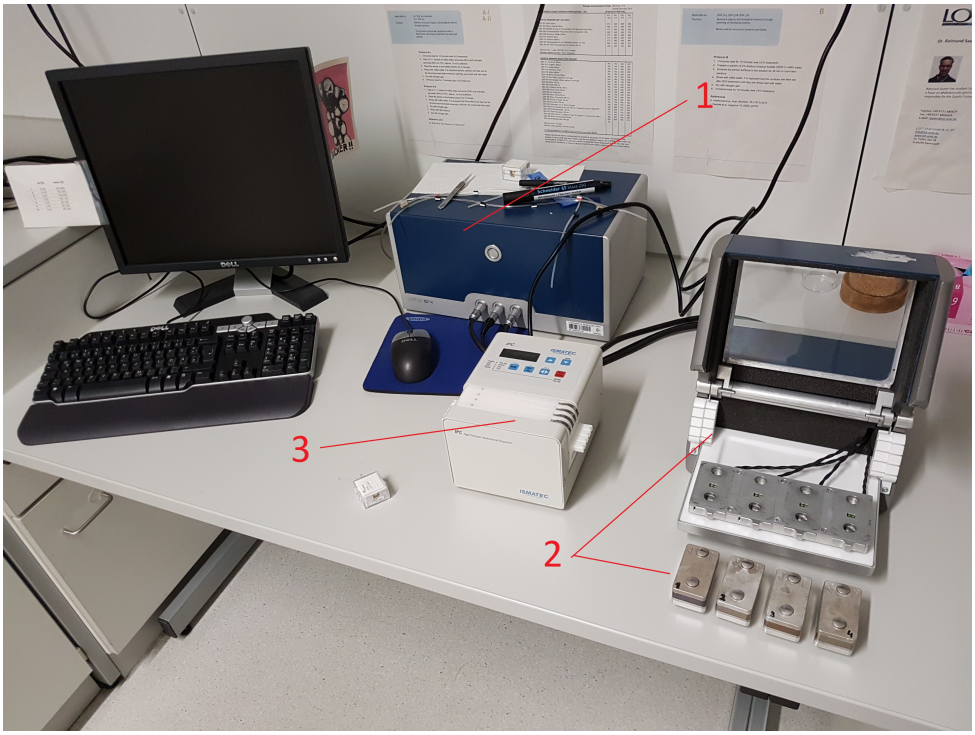


**Figure 1.8:** QCM-D setup and components.

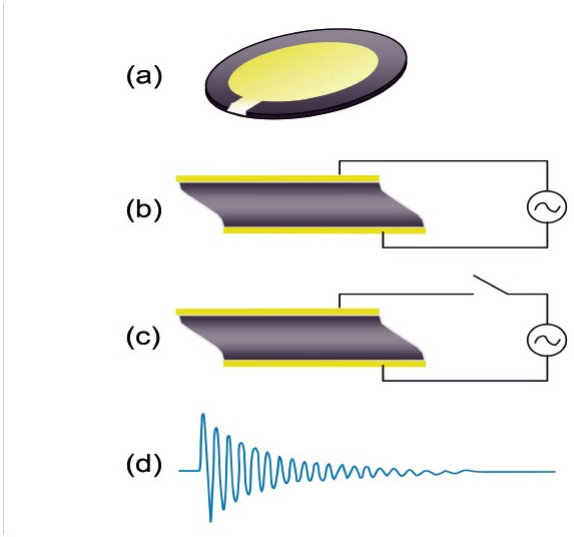


**Figure 1.9:** A brief overview of QCM-D main components. (a): A sensor with gold electrodes for QCM-D method. In practice, it's thickness is around 300 $\mu$m whereas the motion amplitude of the crystal is known to be in the order of maximum of a few nanometers in aqueous environment (also depends on the overtone order and driving voltage). (b): Quartz crystal having alternating current, which is applied on the electrodes. This results in cyclical deformation, where antiparallel fashion of tangentially moving surfaces are observed. (c): Limiting circuiting of the alternating current. (d): After stopping the periodic electric field driving the crystal oscillation, the quartz crystal is coming to a rest and an oscillatory decay is observed. From this decay curve the energy dissipation and resonance frequency are extracted. Taken from Mathew C. Dixon. [52, 54]

Even though there are a few possibilities to perform QCM experiments, but in this project it was focused towards one, "ring-down" method, where the analysis of the crystal response is in the time domain, through the decay of the freely oscillating crystal [52]. The example of a response signal piezoelectric quartz, where certain voltage is produced in the event of these decaying oscillations, yields two parameters per overtone that are important - the resonance frequency $f_n$ and the dissipation $D_n$, which resolutions are on the order of $\pm 0.1$ Hz and $1 \cdot 10^{-7}$, as a function of temperature and time. The formal may be changed between 15 and 45 °C with an accuracy of 0.05 °C and the latter's resolution is around 0.5 seconds with a stable baseline, which gives the opportunity to monitor an experiment for 36 hours and more. Nevertheless, usually frequency and bandwidth shift (equivalent to dissipation) interpretation can be problematic due to lack of knowledge of the energy dissipation procedures, which function in these film structures as they are mowed across at megahertz frequencies as the experiment takes place. The theory behind this method is that after the collision of a shear wave and the sample/resonator interface the wave encounters an attenuation and as well as frequency shift. It is proportional to the amount adsorbed on the sensor of the heterogeneous adsorbate (expressed in eq 1.20 - known as the Sauerbrey relationship for rigid films such as single lipid bilayers resulting in low dissipation) even though the energy which is dissipated during the process is proportional to the attenuation of the wave. [53, 54, 55, 56, 57]

$$\Delta m = -C_{QCM}\frac{\Delta f_n}{n} \tag{1.20}$$

where $\Delta m$ is denoted as the mass of the adsorbent on the surface, $C_{QCM}$ is the mass sensitivity constant (18 ng $\cdot$ $cm^{-2}Hz^{-1}$ at f = 5 MHz [52]) and $\Delta f_n$ is the shift in resonance frequency at the $n$th harmonic. Consequently, it has different order $n$ numbers (1,3,5,7). However, the mass sensitivity constant is not dependent on $n$. Still, it is known that the Sauerbrey relation is not quite fitting with the data if the experiment is conducted with sufficiently "soft" films. [55] In the method of QCM-D, the shear-quartz resonator is defined by the relationship among the resonance frequency/bandwidth of the resonator, the viscosity $\eta_1$ of the medium and the density $\rho_1$:

$$\Delta f_n = -\Gamma_n = -\frac{f_n}{2}\Delta D_n = -\frac{1}{C}\sqrt{\frac{n\rho_1\eta_1}{2\omega_F}} \tag{1.21}$$

In this equation, $\omega = 2\pi f_F$ and is known as the angular fundamental resonance frequency. While QCM is receptive to the properties of the bulk solution, a reference test in the same liquid is mandatory in order to separate bulk liquid contribution from the film characteristics. [52]

The bandwidth from equation 1.21 holds highly important knowledge, which is often applied for the determination of material's viscoelasticity. If we consider a Newtonian liquid, then the shifts of frequency and bandwidth as well as the viscosity of the molecules of interest are related to the original equations of Mason proved for torsional resonators. The practical value of the bandwidth, in fact, is that it is greatly more insensitive to variations of mechanical stress and temperature compared to frequency. The latter parameters are often not that easily susceptible to control in complicated environments. [58] Also, overall, the bandwidth contains information on losses, while the resonance frequency contains information on storage of energy.

### 1.7.1 Mechanism for supported lipid bilayer formation

In this project QCM-D was mainly used for formation of single lipid bilayers (SLBs; to mimic the membrane model) as well as specific and non-specific interaction experiments with functionalized or bare silica nanoparticles. To begin with, the fusion of the vesicles with the substrate is influenced by three aspects: vesicle-vesicle and vesicle-substrate [59, 60] interaction, and the tension of the membrane [61] itself. The formation of a SLB involves release of entrapped water during adsorption and rupture on the surface of the sensor/substrate to consequently form a SLB with higher resonance frequency and lower dissipation than the adsorbed vesicles. The decrease is explained by the loss of water and the construct of a rigid structure. [54]

In order to go in detail on how a SLB forms, two main points ought to be considered: the adhesion and rupture of liposomes on the substrate and the following development of the supported bilayer adsorbed chunks into a full SLB. The figure 1.11 illustrates the rupture processes, that have been reported so far. [62]

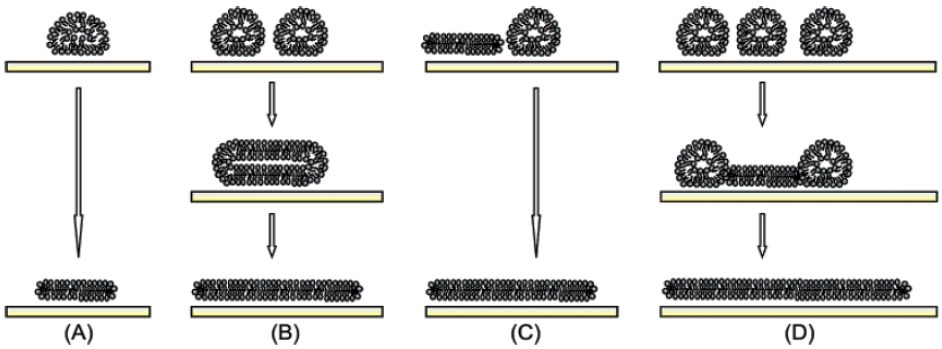


**Figure 1.10:** Processes taking place when liposomes rupture. A) an adsorbed isolated liposome ruptures spontaneously due to induced deformation by the substrate; b) fusion-induced rupturing of the neighbouring liposomes; c) the rupture of the vesicle is promoted by the edge of a nearby formed supported lipid bilayer; d) when the critical liposome coverage is reached, the coordinated action of a few nearby liposomes results in the rupture of a first vesicle. After the first patch of supported lipid bilayer is formed, its edges induce the rupture of adjacent liposomes. Taken from Ralf P. Richter et al. [62]

Zhdanov and Kasemo observed that the deformation propagated by the substrate on the adsorbed liposome is consequently increased by the adsorption of other liposomes in its vicinity. After a definite confinement of adjacent liposomes, matching critical coverage, is achieved, the stress on the liposomes develops into adequate enough to promote rupture (fig. 1.10 d). [63] A typical example of the response achieved by QCM-D technique, when the critical vesicular coverage is taking place is shown in fig. 1.10 c) [62].

A rather unusual effect was observed for liposomes having certain amounts of DOPC and DOPS when they were subjected to mica in a solution containing calcium: in the case of low surface density adsorbing vesicles, at the start they stayed intact, but ruptured individually over a time span of minutes to hours. This observation was rather peculiar in terms that previously it was thought that individual vesicles (the interaction with the same species at their viccinity is negligible) either rupture instantly (e.g., in less than a second) after the adsorption or stay unruptured for days. [64, 62] The possible explanation for such event could be the fact of introduction of two different lipid species within the adsorbed liposomes, which results in the dynamic changes in the vesicle-substrate interaction and in the promoted stability of the liposomes [62]. The seen time span for rupturing is significantly slower than the time required for the lipids contained in the single lipid leaflet to rearrange [65]. Thus, the proposal for the translocation of the lipid molecules between the two leaflets of the liposome is the criterion for the gradual rupturing of the vesicles [62].

After the vesicle ruptures, the resulting chunk of lipid bilayer reveals an edge [66, 67]. They are energetically unfavorable and, from a thermodynamic point of view, anticipated to induce the interaction with the neighbouring lipid material, such as the rupturing event of the adsorbed liposomes or liposomes from bulk solution (fig. 1.10 c)). If the density of adsorbed vesicles is high enough, such process may be promoted across a few adjacent liposomes and result in the formation of the extended lipid bilayer patches [68, 69].

Lipid assemblies as a complete system may have lateral mobility and undergo cooperative form changes. This effect should no be mixed up with the lateral diffusion of individual lipids. An indication about the lipid mobility is observed by the structure of the bilayer patches. Chunks, that are laterally mobile, likely reorganize into circular patches in order to reduce their line tension (seen on mica surfaces) [64]. However, bilayer islands on silica usually retain a strictly noncircular shape, which, evidently, is due to lack of mobility [68].

There are several factors governing the SLB formation: the nature of the support (roughness, surface charge), the liposomes themselves (their charge, composition, size, etc.) and the aqueous environment (ionic strength, pH). However, most important parameters include electrostatic interactions, calcium ions, solid support composition and vesicle size.

Most of the pathways how vesicle adsorbs on a substrate can be produced by changing the charge of the liposomes consequently forming an SLB [62]. In the case of anionic DOPS lipids and mica surface, molecules tend to arrange asymmetrically among two SLB leaflets, however, when subjected to calcium, they may concentrate on the SLB-mica side more, which is an electrostatic interaction mediated SLB formation [64].

In general, divalent ions and, in particular, calcium appear to engage in the screening of charges, thus, altering the electrostatic interactions. However, it was proven that they directly promote the adsorption and rupturing of liposomes, and consequent formation of SLB [68]. Most commonly, small concentrations (in mM range and smaller) of the calcium ions are enough to produce important effects [62].

The formation of SLB is also influenced by the solid support composition [62]. There were previous attempts to form SLBs on surfaces such as gold [59], platinum [70] and others, however, not efficiently successful, leaving mica and silicon-based surfaces as the most conventional supports for SLB formation [62].

It was recently reported [71] that relatively small liposomes form rather full bilayers by rupturing on the substrate, however, the rupture of large vesicles is fragmentary and lead to a mixture of bilayer patches and intact liposomes. The possible explanation for this dependency is that the liposome adsorption is restrained by the diffusion in the solution and the rupturing process only starts at a time, which is relatively proportional to the size of the liposomes. Even though at the critical coverage point, at which rupturing starts is almost independent on the liposome size, but larger vesicles are subjected to sterical

effects, which keep some of them from rupturing. These intact vesicles play a barrier role for lateral lipid molecule diffusion, thus suggesting smaller vesicles to be preferable in the formation of complete SLBs. [71]

In conclusion, it is also important to mention, that QCM-D technique is more advantageous, in this project's case, compared to conventional Surface Plasmon Resonance (SPR) or Elipsometry due to the fact that it enables the possibility of distinguishing adsorbed layer of, e.g., liposomes from a planar bilayer of lipids (figure 1.10) [52].

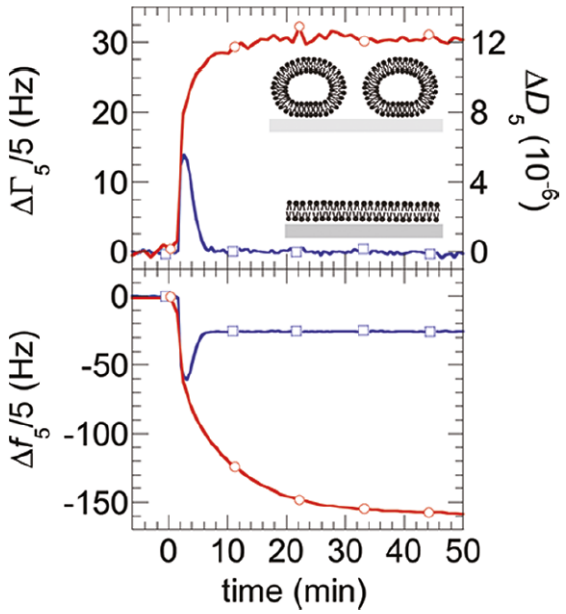


**Figure 1.11:** The figure represents one of the main advantageous points of QCM-D - its sensitivity to discriminate between vesicle adsorption and SLB formation. In the graphs, red lines are denoted as liposome adsorption on the surface without being ruptured. Blue lines show liposomes adsorbing on the surface and then rupturing in to a planar lipid bilayer. However, the frequency shifts are rather unusual due to the fact that adsorbed liposome layer results in a bigger frequency change than a bilayer of lipids. This fact is explained by the fact that the liposome layer is thicker and contains much more water coupled to the crystal oscillation than the planar lipid bilayer. In addition, the liposome layer develops higher energy dissipation, because of the higher water content and overall lower shear viscosity of the layer than for an SLB. Taken from I. Reviakine et al. [52]

Even though, it might seem that qualitative study of the data provided by QCM-D could be rather simple, bandwidth and frequency shift quantification using different overtones lacks understanding of how hydrodynamic and mechanical processes are happening in the system [52]. Up till now, most modeling was performed based on called continuum models, in which the characteristics of a sample in question is explained by a sequence of layers of defined thickness and homogeneous densities, viscosities and elasticities [58]. However, this method is only fully applicable to homogeneous systems, where the sound's wavelength is larger than the length scale of the sample [52]. If heterogeneous systems (e.g. liposomes

or proteins) are considered, the method might be a poor approximation since they are laterally and orthogonally heterogeneous as well as that the connection to the substrate might have significant influence [52].

### 1.7.2 Interpreting QCM-D results

In order to reach an adequate interpretation of achieved QCM-D data one needs to deduct whether the system is laterally heterogeneous or homogeneous as well as is dissipating energy or not. Taking these characteristics into account, conventionally, the received data is explained by several techniques (figure 1.12 that are consolidated by one theory known as the *small load approximation*. Therefore, the review of this concept will be included in the possible situations of QCM-D experiments discussed below. [52]

In the case of homogeneous layers, an induction of rather little or a big shift in dissipation could be observed. Consequently, if one would consider a greater quantitative distinction, a proportion of $\Delta\Gamma/-\Delta f$ should be taken into thought. When $\Delta\Gamma_n$ is significantly smaller than $-\Delta f_n$, the layer is evaluated as having rigid structure, thus, by applying the Sauerbrey estimation, the density of the areal mass of the layer may be well approximated. [52] However, if the layer is highly solvated, then the measured characteristic of the layer will also contain both the solvent, $m_{solvent}$, and the adsorbate, $m_{ads}$ [52]:

$$m_f = m_{ads} + m_{solvent} \tag{1.22}$$

In the situation where $m_{ads}$ is known from a different method, such as SPR [72], or elipsometry [73], the weight part of the solvent in the layer of interest is then possible to be quantified [52]. Even though the width of the adsorbed layer may be evaluated from the equation 1.20 (if the solvent and adsorbate densities are close in value), another estimation has to be considered when the densities are not alike in accordance with already known $m_{ads}$ [74]:

$$h_f = \frac{1}{\rho_{solvent}}\left[m_f - m_{ads}\left(1 - \frac{\rho_{solvent}}{\rho_{ads}}\right)\right] \tag{1.23}$$

where $h_f$ is the thickness of the layer, that is adsorbed, and $\rho_{solvent}$, and $\rho_{ads}$ are the densities of the solvent in the film and the film itself, accordingly.

| type of film | dissipative response | QCM data interpretation: approach | QCM data interpretation: output with QCM alone | QCM data interpretation: output in combination with techniques that quantify areal adsorbate mass density (coverage) |
|---|---|---|---|---|
| laterally homogeneous film | $\Delta\Gamma_n \ll -\Delta f_n$, or[a] low dispersion in $\Delta f_n/n$ | Sauerbrey equation | • areal mass density (may include solvent inside the film) | |
| | $\Delta D > 0$ | viscoelastic model | • areal mass density (may include solvent inside the film)<br>• viscoelastic properties (frequency dependent loss and storage moduli or compliances) | • hydrodynamic film thickness and density<br>• weight fraction of solvent in the film (solvation) |
| | | intrinsic viscosity | • $\Delta\Gamma_n/-\Delta f_n$ ratio has been used to obtain structural information about the molecules in the film.[24] | |
| monolayer of discrete particles or other nanosized objects | $\Delta D$ is small, or [a] low dispersion in $\Delta f_n/n$ | Sauerbrey equation | • areal mass density (including liquid inside the film) | • areal mass density of trapped liquid |
| | | empirical trapped-liquid coat model | | • particle size and height-to-width ratio<br>• lateral distribution of particles (clustering) |
| | $\Delta D \geq 0$ | FEM simulation of hydro-dynamics | • local mechanical properties (linker stiffness)<br>• in principle also particle size, shape and coverage. Quantitative predictions limited by computational resources. | |
| | | model-independent | • $\Delta\Gamma_n/-\Delta f_n$ ratio has been used to obtain adsorbed particle size in a model-independent fashion[26] | |

[a] Either of the two criteria can be applied, though the criteria of low dispersion in $\Delta f_n/n$ is more stringent.

**Figure 1.12:** The table in the figure shows the possible techniques in order to interpret QCM-D data. Taken from I. Reviakine et al. [52]

When $\Delta$D results in a higher value than zero, then the layer is considered thick enough

for the system to detect viscoelastic characteristics of the layer [58, 75, 76, 77, 78]. Then they are conventionally depicted according to complex shear modulus:

$$G = G' + iG" \tag{1.24}$$

where i is known as an imaginary component (or square root out of -1). [52]

The term G' defines the elasticity of the material, also known as the dependence between force that is applied on the material and the magnitude of it's deformation. The other term, G", is defined as the loss modulus and is equal to the angular frequency of deformation $\omega$ multiplied by viscosity $\eta$. When the loss modulus is significantly smaller than the elasticity term, the matter encounters most dominantly elastic demeanor, however, viscous if the relationship is in reverse. In addition, in the situation where the two terms are almost equal, both the viscosity and elasticity play an important role to model the mechanical response of the material. It is also important to note that G' and G" obtain different values according to changing $\omega$ and these numbers may range several orders of magnitude. [52] Consequently, when a finite frequency assortment is established, these reliances are commonly efficiently evaluated through power laws (taking into account exponents $\alpha'$ and $\alpha$"):

$$G'(\omega) = G'_0(\omega/\omega_0)^{\alpha'} \text{ and } G"(\omega) = G_0"(\omega/\omega_0)^{\alpha"} \tag{1.25}$$

where $\omega_0$ is promptly designated frequency for reference. [52] It is also known that $\alpha'$ and $\alpha$" at their certain corresponding frequencies are associated with the movements and interactions on the microscopic level inside the sheared material [79, 80].

When the case of laterally homogeneous viscoelastic layers is in question, the QCM's feedback is conducted through the continuum model, which is established in such a manner that the shear wave transmits across the viscoelastic environment basically as electromagnetic waves in optical research do [81]. However, if the films are significantly thinner than the wave value of the shear-acoustic wave, then areal mass density of the layer (as well as it's viscoelastic characteristics) is associated with the bandwidth and frequency shifts as in these equations [58, 82]:

$$\Delta f_n \approx -\frac{n}{C} m_f \left(1 - n\omega_F \rho_l \eta_l \frac{G_f"}{\rho_f (G'^2_f + G_f"^2)}\right) = -\frac{n}{C} m_f \left(1 - n\omega_F \rho_l \eta_l \frac{J'_f}{\rho_f}\right) \tag{1.26}$$

$$\Delta\Gamma_n \approx \frac{n}{C} m_f n\omega_F \rho_l \eta_l \frac{G'_f}{\rho_f (G'^2_f + G_f"^2)} = \frac{n}{C} m_f n\omega_F \rho_l \eta_l \frac{J'_f}{\rho_f} \tag{1.27}$$

where indexes f and l are depicted as film and liquid, accordingly [52]. The relation $m_f = \rho_f \ h_f$ explains again the layer's areal mass density and the terms J = J' - iJ" = $G^{-1}$ is the compliance of the layer, influenced by the frequency of the wave and J' as well with J" are elastic and viscous units [52]. In order to achieve equal width and z-average viscoelastic characteristics for latterally homogeneous films, with constantly changing mechanical characteristics in the orthogonal direction, one has to establish the model of the profile (e.g. parabolic) and integrate the section in the brackets in the equation 1.27 (results in $\Delta\Gamma$ and $\Delta f$) [82]. A standard case for such layers are polymer brushes.

However, in order to apply the viscoelastic model, it is necessary to keep in mind several aspects [52]. Due to the fact it has five independent parameters to fit, a premise about the density of the layer $\rho_f$ has to be considered with caution - frequency series at which QCM works is rather not probable to correspond to the frequency range in question [58]. To be more precise, if G' is taken as frequency independent component and G" is influenced by the frequency linearly, the disadvantage of the space criterion is observed and commonly not accepted [52].

It is also important to consider cases without laterally homogeneous films, layers that have incorporated discrete objects on the nanoscale such as liposomes, nanoparticles, viruses, etc. Until not that long time ago, the significance of these heterogeneous layers have been taken into consideration due to the fact it was thought that the same viscoelastic model may be applied as for the homogeneous counterpart [52]. However, in the previously mentioned case the main processes taking place are the motion of the particles that are adsorbing on the surface as well as the hydrodynamic influences. Later on it was shown that empirical models [83] and fundamental theory [84, 53] of such example exist and may result in new applications of the whole QCM-D method [52].

Some studies showed that the surface coverage of the film in question does not linearly relate to the frequency shift in QCM-D. Indeed, the liquid that is inside the particles or in spaces between them, contributes to the frequency decline with the increased surface coverage of the layer. In addition, QCM-D is rather significantly more sensitive to the particles being adsorbed at low surface coverage, but a lot less sensitive when particles adsorb at high surface coverage. The example of high coverage correlates to the case of laterally homogeneous layers as mentioned previously, however, the lower coverage is quite different. Due to the fact that liquid is trapped around or in between particles, that are adsorbed on the layer, the complexity of the case increases. For example, the fact that the overall contribution of mass of particles with liquid trapped among them is lower than the identical particle being adsorbed to the plane surface. However, there is no discrete boundary between solvent moving freely or immobilized solvent in crevice of two or more particles, nevertheless, it is a significant factor to consider to total hydrodynamic effects that occur amidst these layers. [52]

Furthermore, an empirical model, that considers the liquid immobilized between the particles as well as the particles are adsorbed on the layer in a random fashion, [85] has shown that it is possible to reproduce coverage-dependent feedbacks of frequency quantitavely [86, 83]. This model is dependent on a measurement of the areal mass density of the particle being adsorbed taken from another experiment in different machinery [52]. Consequently, the fraction of immobilized liquid is taken (H = 1 - $m_{ads}/m_f$ against the adsorbed areal mass density and fitted [52]. The result is particle's size and height-to-width ratio if the oblique distribution and the mass of the particle are noted previously [52]. Also, there is a possibility to achieve the particle degree of clustering or detail of how particles are laterally organized if their size and orientation on the layer are known [86, 52].

Another approach that helps to look at the same problem is known as finite element method (FEM) simulations. In this method, the accumulation of stress over the adsorbed particles of interest is estimated in order to acquire the fluctuations in dissipation and frequency [84, 53]. In addition, this technique does not take into account fitting parameter as mechanical characteristics and molecular geometry are only required initially, and gives information about the coverage-dependent decline of QCM-D's sensitivity in the case of laterally heterogeneous layers [84]. Additionally, it was proven that the main part of energy is depleted through liquid-particle barrier, however, the extent to which it is depleted relies upon the rigidness of the contact and the degree of coverage (particles protect each other from flow conditions) as well [52]. Therefore, if heterogeneous system is taken into account it will dissipate energy even at the point where the adsorbed particles are very rigid, whereas in homogeneous system this will not be observed [52].

According to the continuum viscoelastic model that defines layers which are homogeneous, the previously mentioned relations proves that the barrier-dependent way of energy depletion is superior in heterogeneous layers compared to homogeneous systems. Knowing this, it is insignificant to use the viscoelastic model for single layers of molecules or nanoparticles. [52]

All of these methods and approaches towards QCM-D data interpretation over time led to the development of a unifying approach, which includes an intricate change of frequency:

$$\Delta f* = \Delta f + i\Delta\Gamma \tag{1.28}$$

$$\Delta f* = iZ_L/(2\pi m_q) \tag{1.29}$$

where $m_q$ is the areal quartz crystal's density of the areal mass and $Z_L = Z'_L$ + i$Z_L$" is known as the ratio between velocity and shear stress at the exterior of the fluctuating crystal. [52] The latter sum is known as the *load impedance* [87]. In addition, the linear

relation among the frequency change term as well as the load impedance is named *the small load approximation.* [52]

In the case of laterally homogeneous layers, the load impedance may be estimated through appliance of *Fresnel theory* taken from optics [73, 81]. The acoustic impedance acts as the refractive index of the matter in question [76]:

$$Z = (\rho G)^{1/2} \tag{1.30}$$

When the materials are considered very rigid (G' is significantly bigger than G") or layers with small width, $Z_L = i\omega m$, which results in change of frequency that is evident (no dissipation). In contrast, the estimation may also result into rather complicated changes in frequency (energy dissipation exists). Consequently, if one excludes the dissipation of energy, then both underestimation and overestimation of the true mass load on the QCM crystal can occur. [52]

In heterogeneous systems, the area-averaged stress needs to be estimated numerically, e.g., by obtaining a numerical mean of shear stress that is acquired by FEM modeling around the interface of interest. Even though this technique is more rigorous than viscoelastic modeling based on continuum mechanics, it requires serious amount of computational recourse and prior knowledge of the structure of the adsorbed film.. [52]

In conclusion, it is important to mention that QCM-D is an astonishing qualitative and quantitative technique, but the modelling of the data can be rather complex. When it is applied in combination with other machinery that may evaluate the mass of the adsorbed molecule/particle per area of the surface, a compelling amount of data can be gathered. [52]

# 2. Materials and methods

## 2.1 Materials and chemicals

The lipids used for liposome production POPC, POPG, DOPE-biotinylated, POPS and DSPE-PEG(2000)-biotin are presented in the figures below:

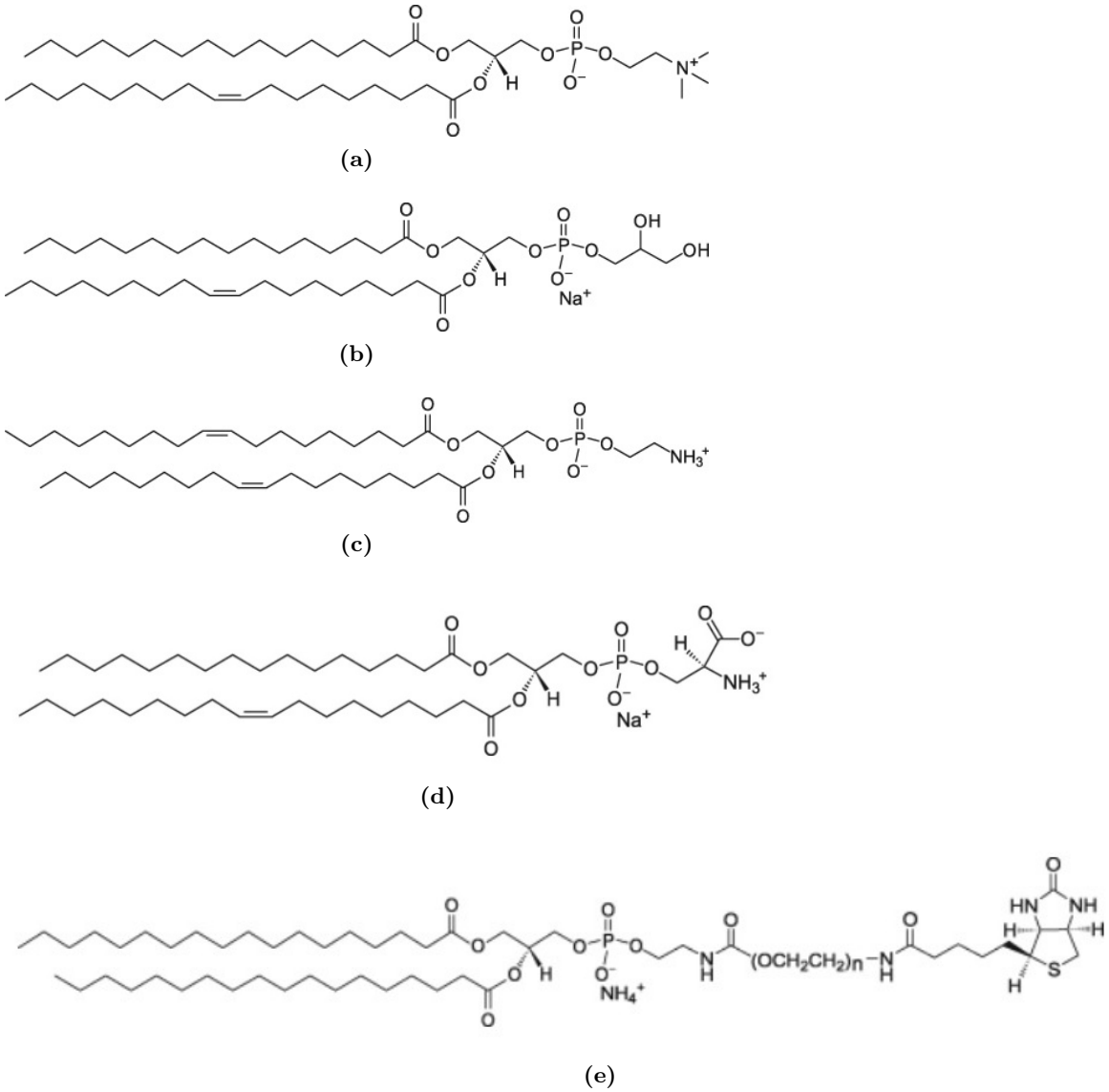

**Figure 2.1:** Lipids used in the project: a) POPC; b) POPG; c) DOPE (It was biotinylated for this project); d) POPS; e) DSPE-PEG(2000)-biotin. Structures taken from Avanti lipids website [88].

**Table 2.1:** Materials used in this thesis

| Material | Manufacturer | Description |
|---|---|---|
| $CaCl_2$(Calcium dichloride) | CARL ROTH | > 94% |
| DOPE(1,2-dioleoyl-sn-glycero-3-phosphoethanolamine)-biotin | Avanti Lipids | (18:1 biotinyl PE Sodium salt); 25 mg/mL in chloroform |
| DSPE-PEG(2000)-biotin (1,2-distearoyl-sn-glycero-3-phosphoethanolamine-N-[biotinyl(polyethyleneglycol)-2000] (ammonium salt) | Avanti Lipids | >99%; 10 mg/mL in chloroform |
| Ethanol | CARL ROTH | >96% |
| HCl(Hydrogen chloride) | CARL ROTH | 6N |
| Isopropanol | Inhouse | 99.5% |
| MilliQ Water | Inhouse | - |
| NaCl(Sodium chloride) | CARL ROTH | >99.8% |
| NaOH(Sodium hydroxide) | CARL ROTH | >99% |
| Neutravidin, biotin binding protein | Thermo Fisher Scientific | - |
| PLL-g-PEG-biotin(Poly(L-Lysine)-g-Poly(ethylene-glycol)-biotin) | SuSOS AG | PLL (20 kDa) grafted with PEG (2 kDa) and PEG-biotin having g (Lys units/PEG chains) = 3.5; |
| POPC(1-palmitoyl-2-oleoyl-sn-glycero-3-phosphocholine) | Avanti Lipids | (16:0 - 18:1 PC Sodium Salt); 25 mg/mL in chloroform |
| POPG(1-palmitoyl-2-oleoyl-sn-glycero-3-phospho-(1'-rac-glycerol)) | Avanti Lipids | (16:0 - 18:1 PG Sodium salt); 25 mg/mL in chloroform |
| POPS(1-palmitoyl-2-oleoyl-sn-glycero-3-phospho-L-serine) | Avanti Lipids | (16:0 - 18:1 PS Sodium Salt); 25 mg/mL in chloroform |
| SDS(Sodium dodecyl sulfate) pellets | CARL ROTH | >99% |
| Silica nanoparticles | Inhouse | - |
| Streptavidin from Streptomyces | Sigma - Aldrich | >13 units/mg protein |
| THF (tetrahydrofuran) | CARL ROTH | >99.5% |
| Trichloromethane | CARL ROTH | >99% |
| Trizma base | Sigma - Aldrich | >99.9% |

## 2.2 Methods

All of the materials and solutions very mainly stored at 4 °C except for lipids and streptavidin/neutravidin, which were stored at -25 °C.

### 2.2.1 Buffer preparation

Both buffers after preparation were filtered through a 0.2 $\mu$m filter.

**Tris 10 x (or 0.1 M):**

1. Dissolve 60.57 mg of Tris in 0.5 L of miliq $H_2O$ and while reaching the final volume adjust the ph with an appropriate acid to pH = 7.5.

**TBS 10 x (or 0.1 M of Tris and 1.5 M of NaCl):**

1. Add 43.83 g of NaCl and 6.057 g of Tris.
2. Reach a final volume of 0.5 L with miliq $H_2O$. The pH should be adjusted with HCl to pH = 7.5.

### 2.2.2 Activation and preparation of silica nanoparticles for coating

1. Incubate Silica Nanoparticles in 0.1 M NaOH solution for 1 hour. Vortex the suspension from time to time during the period.
2. Centrifuge at 6000 RPM for 5 minutes and discard the supernatant.
3. Wash with Ethanol and miliQ $H_2O$ three times by centrifuging with the same parameters as in point 2.
4. Pipette out the supernatant from the nanoparticles and freeze-dry overnight under vacuum.
5. Take 15 mg of Silica Nanoparticles and resuspend them in 10 mL of Tris 10 x. Sonicate this suspension overnight in bath sonicator (37 kHz; 20 °C).

### 2.2.3 Liposome preparation

Liposomes were produced by employing several different methods in order to reach the desired size of the vesicles. In addition, POPC, POPC/DOPE-biotin, inclusion of POPG or POPS and POPC/DSPE-PEG(2000)-biotin liposomes were prepared for the coating with the silica nanoparticles. The exact values of lipid mass are excluded from the protocols due to several different mol% of lipids inclusion through the production.

**1) Initial liposome preparation (Rehydration method; Final liposome concentration 2 mg/mL):**

1. Wash with Ethanol and milliQ $H_2O$ the glass container for liposome production.
2. Under chemical hood wash the glass container with chloroform 2 times.
3. Add lipids according the needed molar percentage of POPC (25 mg/mL) and DOPE-biotin (25 mg/mL) and dry the chloroform with nitrogen under weak stream.
4. Freeze-dry the lipids for at least 30 minutes under vacuum.
5. Resuspend the dried lipids in TBS 1 x buffer to reach the final concentration of 2 mg/mL, vortex for 10 seconds and incubate at room temperature for 15 minutes.
6. Extrude the lipids using one 400 nm and two 50 nm polycarbonate filters (washing with ethanol and milliQ $H_2O$ of the extrudor before use).

**2) Liposome preparation/bath sonication (Rehydration method; Final liposome concentration 2 mg/mL):**

1. Wash with Ethanol and milliQ $H_2O$ the glass container for liposome production.
2. Under chemical hood wash the glass container with chloroform 2 times.

3. Add lipids according the needed molar percentage of POPC (25 mg/mL) or DOPE-biotin (25 mg/mL) and dry the chloroform with nitrogen under weak stream.
4. Freeze-dry the lipids for at least 30 minutes under vacuum.
5. Resuspend the dried lipids in a volume of TBS 1 x buffer to reach the final concentration of 2 mg/mL, vortex for 10 seconds and incubate at room temperature for 15 minutes.
6. Sonicate in bath sonicator for 30 minutes (37 kHz; 20 °C).

**3) Liposome preparation/bath sonication (Solvent injection method; Final liposome concentration 2 mg/mL):**

1. Wash with Ethanol and milliQ $H_2O$ the glass container for liposome production.
2. Under chemical hood wash the glass container with chloroform 2 times.
3. Add lipids according the needed molar percentage of POPC (25 mg/mL) or DOPE-biotin (25 mg/mL) and dry the chloroform with nitrogen under weak stream.
4. Freeze-dry the lipids for at least 30 minutes under vacuum.
5. Add THF solvent (according to the amount of lipids) to the dried lipids.
6. Pipette the THF/lipid solution by drops into certain volume of TBS 1 x (to reach the final concentration) and mix with a magnetic stirrer while blowing with a gentle stream of nitrogen for at least 15 minutes.
7. Sonicate in bath sonicator for 30 minutes (37 kHz; 20 °C).

**4) Liposome preparation/tip sonication (Rehydration method; Final liposome concentration 2 mg/mL):**

1. Wash with Ethanol and milliQ $H_2O$ the glass container for liposome production.
2. Under chemical hood wash the glass container with chloroform 2 times.
3. Add lipids according the needed molar percentage of POPC (25 mg/mL), DOPE-biotin (25 mg/mL), DSPE-PEG(2000)-biotin (10 mg/mL), POPG (25 mg/mL) or POPS (25 mg/mL) and dry the chloroform with nitrogen under weak stream.
4. Freeze-dry the lipids for at least 30 minutes under vacuum.
5. Resuspend the dried lipids in TBS 1 x buffer to reach the final concentration of 2 mg/mL, vortex for 10 seconds and incubate at room temperature for 15 minutes.
6. Freeze in liquid nitrogen and thaw 5 times.
7. Tip sonicate under these settings: 100% duty cycle, 20 minutes, output: 6 with a probe (*Branson Sonifier 250*).
8. Centrifuge for 10 minutes at 8000 RPM to get rid of titanium particles from the probe.
9. Extrude through one 100 nm and two 30 nm polycarbonate membranes.

### 2.2.4 Coating of the silica nanoparticles

The first protocol is the one that was established before I started the project at the institute, however, it was not optimized and not at all reproducible. The second protocol is the one obtained after optimization through the work presented in this thesis to obtain the parameters for best yield of uniformly membrane-coated nanoparticles suitable for the interaction measurements. The optimization procedure will be discussed more in detail in section 3.2.

**1) Initial coated silica nanoparticle preparation:**

1. Add in this order: 200 $\mu$L of vesicles (2 mg/mL), 80 $\mu$L of TBS 10x, 320 $\mu$L of miliQ$H_2O$ and 400 $\mu$L of silica nanoparticles (in Tris buffer). Final concentration of TBS should reach 1x.
2. Mix 10 times with a pipette.
3. Centrifuge at 1000 rcf for 30 minutes.
4. Discard the supernatant.
5. Resuspend the pellet in 1 mL of TBS 1x.
6. Repeat the steps 3,4 and 5 three times.

**2) The most optimized and reproducible silica nanoparticle coating procedure obtained in the project:**

1. Sonicate silica nanoparticles in bath sonicator for at least 2 hours (37 kHz; room temperature).
2. Add 159.7 $\mu$L of liposomes (2 mg/mL), 740.3 $\mu$L of TBS 1 x and 100 $\mu$L of activated and prepared silica nanoparticles.
3. Vortex for 25 minutes at 600 rpm in room temperature.
4. Centrifuge at 6000 rpm for 5 minutes.
5. Discard the supernatant (pipette out around 900 $\mu$L of solution).
6. Add 900 $\mu$L of Tris 10 x.
7. Vortex for 10 seconds.
8. Repeat the cycle (Points 3-6) two more times.

### 2.2.5 Dynamic light scattering

Size distribution measurements were performed on a Zetasizer Nano ZS. Cuvettes used for DLS size distribution measurements were semi-micro PMMA cuvettes and Disposable Capillary Cell (DTS1070) for zeta potential measurements. For each size distribution or zeta potential evaluation there were 3 measurements (averaged in plots, which are presented in the result section) consequent one after another done having at least 12 assessments per one sample for size distribution and 100 for zeta potential.

A pre-wash with a certain buffer (10 x Tris or 1 x TBS) of the cuvette was made before evaluating size distributions or zeta potential of the liposomes/particles in order to avoid

additional contamination during measurements. Dispersants were chosen accordingly (Tris 10x or TBS 1x) and equilibration time was set to 10 seconds for each sample. The concentrations for the appropriate measurements were 2 mg/mL for liposomes, 1.5 mg/mL for bare silica nanoparticles and 0.15 mg/mL for coated silica nanoparticles. In addition, the laser wavelenght of zetasizer was 633 nm. The calculation method for the size distributions from dynamic light scattering data was the CONTIN algorithm.

### 2.2.6 Sensor cleaning protocol for quartz crystal microbalance with dissipation monitoring measurements

1. Put the needed number of silicon dioxide QSensors (around 1 $cm^2$ active surface diameter; crystal type QSX303) in compact uv-ozone cleaner (ProCleaner™; BioForce Nanosciences) with 4"x 4" Chamber - EQ-PCE-44-LD for 10 minutes with blunt tweezers.
2. Turn of the chamber and wait 5-10 minutes.
3. Sonicate the silicon dioxide QSensors in 2% SDS solution for 15 minutes in bath sonicator (37 kHz; 20 °C) and incubate for additional 15 minutes.
4. Clean the sensors thoroughly with milliQ $H_2O$ in the direction of the tweezers (to avoid possible contamination from the tweezers).
5. Blow off the residual milliQ $H_2O$ from the QSensors with nitrogen stream.
6. Put the silicon dioxide QSensors in the uv-ozone cleaner with 4"x 4" Chamber - EQ-PCE-44-LD for 10 minutes with blunt tweezers.
7. Wait for 5-10 minutes after the uv-ozone treatment is complete.
8. Blow of the possible dust from the QSensors while transferring from the uv-ozone chamber to the QSense flow cell.

### 2.2.7 Quartz crystal microbalance with dissipation monitoring

QCM-D measurements were done with QSense Analyzer 4-channel system (presented in 1.5 section). The fundamental frequency of the silicon dioxide QSensor was 4.95 MHz. Also, the pump for the QCM-D experiment was set to 0.51 mm diameter tubing system. Concentrations, dispersants and flow rates for different materials for QCM-D experiments are shown in table 2.2:

| Material | Buffer | Concentration | Flow rate |
|---|---|---|---|
| Liposomes for SLB formation | TBS 1 x | 0.1 mg/mL | 50 $\mu$L/min |
| PLL-g-PEG(2000)-biotin | Tris 10 x | 0.1 mg/mL | 50 $\mu$L/min |
| Streptavidin | TBS 1 x | 0.05 mg/mL | 50 $\mu$L/min |
| Neutravidin | TBS 1x | 0.05 mg/mL | 50 $\mu$L/min |
| Coated silica nanoparticles | TBS 1x | 0.1 mg/mL | 10 $\mu$L/min |
| TBS buffer | - | 1 x | 50 $\mu$L/min |
| Tris buffer | - | 10 x | 50 $\mu$L/min |

**Table 2.2:** Materials, buffers, their concentrations and flow rates used for QCM-D experiments

In addition, most of the QCM-D experiments were conducted in such manner: establishing a baseline with a certain buffer (mostly 1x TBS); assembling a single lipid bilayer (with liposomes); washing step with a buffer; addition of streptavidin/neutravidin; washing step with a buffer; addition of bare or coated silica nanoparticles; washing step with an appropriate buffer (fig. 2.2).

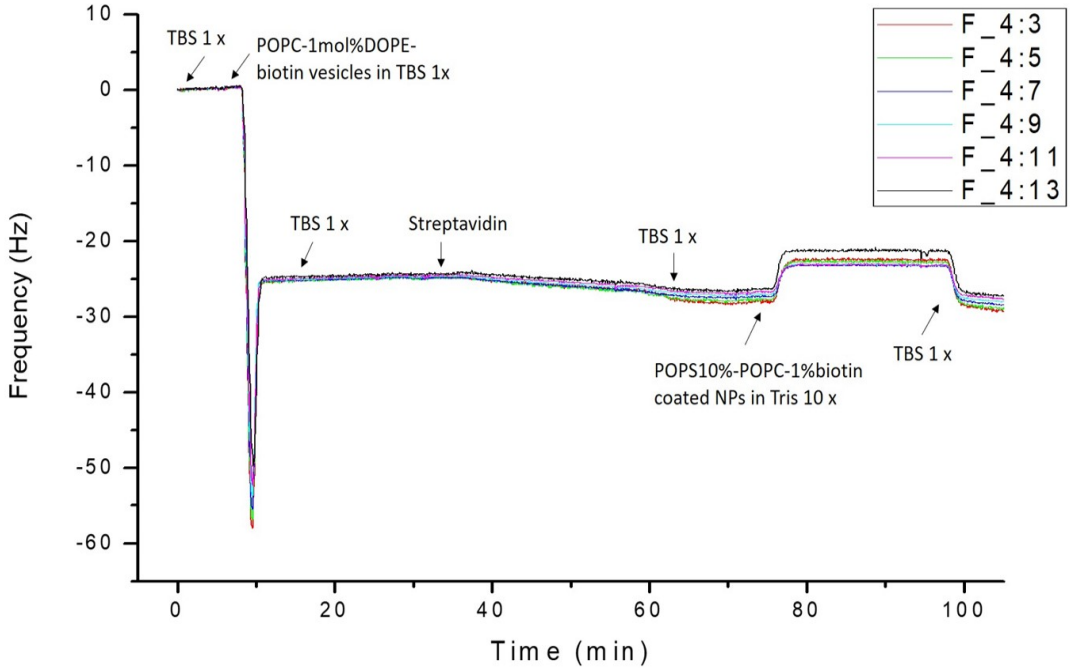


**Figure 2.2:** The manner, in which, QCM-D experiments were mostly proceeded. In the legend, first numerical value indicates the sensor and the second - the overtone.

# 3. Results and discussion

## 3.1 Liposome production method results

In this project, several liposome production methods were tested to achieve the necessary size unilamellar vesicles for the coating procedure of silica nanoparticles. A reasonably uniform vesicle size smaller than the silica nanoparticle size as well as a high relative concentration of liposomes compared to nanoparticles is required to coat nanoaprticles uniformly and without aggregation. As described above, most techniques used to produce unilamellar nanoscale liposomes start using rehydration in combination with extrusion, sonication and freeze-thaw. The size distributions of the liposomes will mostly be presented as intensity distributions from DLS data, however, there will also be a table showing standard errors of all produced liposome z-average diameters in the end of this chapter (table 3.1).

The first protocols for liposome preparation included methods from section 2.2.3 1) - 3). The vesicle size range at z-average = 85 - 112 nm with relatively low or moderate polydispersity (figures 3.1 and 3.2; PDI = 0.2 - 0.3) in accordance to the results of Oliver Bixner and Erik Reimhult [89]. In the picture 3.1 a) and b) represent the same method to produce liposomes containing different components. An amount of lipids with biotin functionalized headgroups (1 mol%; $\approx$ 910 molecules per coated silica nanoparticle of z-average $\approx$ 135 nm) was incorporated in the liposome structure for later interaction experiments on QCM-D. Due to the fact, that via the employed protocol (2.2.3. 1)) the produced liposomes were relatively large for this project, optimization or changes in the protocol steps to reduce the size in order for them to fuse more easier during coating or rupture for the supported lipid bilayer assembly. Thus, firstly bath sonication (30 and 60 min; 3.1 c) and d); 2.2.3. 2)) after the extrusion of the liposomes was applied in order to possibly break up the current vesicles into smaller ones or membrane fragments. However, as seen in 3.1 d), longer sonication time increases the risk of introducing artifacts (z-average $\approx$ 1 - 20 nm) rather than decreasing the overall liposome z-average size.

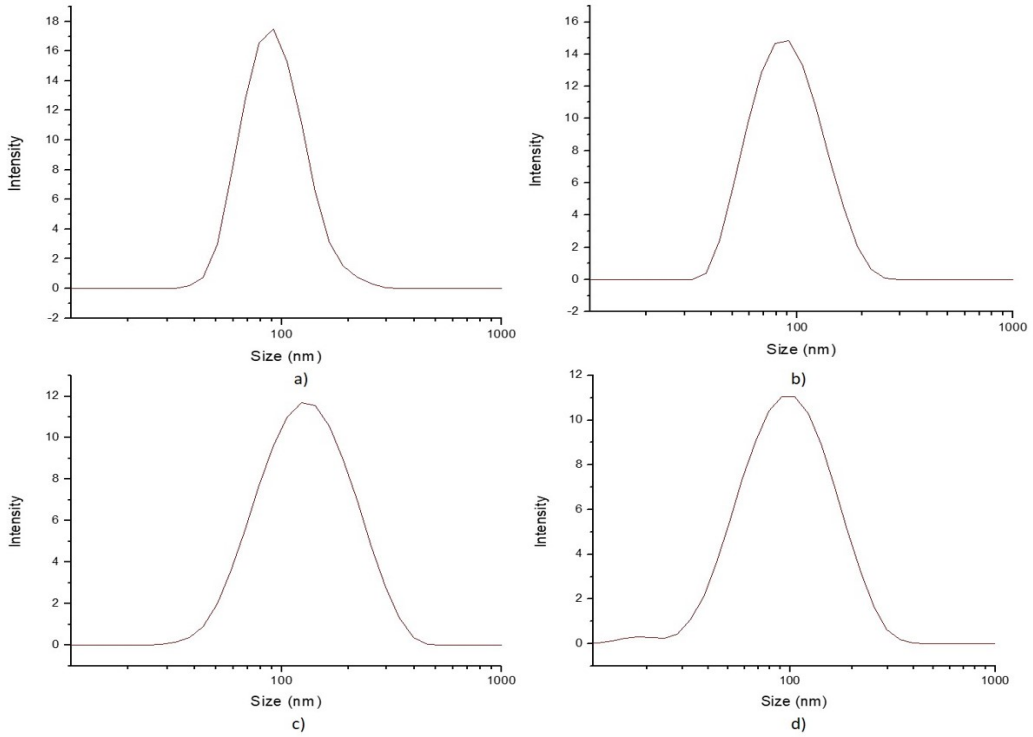


**Figure 3.1:** DLS intensity size distribution measurements on the first attempts to produce liposomes. Rehydration methods (2.2.3. 1) and 2)). A) POPC liposomes; z-average diameter = 96.2 nm b) POPC-1mol%DOPE-biotin liposomes; z-average diameter = 92.2 nm c) POPC liposomes, 30 min. bath sonication; z-average diameter = 112.4 nm d) POPC liposomes, 60 min. bath sonication; z-average diameter = 84.7 nm.

Furthermore, fig. 3.2 represents another set of first attempts on liposome development in order to achieve smaller vesicle size, however, with other, solvent injection method (2.2.3. 3); this protocol uses solvent injection with THF as the carrier solvent to first produce unilamellar vesicles in the 100-200 nm size range, which are then bath sonicated to achieve a reduced size. Due to the fact that method includes bath sonication as well as the previously mentioned technique, it is essential to take into account that the size of the vesicles vary in correspondence to different sonication times and salt concentration. By increasing the salt concentration and sonication time, one can expect smaller vesicles in the 20 - 40 nm region (fig. 3.2 c). In the first three subfigures in fig. 3.2 it is observable that the z-average diameter is $\approx$ 75 - 123 nm, which is almost the same as with the first technique and the polydispersity is higher, thus, this method was not further pursued. Nevertheless, statistical two tailed t-tests were performed to see whether varying salt concentration and sonication time is significant for the z-average diameter of the POPC liposomes. In the case of 1x TBS or 10x TBS buffer concentrations in POPC vesicle solutions during production (subfigures a) and b) in fig. 3.2) alternative hypothesis at significance level 0.05 was accepted stating that z-average diameter depends on the salt concentration (t-critical value = 22.52978324, corresponds to p-value $< 0.001$). In addition, bath sonication

time (subfigures b) and c) in fig. 3.2), according to two-sided t-test, proved to have influence on z-average diameter of the POPC vesicles (t-critical value = 54.30422871, corresponds to p-value $< 0.001$) as the alternative hypothesis at significance level 0.05 was accepted as well. The last subfigure d) in fig. 3.2 represents an inclusion of a freeze-thaw step, which according to Jonathan et.al. [90] should impose vesicle size reduction by immersing the sample solution into liquid nitrogen and thawing correspondingly at room temperature, in this case. However, the overall intensity size distribution profile remained not monodispersed enough and the size has not decreased adequately. Also, the two-sided t-test has shown the z-average diameter of the POPC vesicles is influenced by the freeze-thaw step inclusion due to the fact that the alternative hypothesis (freeze-thaw influences z-average diameter of liposomes) was accepted at significance level 0.05 (t-critical value = 8.422938864, corresponds to p-value = 0.001 - 0.002).

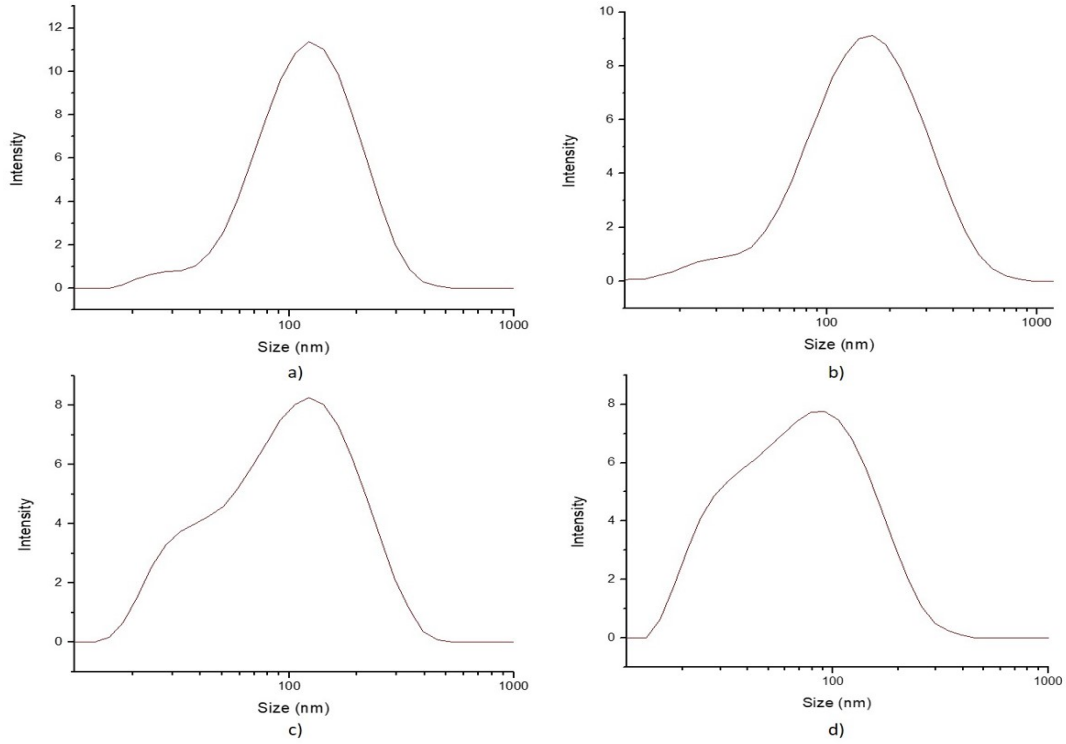


**Figure 3.2:** The first attempts to produce liposomes (DLS intensity size distribution measurements). Solvent injection a), b) and c)) and rehydration (d)) methods (2.2.3. 2) and 3)). A) POPC liposomes, 1x TBS, 30 min. sonication; z-average diameter = 101.8 nm b) POPC liposomes, 10x TBS, 30 min. sonication; z-average diameter = 123.2 nm c) POPC liposomes, 10x TBS, 50 min. bath sonication; z-average diameter = 75.4 nm d) POPC liposomes, freeze-thaw 5x, 30 min. bath sonication, no extrusion; z-average diameter = 56.3 nm.

After the two previous sets of developments not yielding sufficiently small and monodisperse liposomes, we switched to preparation protocols based on tip probe sonication in combination with freeze-thaw has come into consideration. Figure 3.3 demonstrates the application of this approach to liposome production. The first subfigure

a) already shows a decline in vesicle size to z-average = 80.9 nm, which, in turn, suggests that inclusion of tip probe sonication might result in the desired yield if parameters are optimized. Thus the attempts, b) and c), represent the optimization pathway. With the inclusion of smaller (30 nm) polycarbonate membranes in the extrusion step and increase in duty cycle of tip probe sonication to 100 %, the z-average of vesicles became significantly smaller (z-average diameter = 61 - 66 nm) and the PDI decreased gradually to a value of $\approx 0.1$. Consequently, the actual necessity for freeze-thaw step was tested and the results displayed that it leads to a decline in size by a few nanometers. Additionally, the subfigure d) is just an example to see whether the size of liposomes, with the inclusion of lipids with biotin functionalized headgroups in their structure, will remain within the same range. Nevertheless, the z-average diminished even more, to 53.4 nm from 61 - 66 nm, when tip sonication time was increased. However, this was estimated as the maximum time a sample could be sonicated due to the fact of a possibility for sample being overheated and therefore result in change of it's concentration. Long sonication times causing high temperatures are also believed to cause sample damage through lipid degradation.

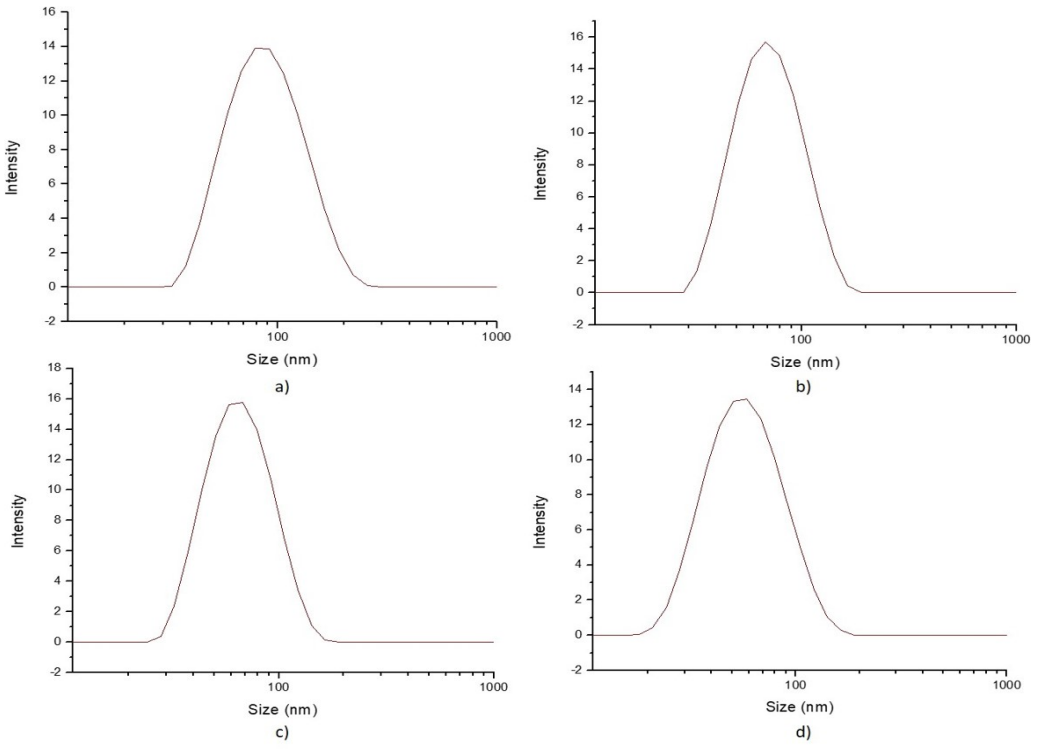


**Figure 3.3:** The figure shows DLS intensity size distribution measurements on liposomes produced via rehydration method (2.2.3. 1)) with inclusion of tip sonication and with or without freeze-thaw. A) POPC liposomes, freeze-thaw 5 times, tip sonication (50% duty cycle, probe, 6 output, 15 minutes), extrusion through one 100 and two 50 nm membranes; z-average diameter = 80.9 nm b) POPC liposomes, no freeze-thaw, tip sonication (100% duty cycle, probe, 6 output, 15 minutes), extrusion through one 100 and two 30 nm membranes; z-average diameter = 65.8 nm c) the same as b), but with freeze-thaw 5 times; z-average diameter = 61.2 nm d) POPC-1mol%DOPE-biotin liposomes, freeze-thaw 5 times, tip sonication (100% duty cycle, probe, 6 output, 15 minutes), extrusion through one 100 and two 30 nm membranes; z-average diameter = 53.4 nm.

Finally, the latest protocol involving rehydration method with tip sonication and extrusion was used for further liposome production during the project, however, as it will be shown later on in the section of the results of the nanoparticle coating, the need for inclusion of anionic lipids into the vesicle structure was inevitable in order to obtain a stable and needed size colloidal systems. The idea for anionic lipids has risen as well due to the fact that the silica nanoparticles, to begin with, are negatively charged in overall (zeta potential ≈ -43 mV; fig. 3.4), thus, as one of the stabilization methods of the colloidal systems, we have chosen electrostatic stabilizing effect by including anionic lipids (different molar percentage of POPG or POPS) in the liposome structure, which would help to prevent aggregation and keep the negative potential high during the coating.

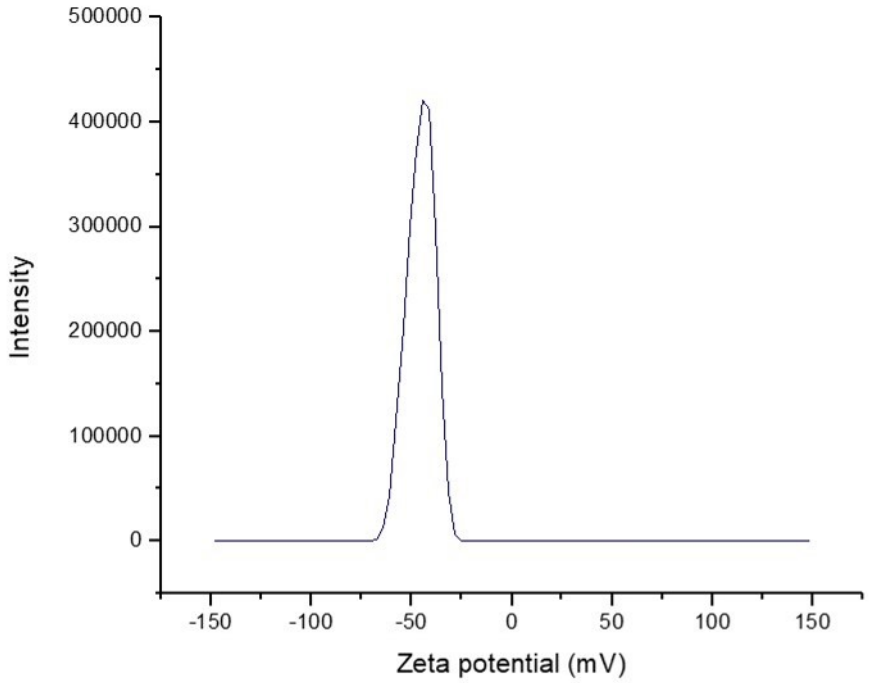


**Figure 3.4:** DLS measurement of silica nanoparticle (z-average diameter ≈ 130 nm) zeta potential in Tris 10x buffer (pH = 7.5). After roughly 3 months keeping the colloids in the solution, the zeta potential shifts to ≈ -49 mV from ≈ -43 mV.

We tried three different anionic POPG molar ratios (4mol%, 10mol% and 25mol%; fig. 3.5 and 3.7) included in the POPC liposome structure. Even though the size differs just by 1-2 nm between these different compositions, the PDI decreased even more for liposomes containing DOPE-biotin ligands (from 0.164 to 0.107) compared to the previous protocol, which does not include anionic lipids. In order to see how the inclusion of each anionic lipid molar percentages in the vesicle structure has influenced the coating of the nanoparticles it is important to look into their monodispersity and stability.

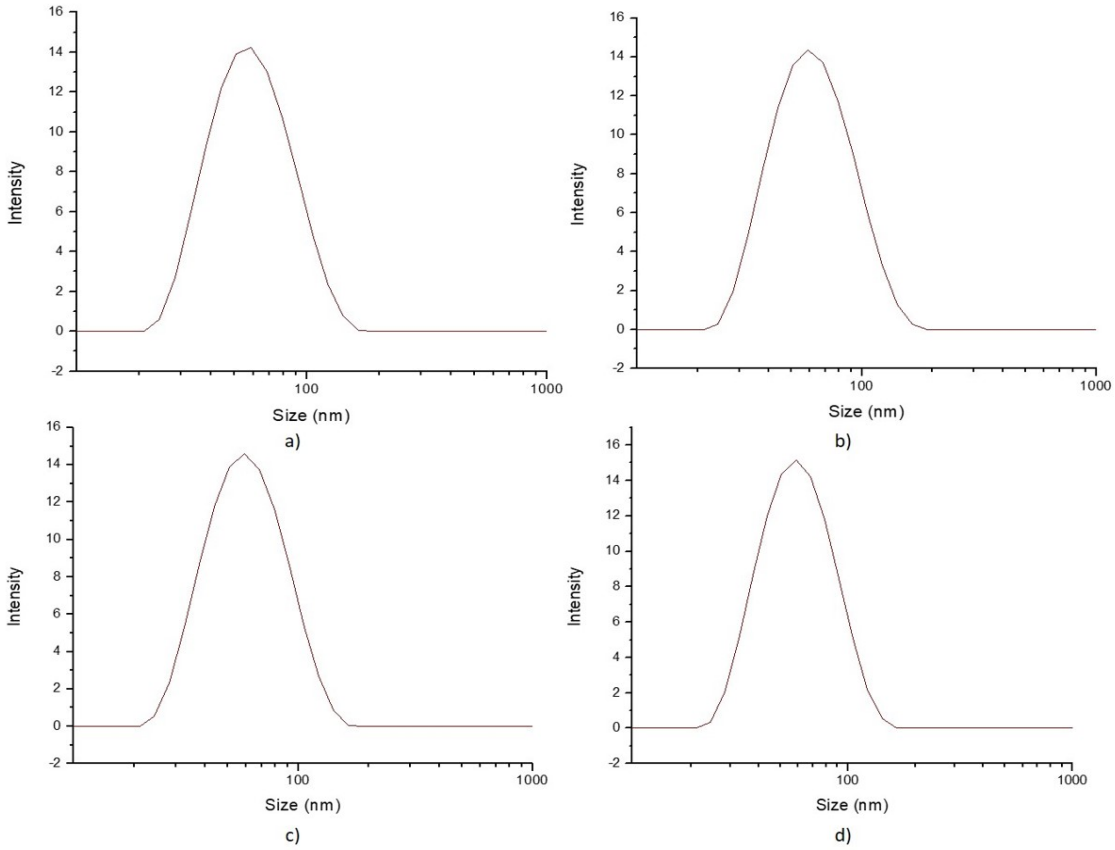


**Figure 3.5:** DLS intensity size distribution measurements of liposomes containing certain molar percentages of anionic POPG lipids. A) POPC-4mol%POPG liposomes, freeze-thaw 5 times, tip sonication (100% duty cycle, probe, 6 output, 15 minutes), extrusion through one 100 and two 30 nm membranes; z-average diameter = 56.3 nm b) POPC-10mol%POPG liposomes, freeze-thaw 5 times, tip sonication (100% duty cycle, probe, 6 output, 15 minutes), extrusion through one 100 and two 30 nm membranes; z-average diameter = 57.1 nm c) POPC-25mol%POPG liposomes, freeze-thaw 5 times, tip sonication (100% duty cycle, probe, 6 output, 15 minutes), extrusion through one 100 and two 30 nm membranes; z-average diameter = 55.5 nm d) POPC-10mol%POPG liposomes-1mol%DOPE-biotin liposomes, freeze-thaw 5 times, tip sonication (100% duty cycle, probe, 6 output, 15 minutes), extrusion through one 100 and two 30 nm membranes; z-average diameter = 55.4 nm.

In addition, there were also attempts to produce liposomes that include POPS anionic lipid (4mol% and 10mol%; fig. 3.6 and 3.7) due to their possible coordination in self-assembly by calcium$^{2+}$ ions [91], however, in the later experiments this decision was excluded due to insignificant changes in the nanoparticle coating procedure and higher costs than POPG anionic lipids. Nevertheless, the inclusion of POPS anionic lipids in the vesicle structure yielded smaller z-average size (drop from 56.3 nm to 52.3 nm for 4mol% and from 57.1 nm to 51.2 nm for 10mol% anionic lipids) as well as polydispersity index (decline from 0.182 to 0.096 for 4mol% and from 0.122 to 0.12 for 10mol% anionic lipids) compared to POPG counterparts.

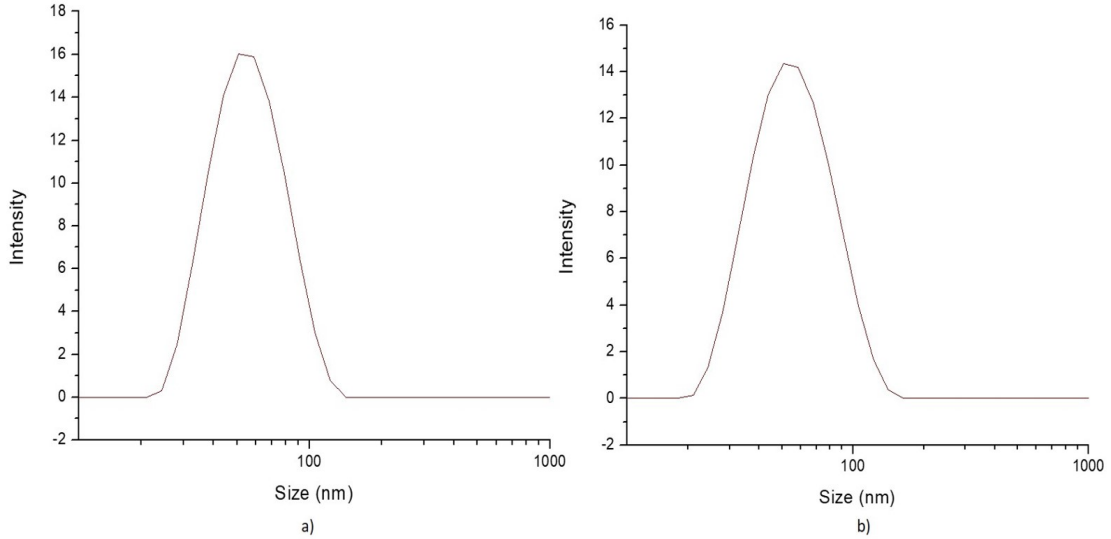


**Figure 3.6:** DLS intensity size distribution measurements of liposomes containing certain molar percentages of anionic POPS lipids. A) POPC-4mol%POPS liposomes, freeze-thaw 5 times, tip sonication (100% duty cycle, probe, 6 output, 15 minutes), extrusion through one 100 and two 30 nm membranes; z-average diameter = 52.3 nm b) POPC-10mol%POPS liposomes, freeze-thaw 5 times, tip sonication (100% duty cycle, probe, 6 output, 15 minutes), extrusion through one 100 and two 30 nm membranes; z-average diameter = 51.2 nm.

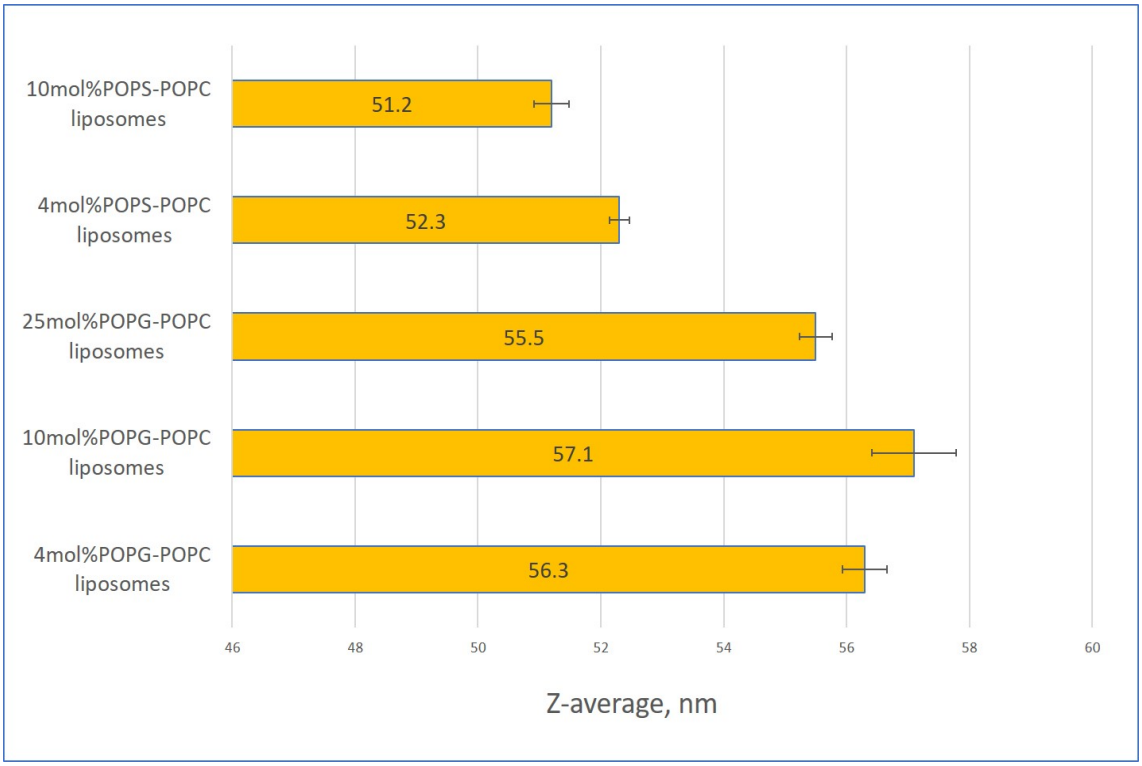


**Figure 3.7:** Z-average sizes of liposomes differing by the molar concentrations of POPG and POPS lipids in their structures.

Statistical two-sided t-tests were performed at significance level 0.05 for POPC vesicles, containing anionic lipids in their structure, z-average values in order to see the significance in varying the molar concentrations. It was found that in the cases between 4mol%POPG and 10mol%POPG (t-critical value = 1.016334647, corresponds to p-value = 0.30 - 0.40) 10mol%POPG and 25mol%POPG (t-critical value = 2.236456054, corresponds to p-value = 0.05 - 0.10), 4mol%POPG and 25mol%POPG (t-critical value = 1.909590092, corresponds to p-value = 0.10 - 0.20) null hypothesis is accepted at 0.05 significance level (two-sided test), which states that the POPG molar concentrations (4mol%, 10mol% and 25mol%) have no influence on the z-average diameter of the POPC vesicles. The examples of 4mol%POPS and 10mol%POPS (t-critical value = 3.114395225, corresponds to p-value = 0.05 - 0.02) and 10mol%POPG, and 10mol%POPS (t-critical value = 7.877165741, corresponds to p-value $< 0.001$) result in alternative hypothesis acceptance at 0.05 significance level (two-sided test) stating that the z-average diameter depends on appropriate anionic lipid (10mol%POPS or 10mol%POPG) or their molar concentration (4mol%POPS or 10mol%POPS) inclusion in the POPC liposome structure.

**Table 3.1:** Different methods for liposome production and their statistics (Each sample having 3 measurements)

| Nr. | Sample; Subsection in method part; | Z-average, nm | PDI | St. error of mean, ±nm |
|---|---|---|---|---|
| 1 | First POPC liposome preparation; 2.2.3. 1) | 96.2 | 0.242 | 1.17 |
| 2 | First POPC-1mol%-DOPE-biotin liposomes; 2.2.3. 1) | 92.2 | 0.17 | 2.31 |
| 3 | POPC liposomes, 30 min bath sonication after extrusion; 2.2.3. 1); | 112.4 | 0.192 | 1.04 |
| 4 | POPC liposomes, 60 min bath sonication after extrusion; 2.2.3. 1); | 84.7 | 0.202 | 0.82 |
| 5 | POPC liposomes, 30 min bath sonication 1x TBS; 2.2.3. 3); | 101.8 | 0.216 | 0.37 |
| 6 | POPC liposomes, 30 min bath sonication; 10 x TBS; 2.2.3. 3); | 123.2 | 0.292 | 0.87 |
| 7 | POPC liposomes, 50 min bath sonication; 10 x TBS; 2.2.3. 3); | 75.4 | 0.293 | 0.1 |
| 8 | POPC liposomes, freeze-thaw 5 times before sonication; 2.2.3. 2) | 56.3 | 0.273 | 0.82 |
| 9 | POPC liposomes; 2.2.3. 1) Tip sonication[1] | 80.9 | 0.13 | 0.29 |
| 10 | POPC liposomes; 2.2.3. 1) Tip sonication[2] | 65.8 | 0.102 | 0.23 |

| | | | | |
|---|---|---|---|---|
| 11 | POPC liposomes; 2.2.3. 1) Tip sonication[3] | 61.2 | 0.101 | 0.5 |
| 12 | POPC-1mol%-DOPE-biotin; 2.2.3. 1) Tip sonication[4] | 53.4 | 0.164 | 0.47 |
| 13 | POPC-4mol%POPG; 2.2.3. 1) Tip sonication[4] | 56.3 | 0.182 | 0.36 |
| 14 | POPC-10mol%POPG; 2.2.3. 1) Tip sonication[4] | 57.1 | 0.122 | 0.69 |
| 15 | POPC-25mol%POPG; 2.2.3. 1) Tip sonication[4] | 55.5 | 0.124 | 0.26 |
| 16 | POPC-10mol%POPG-1mol%-DOPE-biotin; 2.2.3. 1) Tip sonication[4] | 55.4 | 0.107 | 0.51 |
| 17 | POPC-10mol%POPG; 2.2.3. 1) Tip sonication[4]; Diluted to 20 mM NaCl | 58.3 | 0.102 | 0.4 |
| 18 | POPC-10mol%POPG; 2.2.3. 1) Tip sonication[4]; Diluted to 10 mM NaCl | 56.5 | 0.104 | 0.17 |
| 19 | POPC-10mol%POPG; 2.2.3. 1) Tip sonication[4]; Diluted to 50 mM NaCl | 55.7 | 0.08 | 0.3 |
| 20 | POPC-4mol%POPS; 2.2.3. 1) Tip sonication[4] | 52.3 | 0.096 | 0.16 |
| 21 | POPC-10mol%POPS; 2.2.3. 1) Tip sonication[4] | 51.2 | 0.12 | 0.28 |
| 22 | POPC-1.5mol%-DOPE-biotin; 2.2.3. 1) Tip sonication[4] | 58.7 | 0.146 | 0.29 |
| 23 | POPC-2mol%-DOPE-biotin; 2.2.3. 1) Tip sonication[4] | 55.5 | 0.128 | 0.46 |
| 24 | POPC-2.5mol%-DOPE-biotin; 2.2.3. 1) Tip sonication[4] | 57.7 | 0.113 | 0.45 |
| 25 | POPC-3.5mol%-DOPE-biotin; 2.2.3. 1) Tip sonication[4] | 61.3 | 0.135 | 1.11 |
| 26 | POPC-1mol%-PE-PEG-biotin; 2.2.3. 1) Tip sonication[4] | 64.4 | 0.137 | 1.01 |
| 27 | POPC-5mol%-PE-PEG-biotin; 2.2.3. 1) Tip sonication[4] | 59.4 | 0.106 | 0.54 |
| 28 | POPC-10mol%POPG-0.1mol%-PE-PEG-biotin; 2.2.3. 1) Tip sonication[5] | 55 | 0.174 | 0.53 |

| | | | | |
|---|---|---|---|---|
| 29 | POPC-10mol%-POPG-1mol%-PE-PEG-biotin; 2.2.3. 1) Tip sonication[5] | 61.3 | 0.106 | 0.65 |

[1] 15 minutes, 50% duty cycle; probe sonication and output level 6; Freeze-thaw 5 times; extrusion through one 100 and two 50 nm membranes

[2] 15 minutes, 100% duty cycle; probe sonication, output level 6; extrusion through one 100 and two 30 nm membranes; No freeze-thaw

[3] 30 minutes. 100% duty cycle; probe sonication, output level 6; extrusion through one 100 and two 30 nm membranes; Freeze-thaw 5 times

[4] 20 minutes. 100% duty cycle; probe sonication, output level 6; extrusion through one 100 and two 30 nm membranes; Freeze-thaw 5 times

[5] 20 minutes. 100 % duty cycle; probe sonication, output level 6; extrusion through one 100 and two 30 nm membranes; Freeze-thaw 5 times; Centrifugation step (8000 rpm; 10 min) after tip sonication

## 3.2 Silica nanoparticles and their coating procedure

In this section, the DLS intensity size distribution and some zeta potential measurements regarding bare and coated silica nanoparticles as well as the effects influencing the coating procedure will be discussed. The coating protocol, in general, involves the mixture of liposomes in TBS 1x buffer, bare silica NPs in Tris 10x buffer, TBS 1x buffer, consequent vortexing and purification by centrifugation.

Due to the fact of a vast amount of DLS measurements, the reproduced coated silica nanoparticles under a certain method will not be shown, thus, it is essential to note that a graph or z-average value presented is the best achieved value or plot out of at least 2-3 productions. All the bare silica nanoparticle and coated-silica nanoparticle DLS measurements with statistics are depicted in the appendix table 5.1.

The silica nanoparticles synthesized by Stöber synthesis have shown to have different average size and polydispersities under contrasting dispersion conditions marked in the standard operating procedure (SOP) in DLS and whether they are activated (method 2.2.2) or not (fig. 3.8).

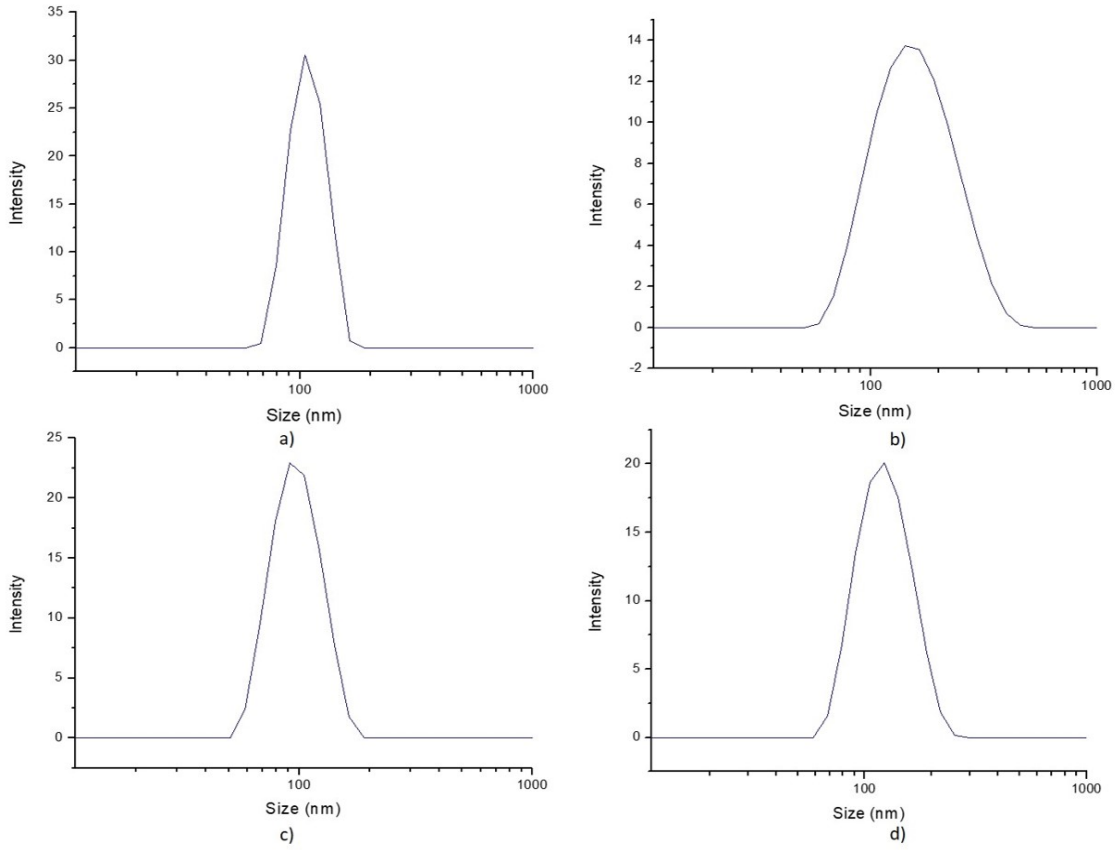


**Figure 3.8:** DLS intensity size distribution measurements of silica nanoparticles. a) Silica nanoparticles - not activated with hydroxy groups and in 10x Tris; z-average diameter = 156.2 nm b) Silica nanoparticles - not well-activated with hydroxy groups and in 10 x Tris; z-average diameter = 146.3 nm c) Silica nanoparticles - not well-activated with hydroxy groups and in 1x TBS; z-average diameter = 192.3 nm d) Activated silica NPs with hydroxy groups in 10 x Tris; z-average diameter = 129.1 nm.

In the figure it is observed that the intensity size distributions differ to some extent. The subfigure a) represents nanoparticles that are dispersed in 10 x Tris buffer, however, they were not activated right after due to the fact that the activation degree with hydroxy groups thought to be sufficient to begin with. Thus, the first attempts of nanoparticle coating included these silica nanoparticles (figures 3.9 and 3.10) with z-average of 156.2 nm and PDI = 0.295. The b) and c) plots present silica nanoparticles, which were supposedly activated (protocol in method 2.2.2), however, not efficient steps of cleaning with ethanol resulted in nanoparticles with z-average sizes of 146.3 (PDI = 0.166) and 192.3 nm (PDI = 0.333) in 10x Tris and 1x TBS buffers, respectively. In the end, silica nanoparticles were properly activated (covalently bonded) with hydroxy groups (as will be seen in improved coating of the nanoparticles later on; fig. 3.8 d)) and resulted in z-average = 129.1 nm (PDI = 0.225), and were used throughout the project for the rest of the coating procedures. It is important to point out that both for bare and single lipid bilayer coated silica nanoparticle aggregation is usually driven by Van der Waals attraction force in the absence of electric

double layer repulsion as well as during coating of the nanoparticles with lipid vesicle bilayers the event of bridging of the particles by the lipid vesicles.

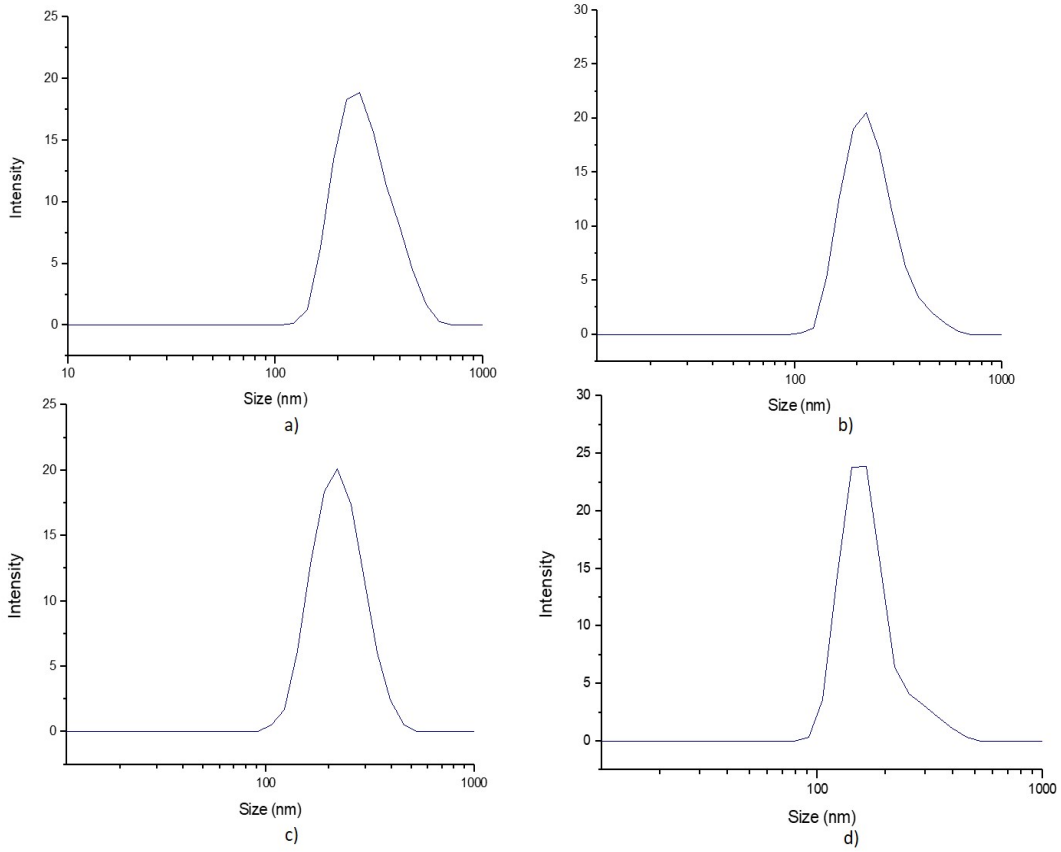


**Figure 3.9:** DLS intensity size distribution measurements of coated silica nanoparticles. a) POPC-coated silica nanoparticles (with non-activated bare NPs) in TBS 1x; z-average diameter = 279.9 nm b) POPC-1mol%biotin-coated silica nanoparticles (with non-activated bare NPs) in TBS 1x; z-average diameter = 334.8 nm c) POPC-coated silica nanoparticles (with non-activated bare NPs), 15 minutes bath sonicated after production in TBS 1x; z-average diameter = 249.4 nm d) POPC-1mol%DOPE-biotin-coated silica nanoparticles (with non-activated bare NPs), 15 minutes bath sonicated after production in TBS 1x; z-average diameter = 300.5 nm.

In the figure 3.9 the first attempts to coat the nanoparticles via procedure 2.2.4.1) can be seen, where POPC or POPC-1mol%DOPE-biotin liposomes are mixed with silica nanoparticles in the presence of TBS 1x buffer and afterwards purified by centrifugation. Subfigures a) and b) represent two different structures of supposed supported lipid bilayers on the silica nanoparticles and c) and d) are the same coated nanoparticles, but bath sonicated after coating in order to try and reduce their z-average size. Keeping in mind that well-activated silica nanoparticles (fig. 3.8 d)) are 129.1 nm in diameter according to DLS measurements, one can expect that after coating procedure they should be in the range of 135-140 nm, because the supported lipid bilayer width is 5-7 nm [92], however, as seen in all of the subfigures that is not the case. During the coating procedure the silica

nanoparticles aggregated, possibly, due to cross-reactions between lipids or the absence of electrostatic repulsion between particles, hence, resulting in z-average sizes of 279.9 nm (PDI = 0.209) for POPC-coated silica NPs and 334.8 nm (PDI = 0.426) for POPC-1mol%DOPE-biotin. Even though, the post-coating bath sonication step diminished the size of the coated particles to 249.4 nm (PDI = 0.276) for POPC-coated silica and 300.5 nm (PDI = 0.31) for POPC-1mol%DOPE-biotin NPs, this step was excluded later on due to the fact of a risk of introducing liposomes in the solution, since it is possible that the nanoparticles not only deaggregate, but that lipids are ripped lose and reform as liposomes. The difference from these coated nanoparticles and the ones presented in fig. 3.10 is that in the latter a point of incubation of 30 minutes was added after the addition of vesicles, nanoparticles and buffer in order to achieve knowledge about the stability of the systems in terms of aggregation, when the mixture is not purified for a certain period of time. Still, for POPC-coated silica NPs the diameter and polydispersity increased (Z-average = 338.3 nm, PDI = 0.291) whereas for POPC-1mol%DOPE-biotin NPs the size and polydispersity have decreased (Z-average = 308.2 nm, PDI = 0.321).

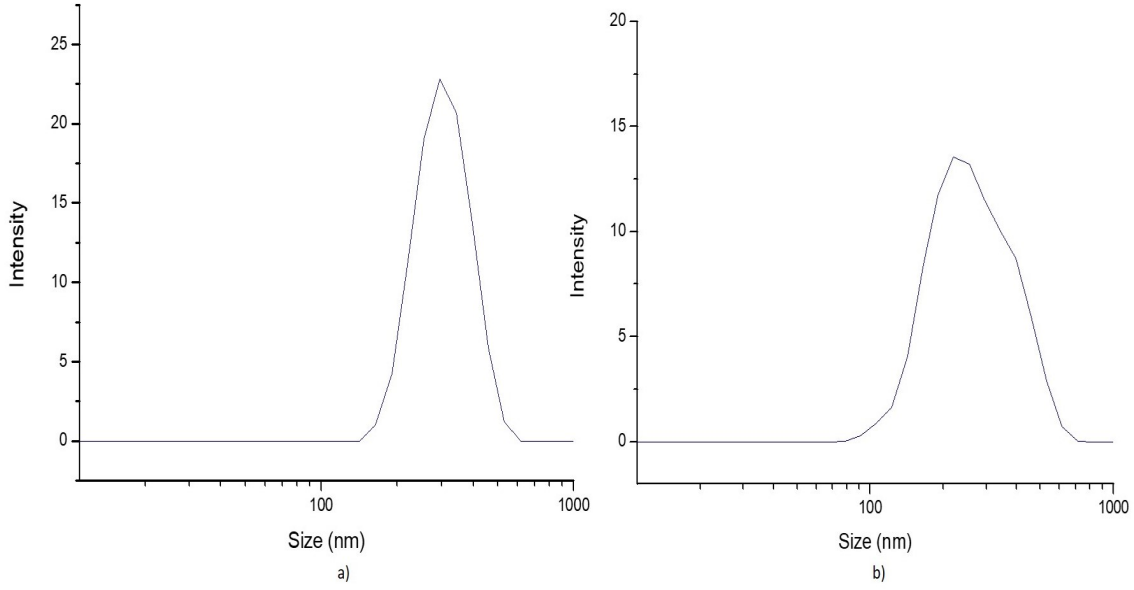


**Figure 3.10:** DLS intensity size distribution measurements of coated silica nanoparticles. a) POPC-coated NPs (with non-activated bare NPs) in TBS 1x; z-average diameter = 338.3 nm b) POPC-1mol%DOPE-biotin-coated silica nanoparticles (with non-activated bare NPs) in TBS 1x; z-average diameter = 308.2 nm.[6]

By considering these results, attempts for even longer incubation of liposomes with silica nanoparticles in the presence of TBS 1x buffer at room temperature conditions were made as well as for bare silica nanoparticle activation (fig. 3.11).

[6] 30 minute incubation after mixing silica nanoparticles, vesicles and 1x TBS buffer together. Not activated NPs.

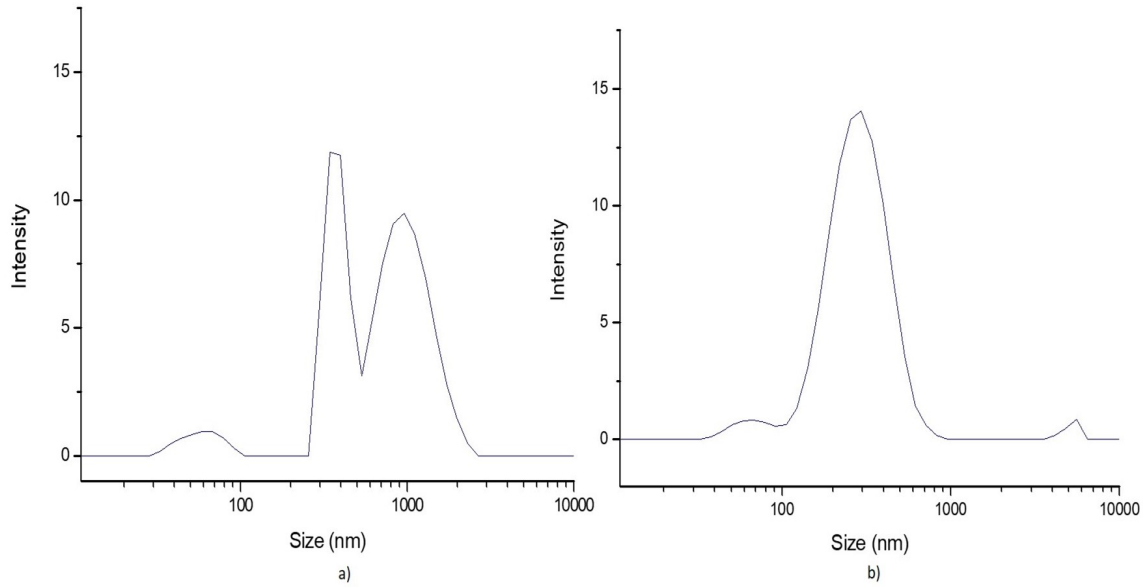


**Figure 3.11:** DLS intensity size distribution measurements of coated silica nanoparticles. a) POPC-coated NPs (with not efficiently enough activated bare NPs) in TBS 1x; z-average diameter = 741.1 nm b) POPC-1mol%DOPE-biotin-coated silica nanoparticles (with not efficiently enough activated bare NPs) in TBS 1x; z-average diameter = 279.8 nm.[7]

Apparently, the latter decision led to liposome formation or reformation (smaller peaks in fig. 3.11 a) in the range of 20-100 nm) as well as aggregation in the case of POPC-coated silica NPs (z-average = 741.1 nm, PDI = 0.654; results not reliable as for very polydisperse samples the CONTIN fit is not suitable). In addition, even though, for POPC-1mol%DOPE-biotin NPs (fig. 3.11 b); z-average = 279.8 nm, PDI = 0.380) degree of aggregation was not significantly increased, as it was for POPC-coated silica nanoparticles, the introduction of small particles (<90 nm) concluded that the procedure needs more optimization. After a few reproducibility procedures, it was also decided that the silica nanoparticles were not sufficiently enough activated due to, probably, not efficient cleaning steps by ethanol and miliq$H_2O$, thus, were reactivated (as seen in fig. 3.8 d)). Nevertheless, it was established that different ways of mixing, after the addition of vesicles with nanoparticles, should be experimented with next.

In the figure 3.12 two different ways of mixing after the addition of the coating materials were added together are presented. Moreover, it is important to note that a longer bath sonication time (2 hours) before the start of the nanoparticle coating results in more uniform z-average size compared to only 30 minute sonication, meaning that after a certain period of time (1-2 weeks) nanoparticles in 10x Tris solution tend to start to aggregate up to the size roughly 150-160 nm in diameter and it takes more than 30 minutes to bring them to their original size.

[7] Sonicate NPs for 30 minutes before addition; Add everything in the same order as in 2.2.4.1); shake overnight at 4 °C at 500 rpm; bath sonicate solution for 30 minutes; centrifuge at 500 rcf for 30 minutes; resuspend in 1x TBS and repeat centrifugation steps 3. Not sufficiently enough activated silica NPs.

In addition, the liposome/nanoparticle surface area ratio was calculated to be ≈90 as well as the centrifugation power modified to 6000 rpm from 500 rcf. Consequently, by optimizing these parameters the size of the coated nanoparticles were brought to 241.2 nm (PDI = 0.458) and to 236.6 nm (PDI = 0.476) for POPC-coated NPs and POPC-1mol%DOPE-biotin NPs, accordingly. However, the aggregates observed in fig. 3.12 b) implies that pipetting should be optimized or rejected as the appropriate mixing approach. Furthermore, the small peak reaching over 4 $\mu$m in z-average are most likely dust accumulating in the dispersion as it was seen through many different DLS measurements.

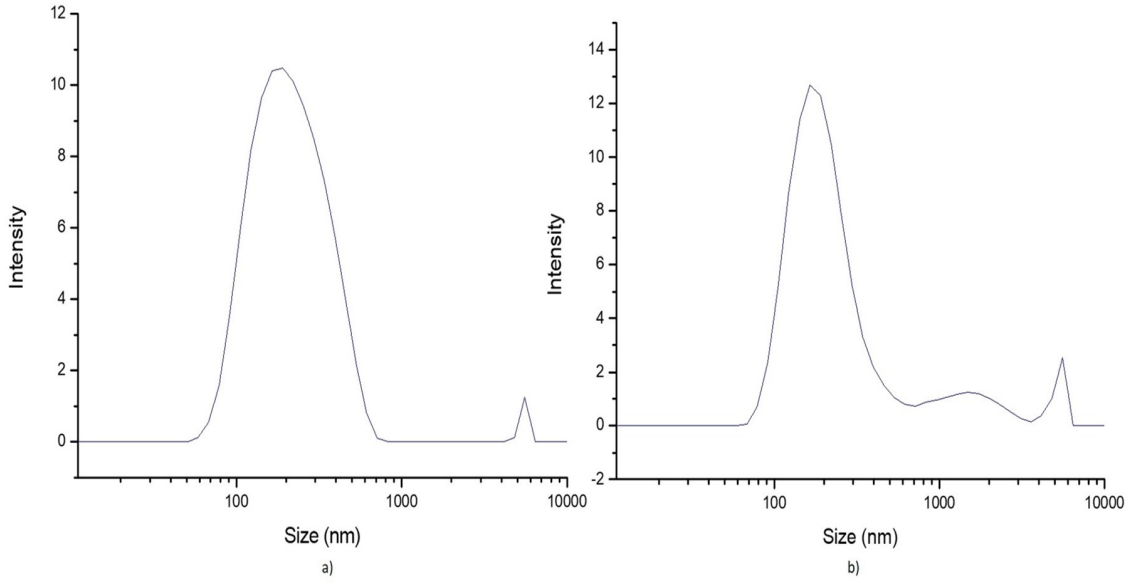


**Figure 3.12:** DLS intensity size distribution measurements of coated silica nanoparticles. a) POPC-coated NPs in TBS 1x, 30 minutes vortexing after mixing (2000 rpm), 30 minutes incubation; z-average diameter = 241.2 nm b) POPC-1mol%DOPE-biotin-coated silica nanoparticles in TBS 1x, 30 minutes pipetting after mixing, 30 minutes incubation; z-average diameter = 236.6 nm.[8]

Additional experiments for the established coating[8] method were conducted (fig. 3.13). In pictures a) and b) the reduction of mixing time to 20 minutes as well the effect of omitting the incubation step is observed. These attempts concluded that the most appropriate mixing approach is vortexing, as it produces the least aggregates, even though it might still be needed to optimize. Moreover, in subfigures c) and d) in fig. 3.13 and in fig. 3.14 attempts of resuspension in different media can be seen. This leads to a conclusion that during and after centrifugation step the coated nanoparticles should be redispersed in 10x Tris, which does not include any NaCl and does not bring upon significant aggregates (as seen in fig. 3.13 c)) as resuspension just in miliq$H_2O$ does possibly due to the small change in pH and the higher ionic strength of Tris. Consequently, even though the diameter of the coated nanoparticles were not reduced to an expected value, a sufficient, in terms of polydispersity (PDI = 0.2-0.3), intensity size distribution profile has been achieved.

[8] Sonicate NPs for 2 hours before addition; add 159.7 $\mu$L of liposomes (2 mg/mL), 740.3 $\mu$L of 1x TBS and 100 $\mu$L of NPs; Apply appropriate mixing; centrifuge at 6000 rpm for 5 minutes; resuspend in 1x TBS and repeat centrifugation steps 3 times. With well activated NPs.

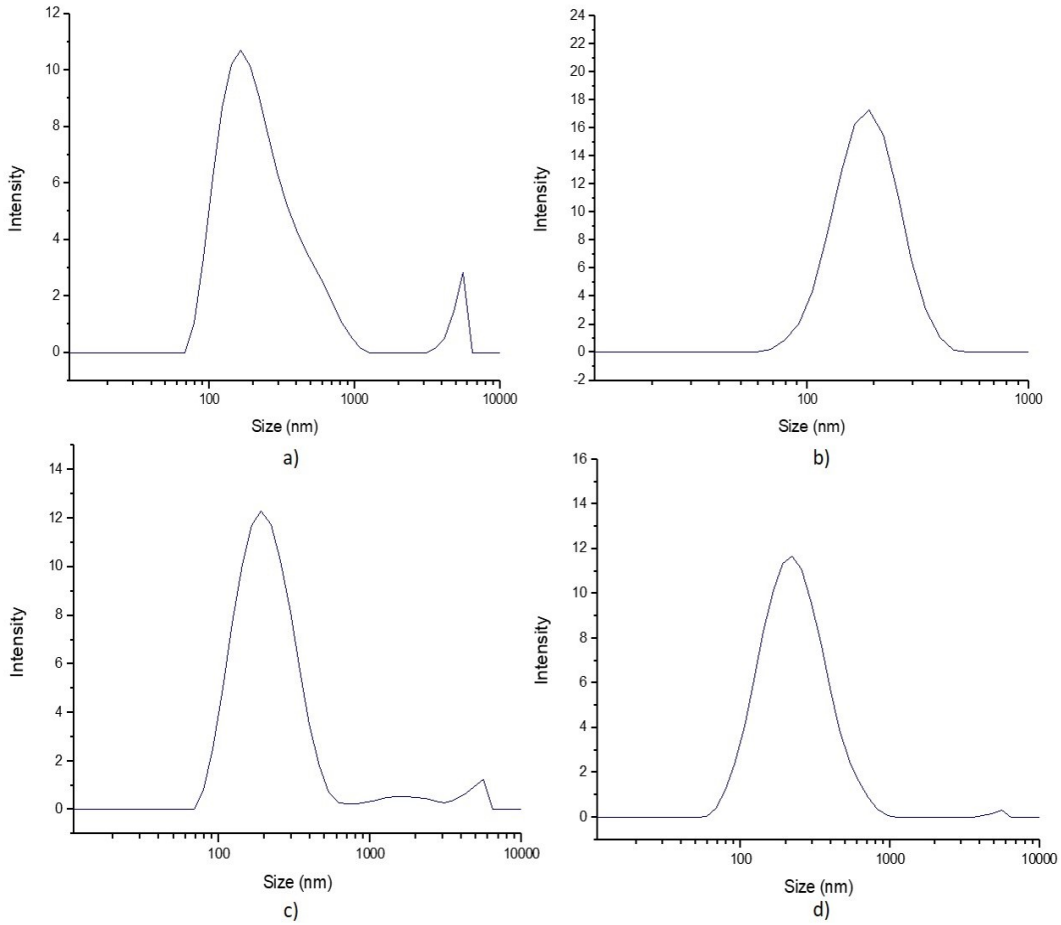


**Figure 3.13:** DLS intensity size distribution measurements of coated silica nanoparticles. a) POPC-coated NPs in TBS 1x, 20 minutes vortexing after mixing (2000 rpm); z-average diameter = 160.7 nm b) POPC-1mol%DOPE-biotin-coated silica nanoparticles in TBS 1x, 20 minutes pipetting after mixing; z-average diameter = 266.2 nm c) POPC-coated NPs in miliQwater, 20 min vortexing after mixing (2000 rpm) and resuspension in miliQwater during centrifugation; z-average diameter = 202.1 nm d) POPC-coated NPs in Tris 10x, 20 min vortexing after mixing (2000 rpm) and resuspension in 10x Tris during centrifugation; z-average diameter = 204.6 nm.[8]

Statistical two-sided t-tests were performed at significance level of 0.05 for the three resuspension buffers: TBS 1x, Tris 10x and milliQwater. The cases of TBS 1x and Tris 10x (t-critical value = 6.967863204, p-value = 0.002 - 0.01), and TBS 1x and milliQwater (t-critical value = 7.066986973, p-value = 0.002 - 0.01) yielded the acceptance of an alternative hypothesis - NaCl salt concentration has an effect on POPC-coated NP z-average diameter. However, the difference between Tris 10x and milliQwater (t-critical value = 0.916461194, p-value = 0.40 - 0.50) statistically has not been seen (as expected, because both of these buffers do not contain NaCl) and null hypothesis was accepted stating that NaCl salt concentration has no effect on the POPC-coated NPs z-average diameter.

[8] Sonicate NPs for 2 hours before addition; add 159.7 $\mu$L of liposomes (2 mg/mL), 740.3 $\mu$L of 1x TBS and 100 $\mu$L of NPs; Apply appropriate mixing; centrifuge at 6000 rpm for 5 minutes; resuspend in 1x TBS and repeat centrifugation steps 3 times. With well activated NPs.

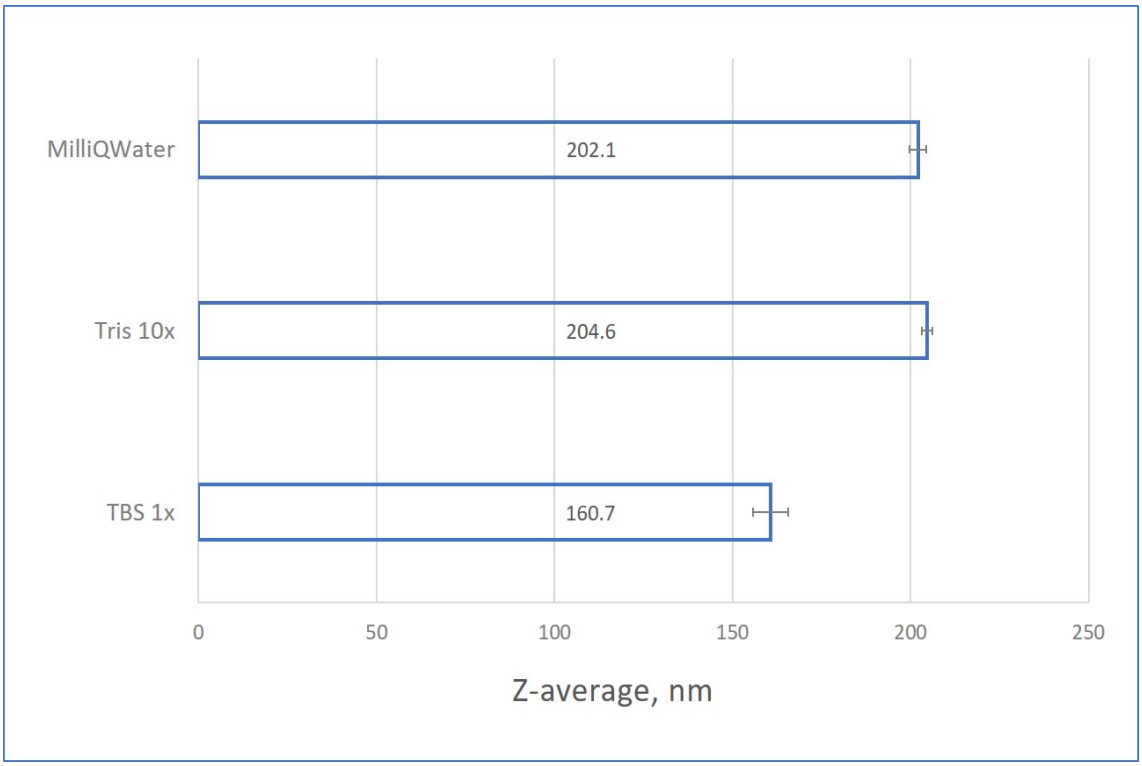


**Figure 3.14:** Z-average sizes of liposomes differing by the molar concentrations of POPG and POPS lipids in their structures.

From this point forward, the idea of incorporating anionic lipids in the liposome structure to form more stable colloidal dispersion as well as possibly reduce the z-average to the expected value of the coated silica nanoparticles will be discussed.

As seen in figures 3.15, 3.16 and 3.19 different molar percentage of POPG anionic lipid in the liposome structure lead to a more uniform profile of intensity size distribution (except for the case of POPC-4mol%POPG-coated NPs). There is a clear difference of degree of aggregation or the boundary of molar concentration of POPG, at which, the colloidal dispersion becomes stable, between POPC-4mol%POPG-coated NPs, POPC-10mol%POPG-coated NPs and POPC-25mol%POPG-coated NPs. Hence, the further nanoparticle coatings in this project did not include POPC-4mol%POPG-coated NPs due to insufficient stability over a period of time. However, in order to compare POPC-10mol%POPG-coated NPs and POPC-25%POPG-coated NPs, one needs to look more in detail in their z-average sizes and PDIs. The z-average and PDI are 185.9 nm and 0.237, and 186.4 nm and 0.286 for POPC-10mol%POPG-coated NPs and POPC-25mol%POPG-coated NPs, respectively, which seems not that significant.

However, after a certain period of time, 48 hours for POPC-10mol%POPG-coated NPs and 24 hours for POPC-25mol%POPG-coated NPs (figures 3.16 and 3.19), it is observed that the z-average of both coated NPs as well as their PDI diminish even more, 171 nm (PDI = 0.224) for POPC-10mol%POPG-coated NPs, and 175.4 nm (PDI = 0.265) for POPC-25mol%POPG-coated NPs. Thus, for further nanoparticle coatings the inclusion of 10mol%POPG was selected over the others due to it's result in a more stable dispersion, close proximity to the expected value of the coated silica NPs (z-average diameter = 171 nm in accordance to the expected value of z-average

diameter = 135-140 nm) and the possible lesser influence in electric double layer interaction in QCM-D experiments POPC-coated silica nanoparticles that include 25mol%POPG lipids in their structure. The possible reasons for the remaining discrepancy in POPC-10mol%POPG-coated NPs size in comparison to the expected value could be not perfectly optimized molar concentration of POPG (as there where only 4mol%, 10mol% and 25mol% chosen) as well as some unavoided lipid bridging interactions during coating procedure.

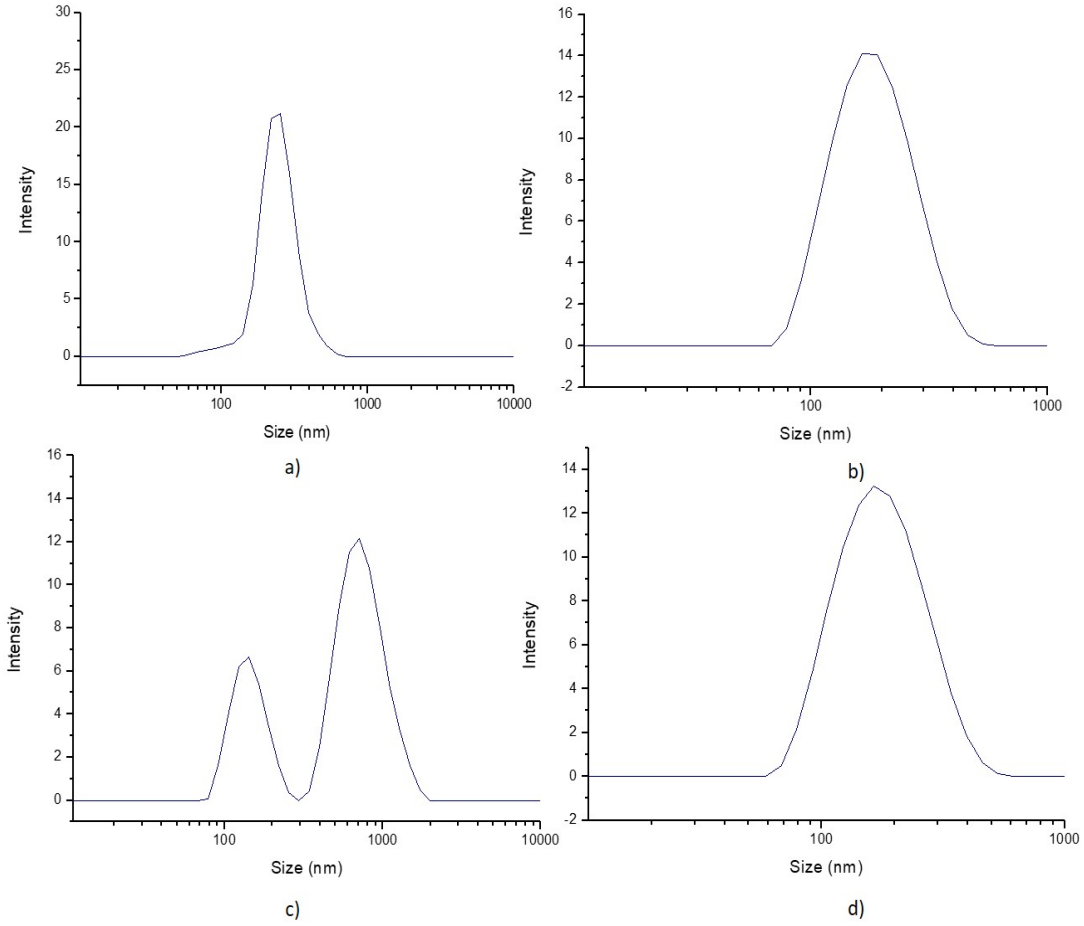


**Figure 3.15:** DLS intensity size distribution measurements of coated silica nanoparticles. a) POPC-4mol%POPG-coated NPs in Tris 10x; z-average diameter = 273.6 nm b) POPC-10mol%POPG-coated silica nanoparticles in Tris 10x; z-average diameter = 185.9 nm c) POPC-4mol%POPG-coated NPs after 48 hours after purification in Tris 10x; z-average diameter = 462.1 nm d) POPC-10mol%POPG-coated silica nanoparticles after 48 hours after purification in Tris 10x; z-average diameter = 171 nm.[9]

[9] Sonicate NPs for 2 hours before addition; add 159.7 $\mu$L of liposomes (2 mg/mL), 740.3 $\mu$L of 1x TBS and 100 $\mu$L of NPs; 20 minutes vortex at 2000 rpm; centrifuge at 6000 rpm for 5 minutes; resuspend in 1x TBS and repeat centrifugation steps 3 times. With well activated NPs.

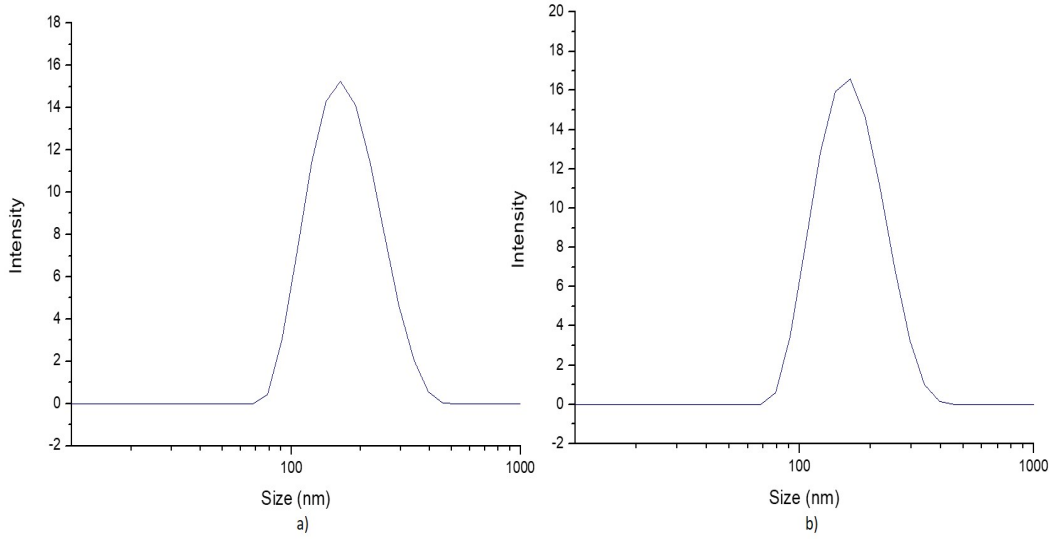


**Figure 3.16:** DLS intensity size distribution measurements of coated silica nanoparticles. a) POPC-25mol%POPG-coated NPs in Tris 10x; z-average diameter = 186.4 nm b) POPC-25mol%POPG-coated silica nanoparticles after 24 hours after purification in Tris 10x; z-average diameter = 175.4 nm.[9]

The experiments for POPC-coated silica nanoparticles with POPS anionic lipids in their structure were attempted as well (figures 3.17 and 3.19). Nevertheless, the case of 25mol%POPS was excluded due to cost issues, thus, only the inclusion of 4mol%POPS and 10mol%POPS can be seen in the graphs. In addition, as mentioned before, the influence of $Ca^{2+}$ was tested, which concluded that these ions do not impact highly the coating procedure, in fact, the coating of the nanoparticles without $Ca^{2+}$ ions leads to better results in terms of z-average sizes. Coated silica nanoparticles with POPC-4mol%POPS and POPC-10mol%POPS with $Ca^{2+}$ culminated to z-average sizes of 213.5 nm (PDI = 0.373; fig. 3.17 a)) and 191.7 nm (PDI = 0.277; fig. 3.17 b)), respectively, whereas the same structures without $Ca^{2+}$ ions derived into z-average sizes of 210.2 nm (PDI = 0.366; fig. 3.17 c)) and 185.2 nm (PDI = 0.288; fig. 3.17 d)), accordingly. Furthermore, an additional experiment with POPC-10mol%POPS-1mol%biotin coated NPs without $Ca^{2+}$ ions during the coating procedure was done in order to observe whether same or similar z-average size and polydispersity is achieved (fig. 3.18). Hence, the results were almost alike compared to POPC-10mol%POPS coated NPs, which does not contain biotin ligands, - 190.3 nm (PDI = 0.245; POPC-10mol%POPS-1mol%biotin coated NPs). Lastly, as mentioned before, POPS anionic lipids were not used anymore for production of liposomes or coated nanoparticles due to their price as well as not significant enough difference from POPG anionic lipids. The significance was proven by applying statistical two-tailed t-tests were performed at the significance level of 0.05 on POPC-coated silica NPs containing POPG or POPS and different molar concentrations in their structure in order see whether the changes in z-average diameter between different molar concentrations are statistically significant.

[9] Sonicate NPs for 2 hours before addition; add 159.7 $\mu$L of liposomes (2 mg/mL), 740.3 $\mu$L of 1x TBS and 100 $\mu$L of NPs; 20 minutes vortex at 2000 rpm; centrifuge at 6000 rpm for 5 minutes; resuspend in 1x TBS and repeat centrifugation steps 3 times. With well activated NPs.

It was observed that between 4mol%POPG and 25mol%POPG (t-critical value = 12.97659917, p-value < 0.001), and 4mol%POPG and 10mol%POPG (t-critical value = 12.3526649, p-value < 0.001) there is a significant difference at the significance level of 0.05 in terms of z-average diameter of the POPC-coated NPs. However, between 10mol%POPG and 25mol%POPG (t-critical value = 0.168816933, p-value = 0.50 - 1.00) there was no significant difference in terms of z-average diameter calculated. Also, in the case of 4mol%POPS and 10mol%POPS anionic lipid inclusion (t-critical value = 9.658504235, p-value < 0.001) in the POPC-coated NP structure, it was deducted that there is a significant difference in z-average diameter at 0.05 significance level. And lastly, there was no significant difference between 10mol%POPG and 10mol%POPS (t-critical value = 0.261397393, p-value = 0.50 - 1.00) in terms of z-average diameter of the POPC-coated NPs.

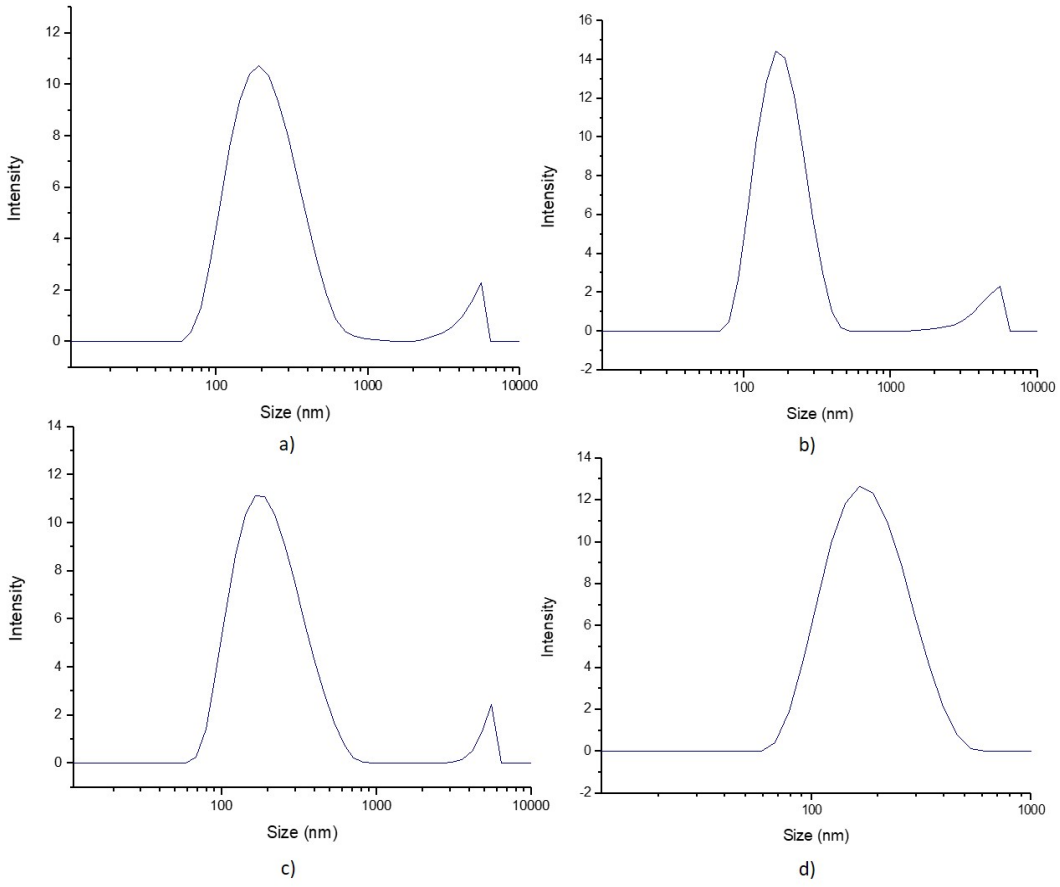


**Figure 3.17:** DLS intensity size distribution measurements of coated silica nanoparticles. a) POPC-4mol%POPS-coated NPs with $Ca^{2+}$ ions in Tris 10x; z-average diameter = 213.5 nm b) POPC-10mol%POPS-coated NPs with $Ca^{2+}$ ions in Tris 10x; z-average diameter = 191.7 nm c) POPC-4mol%POPS-coated NPs without $Ca^{2+}$ ions in Tris 10x; z-average diameter = 210.2 nm d) POPC-10mol%POPS-coated NPs with $Ca^{2+}$ ions in Tris 10x; z-average diameter = 185.2 nm .[9]

[9] Sonicate NPs for 2 hours before addition; add 159.7 $\mu$L of liposomes (2 mg/mL), 740.3 $\mu$L of 1x TBS and 100 $\mu$L of NPs; 20 minutes vortex at 2000 rpm; centrifuge at 6000 rpm for 5 minutes; resuspend in 1x TBS and repeat centrifugation steps 3 times. With well activated NPs.

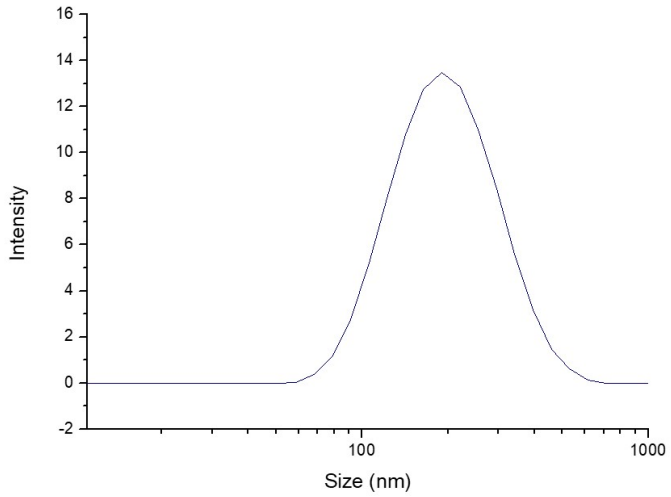


**Figure 3.18:** DLS intensity size distribution measurements of coated silica nanoparticles. a) POPC-10mol%POPS-1mol%biotin coated NPs without $Ca^{2+}$ ions in Tris 10x; z-average diameter = 190.3 nm .[9]

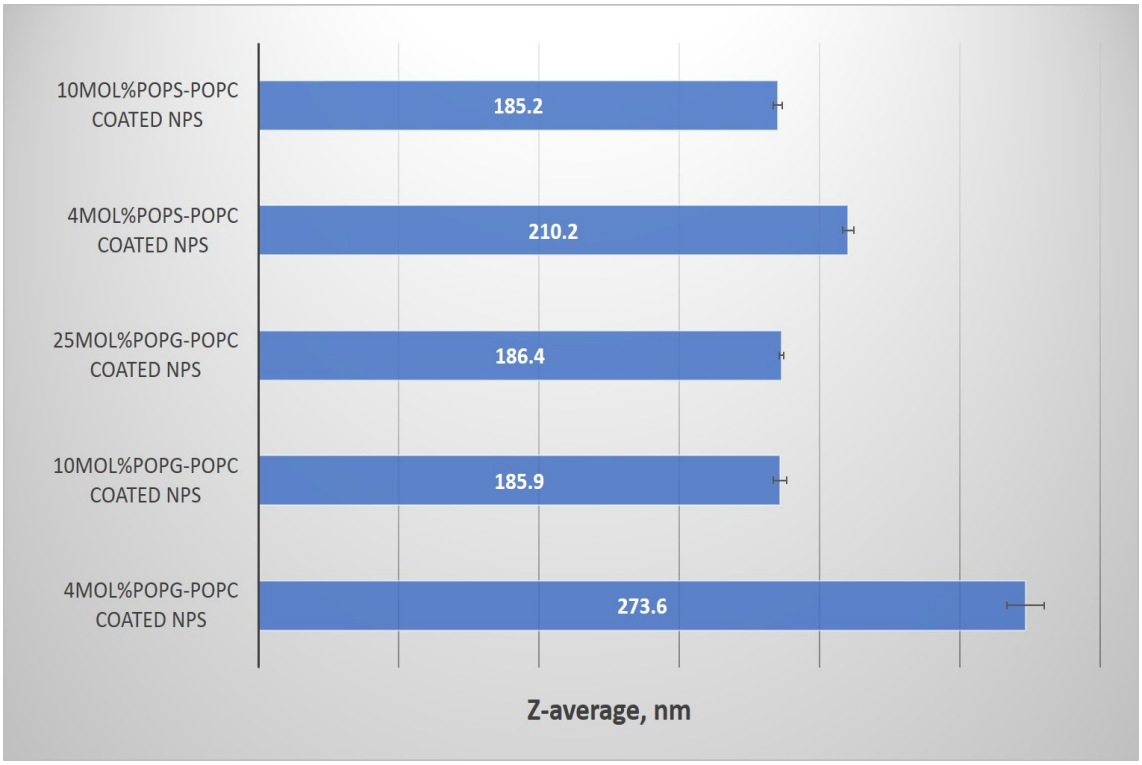


**Figure 3.19:** Z-average diameters of POPC-coated silica NPs containing POPG or POPS lipids in their structures.

[9] Sonicate NPs for 2 hours before addition; add 159.7 $\mu$L of liposomes (2 mg/mL), 740.3 $\mu$L of 1x TBS and 100 $\mu$L of NPs; 20 minutes vortex at 2000 rpm; centrifuge at 6000 rpm for 5 minutes; resuspend in 1x TBS and repeat centrifugation steps 3 times. With well activated NPs.

Due to the fact that the z-average size of the best coating protocol uptil this point still has not reached the desired z-average value, additional optimization was needed. In according to this, the vortex speed after mixing the silica NPs, vesicles and 1x TBS buffer was firstly reduced to 1000 rpm (fig. 3.20 a) - c)) and later on to 600 rpm (fig. 3.20 d)) as well as it was noticed throughout the production of liposomes that due to inclusion of tip sonication in the preparation, titanium particles sediment at the bottom of the sample tube, thus, an additional step of centrifugation after tip sonication at 8000 rpm for 10 minutes was added in order to remove as much titanium particles as possible from the dispersion. These changes led to further size reduction of POPC-10mol%POPG-1mol%biotin coated NPs to z-average diameter = 166.8 nm (desired value z-average diameter = 135-140 nm) and to final protocol for the coating of silica NPs. The remaining discrepancy is thought to be attributed to not fully optimized molar concentration of POPG in the vesicle structure and possible lipid bridging interaction during coating of the nanoparticles.

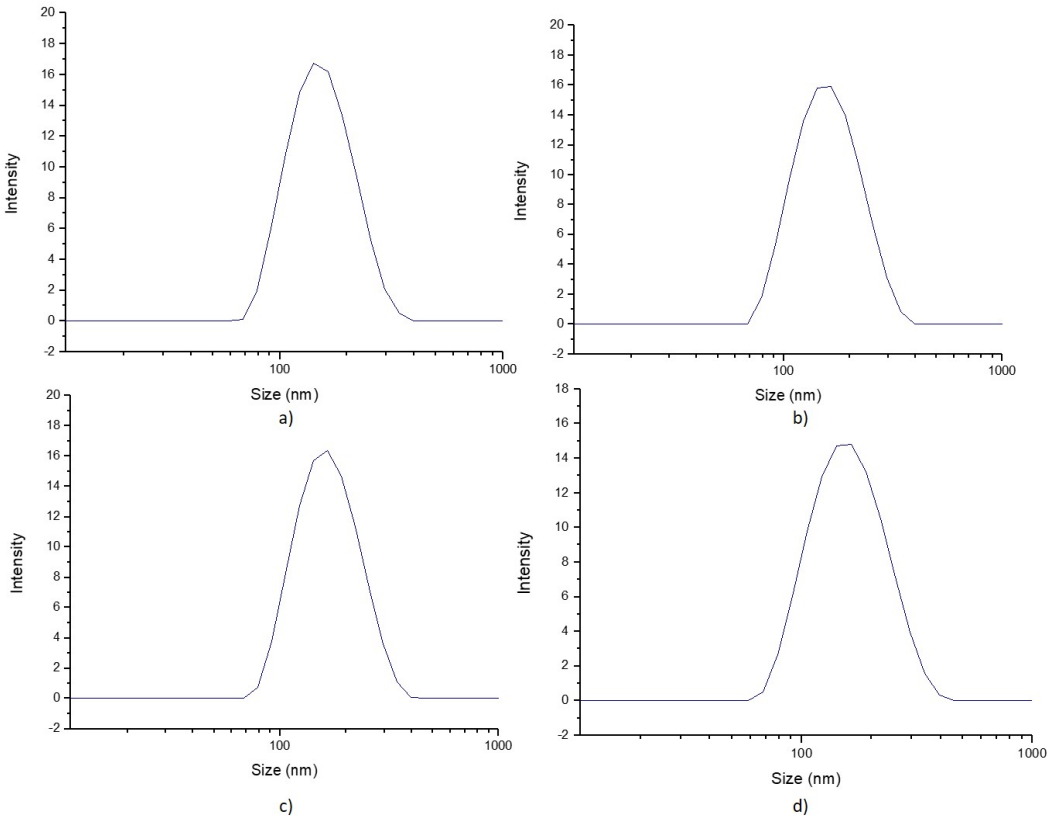


**Figure 3.20:** DLS intensity size distribution measurements of coated silica nanoparticles. a) POPC-10mol%POPG coated NPs in Tris 10x. Vortex at 1000 rpm after mixing; z-average diameter = 169.3 nm b) POPC-10mol%POPG-1mol%biotin coated NPs in Tris 10x. Vortex at 1000 rpm after mixing; z-average diameter = 166.5 nm c) POPC-10mol%POPG-5mol%biotin coated NPs in Tris 10x. Vortex at 1000 rpm after mixing; z-average diameter = 172.5 nm d) POPC-10mol%POPG-1mol%biotin coated NPs in Tris 10x. Vortex at 600 rpm after mixing; z-average diameter = 166.8 nm.[9]

[9] Sonicate NPs for 2 hours before addition; add 159.7 $\mu$L of liposomes (2 mg/mL), 740.3 $\mu$L of 1x TBS and 100 $\mu$L of NPs; 20 minutes vortex at 2000 rpm; centrifuge at 6000 rpm for 5 minutes; resuspend in 1x TBS and repeat centrifugation steps 3 times. With well activated NPs.

The z-average size presented in fig. 3.20 a) - c) and obtained by the final protocol was 169.3 nm (PDI = 0.275), 166.5 nm (PDI = 0.260), 172.5 nm (PDI = 0.250) for POPC-10mol%POPG coated NPs, POPC-10mol%POPG-1mol%biotin coated NPs and POPC-10mol%POPG-5mol%biotin coated NPs, respectively. They were vortexed after mixing of bare silica NPs, vesicles and 1x TBS buffer at 1000 rpm for 20 minutes. The POPC-10mol%POPG-5mol%biotin coated NPs were included due to interaction experiments in QCM-D and will be discussed later on in more detail. In addition, fig. 3.20 d) displays POPC-10mol%POPG-1mol%biotin vortexed at 600 rpm for 20 minutes after mixing of the appropriate materials in question and results in 166.8 nm (PDI = 0.273) in z-average size, which is almost equivalent for the same coated NPs with vortexing at 1000 rpm for 20 minutes. Nevertheless, vortexing at 600 rpm for 20 minutes was chosen over 1000 rpm due to results in repeated productions with the same parameters, which led to more excellent reproducibility. Furtheremore, in parallel to the lately established protocol, the coating of the silica nanoparticles just with (without POPG or POPS) POPC liposomes were assesed (fig. 3.21).

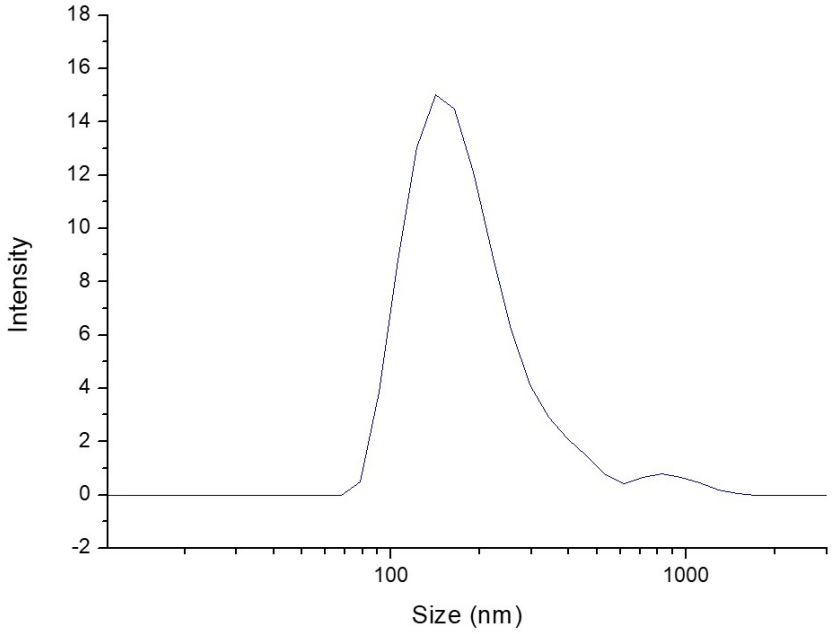


**Figure 3.21:** DLS intensity size distribution measurements of coated silica nanoparticles. POPC coated silica NPs in Tris 10x; z-average diameter = 232.8 nm. Vortex at 500 rpm after mixing.[9]

However, the exclusion of anionic lipids resulted in aggregates and in not sufficiently enough monodisperse particles. The z-average size of POPC coated nanopartiles produced in such manner is 232.8 nm (PDI = 0.402). In addition, there was an attempt to reduce the vortexing speed after mixing of vesicles with nanoparticles to 500 rpm in this case, but was disregarded later on due to no noticeable difference from 600 rpm.

[9] Sonicate NPs for 2 hours before addition; add 159.7 $\mu$L of liposomes (2 mg/mL), 740.3 $\mu$L of 1x TBS and 100 $\mu$L of NPs; 20 minutes vortex at 2000 rpm; centrifuge at 6000 rpm for 5 minutes; resuspend in 1x TBS and repeat centrifugation steps 3 times. With well activated NPs.

As the final protocol for silica nanoparticle coating is set up, it is important to show, in terms of zeta potential, that the nanoparticles are coating with lipid bilayer in the first place (fig. 3.22).

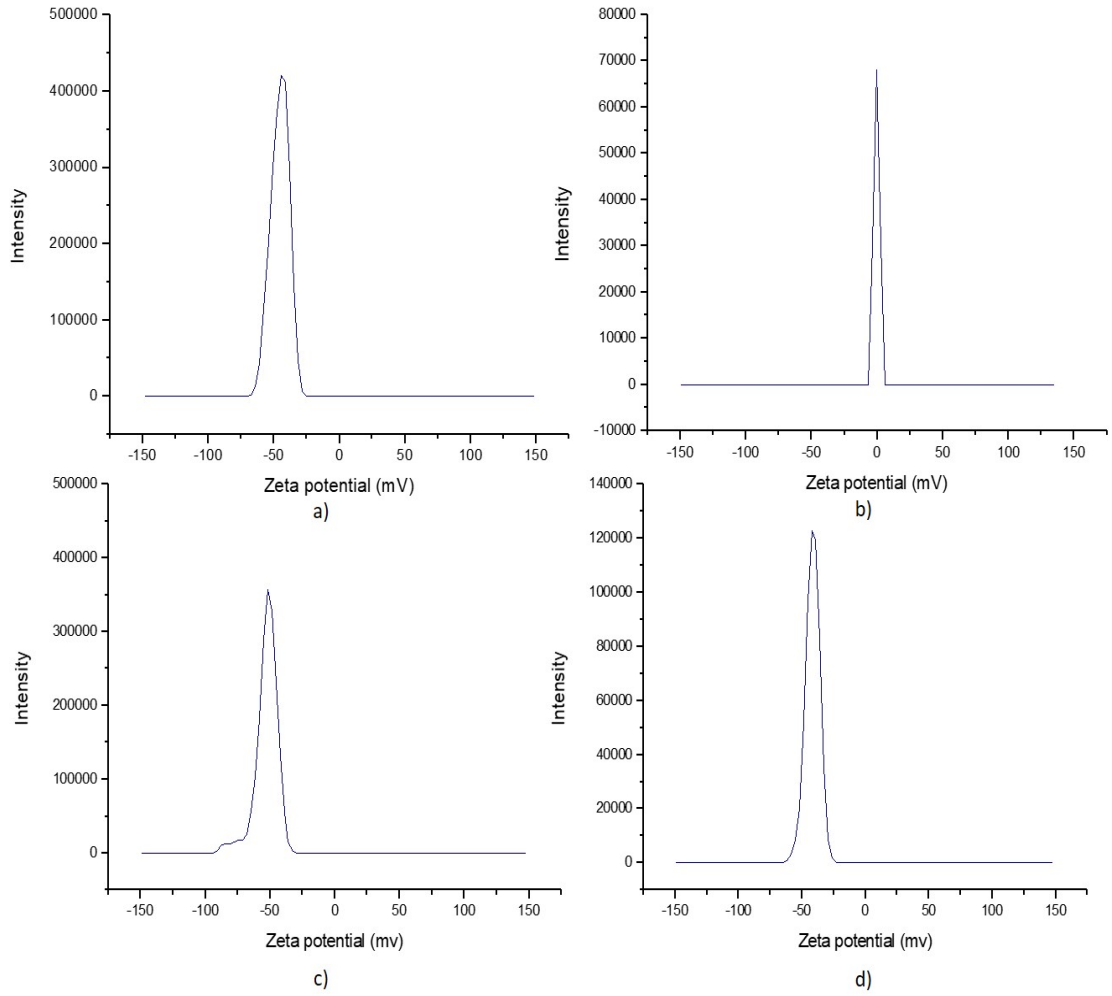


**Figure 3.22:** DLS zeta potential measurements of bare and coated silica nanoparticles. a) Bare silica NPs in Tris 10x; b) POPC coated silica NPs in Tris 10x; c) 3 month old bare silica NPs in Tris 10x; d) POPC-10mol%POPG coated silica NPs in Tris 10x.[9]

As mentioned before, the bare activated silica NP zeta potential is ≈ -43 mV and in time it shifts to even more negative potential (fig. 3.22 c)). However, as evidence that the silica nanoparticles are coated with a supported lipid bilayer, the zeta potential for POPC coated silica NPs is ≈ 0 due to the fact that POPC itself is neutral. However, if the nanoparticles are coated with anionic lipid containing liposomes, POPC-10mol%POPG in this case (fig. 3.22 d)), then it is impossible to declare whether the nanoparticles are coated due to the fact that the zeta potential becomes almost identical (≈ -43 mV) as for bare activated silica nanoparticles.

[9] Sonicate NPs for 2 hours before addition; add 159.7 $\mu$L of liposomes (2 mg/mL), 740.3 $\mu$L of 1x TBS and 100 $\mu$L of NPs; 20 minutes vortex at 2000 rpm; centrifuge at 6000 rpm for 5 minutes; resuspend in 1x TBS and repeat centrifugation steps 3 times. With well activated NPs.

Even though the results have not included QCM-D interaction experiments yet, the remaining intensity size distributions of activated silica nanoparticles coatings, which beside anionic lipids include polyethylene glycol (PEG) linker and higher biotin ligand density (their relevance will be explained in the section of QCM-D interaction experiment results), will be presented in this chapter.

As stated as one of the goals of the project, the ligand density influence on the effect of overall coated nanoparticle avidity will be investigated. Thus, liposomes, containing higher molar percentage of biotin as well as different PEG linker molar concentrations (needed to prove a hypothesis for interaction experiments in QCM-D due to possible non-binding of coated NP with functionalized biotin headgroups without PEG linkers), in connection with included anionic lipids in the structure, DLS intensity size distributions are presented in figures 3.23 and 3.24 (both types of liposomes were produced via the optimized protocol 2.2.3. 4)).

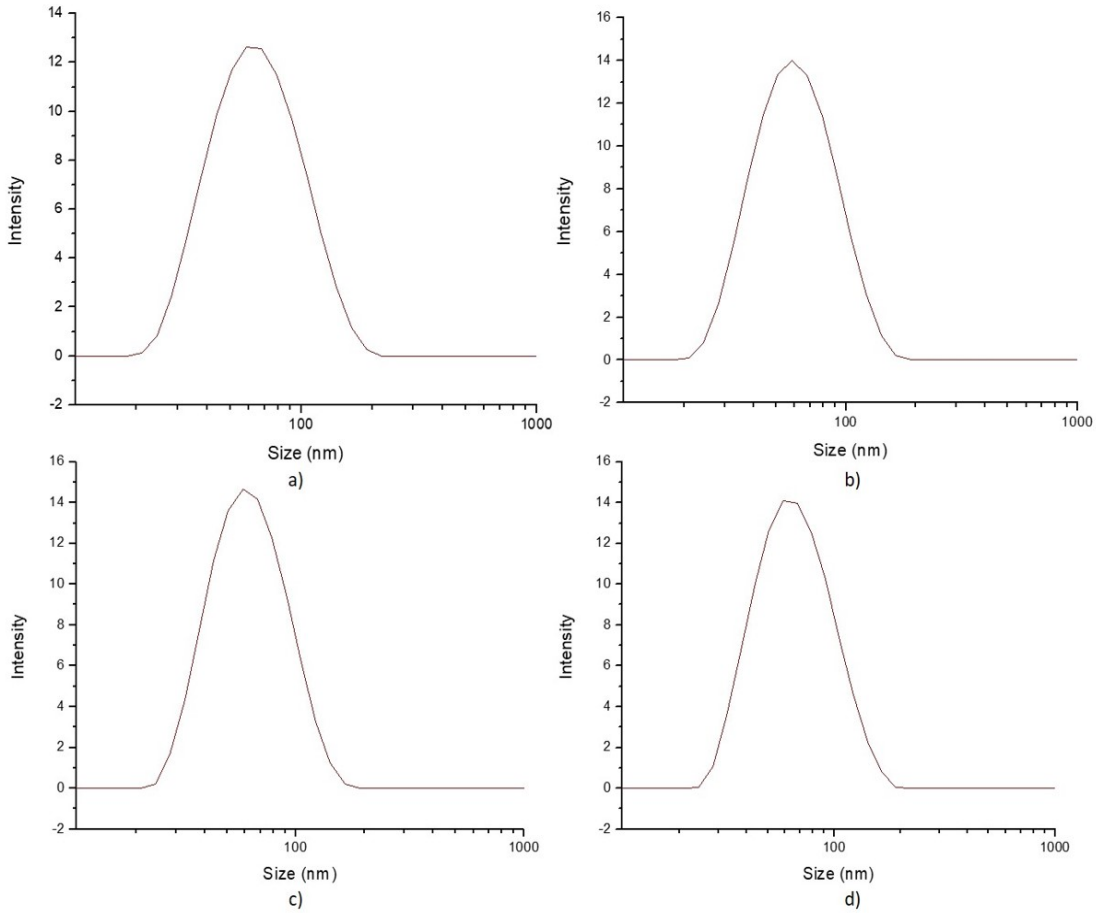


**Figure 3.23:** DLS intensity size distribution measurements on vesicles containing anionic lipids and different biotin density on their surfaces. a) POPC-1.5mol%DOPE-biotin liposomes in TBS 1x; z-average diameter = 58.7 nm b) POPC-2mol%DOPE-biotin liposomes in TBS 1x; z-average diameter = 55.5 nm c) POPC-2.5mol%DOPE-biotin liposomes in TBS 1x; z-average diameter = 57.7 nm d) POPC-3.5mol%DOPE-biotin liposomes in TBS 1x; z-average diameter = 61.3 nm.

All of the liposome intensity size distributions displayed in fig. 3.23 even with increasing biotin ligand density stay roughly in the same z-average range of 50-60 nm (58.7 nm (PDI = 0.146) for POPC-1.5mol%DOPE-biotin liposomes; 55.5 nm (PDI = 0.128) for POPC-2mol%DOPE-biotin liposomes; 57.7 nm (PDI = 0.113) for POPC-2.5mol%DOPE-biotin liposomes and 61.3 nm (PDI = 0.135) for POPC-3.5mol%DOPE-biotin liposomes).

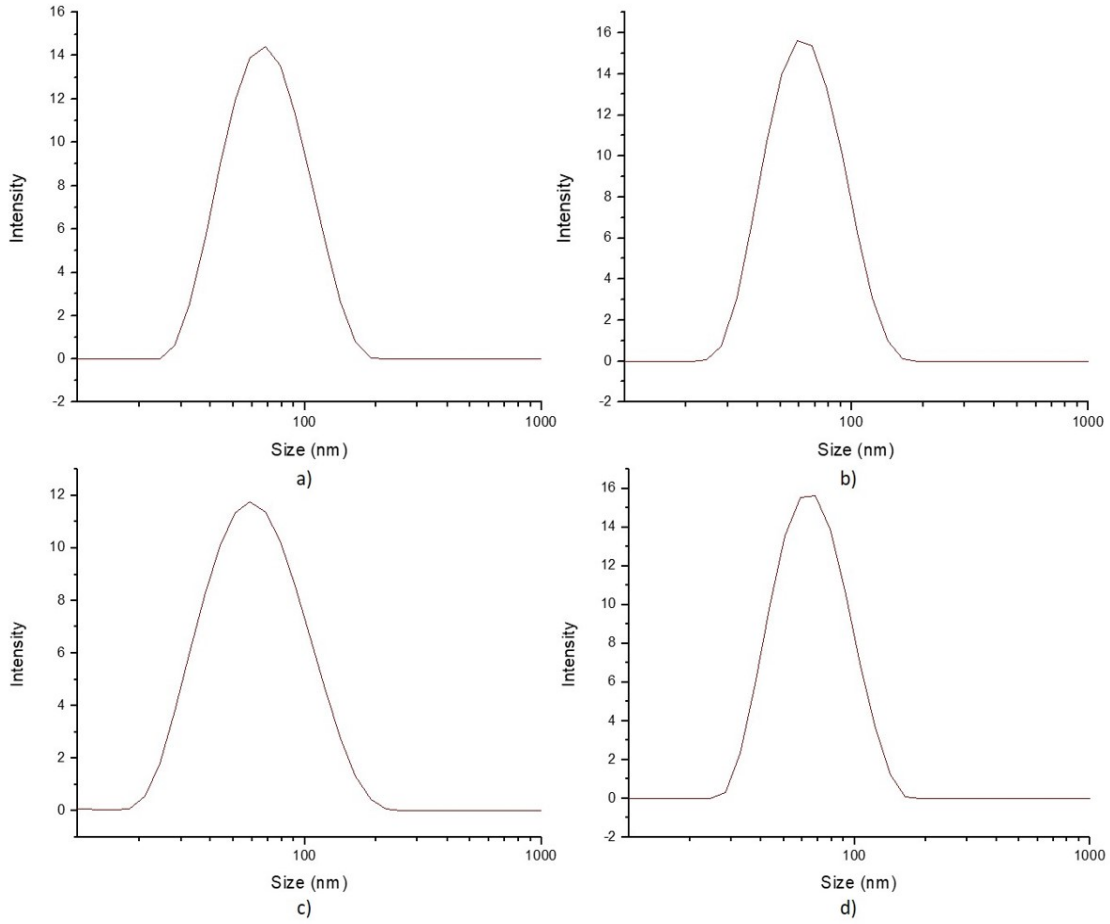


**Figure 3.24:** DLS intensity size distribution measurements on vesicles containing anionic lipids and PEG linkers. a) POPC-1mol%PE-PEG-biotin liposomes in TBS 1x; z-average diameter = 64.4 nm b) POPC-5mol%PE-PEG-biotin liposomes in TBS 1x; z-average diameter = 59.4 nm c) 10mol%POPG-POPC-0.1mol%PE-PEG-biotin liposomes in TBS 1x; z-average diameter = 55 nm d) 10mol%POPG-POPC-1mol%PE-PEG-biotin liposomes in TBS 1x; z-average diameter = 61.3 nm.

The same statement is reflected for liposomes including PEG linkers as well (fig. 3.24). The z-average is almost in the same range of 55-65 nm (64.4 nm (PDI = 0.137) for POPC-1mol%PE-PEG-biotin liposomes; 59.4 nm (PDI = 0.106) for POPC-5mol%PE-PEG-biotin liposomes; 55 nm (PDI = 0.174) for 10mol%POPG-POPC-0.1mol%PE-PEG-biotin liposomes and 61.3 nm (PDI = 0.106) for 10mol%POPG-POPC-1mol%PE-PEG-biotin liposomes). In order to see difference between including anionic lipids in the PEGylated structure or not, one needs to look into the DLS intensity size distributions of corresponding coated silica NPs.

The first silica nanoparticle coatings, which include PEG linker, are displayed in figures 3.25, 3.26 and 3.27. These coatings followed the same protocol[9] as established beforehand.

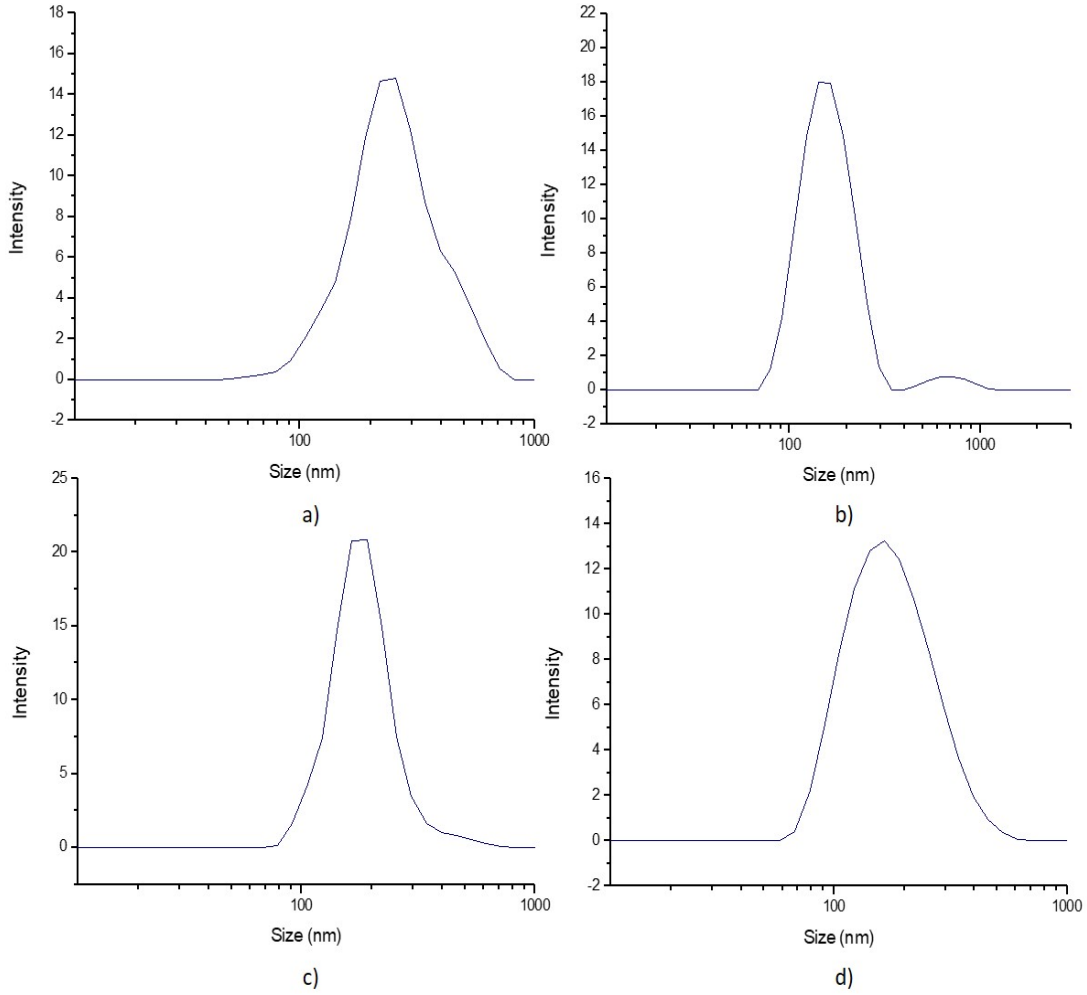


**Figure 3.25:** DLS intensity size distribution measurements on coated silica nanoparticles containing anionic lipids and PEG linkers. a) POPC-1mol%PE-PEG-biotin coated silica NPs in Tris 10x; z-average diameter = 351.1 nm b) POPC-0.1mol%PE-PEG-biotin coated silica NPs in Tris 10x; z-average diameter = 272.4 nm c) POPC-10mol%POPG-1mol%PE-PEG-biotin coated silica NPs in Tris 10x; z-average diameter = 227.6 nm d) POPC-10mol%POPG-0.1mol%PE-PEG-biotin coated silica NPs in Tris 10x; z-average diameter = 187 nm.[9]

[9] Sonicate NPs for 2 hours before addition; add 159.7 $\mu$L of liposomes (2 mg/mL), 740.3 $\mu$L of 1x TBS and 100 $\mu$L of NPs; 20 minutes vortex at 2000 rpm; centrifuge at 6000 rpm for 5 minutes; resuspend in 1x TBS and repeat centrifugation steps 3 times. With well activated NPs.

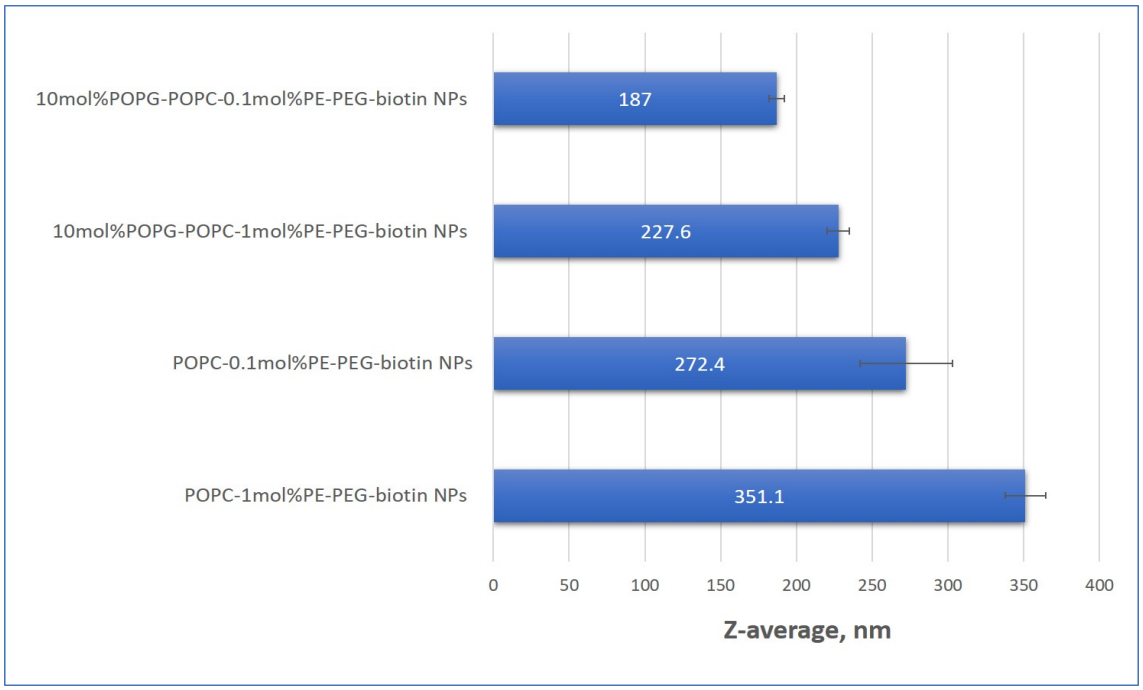


**Figure 3.26:** Z-average diameters of POPC-coated silica NPs with or without 10mol%POPG and with 0.1mol%PE-PEG-biotin and 1mol%PE-PEG-biotin linkers in their structure.

The subfigures c) and d) in fig. 3.25 display coated silica NPs, which include both - POPG anionic lipids and PEG linkers. Their z-average sizes are 227.6 nm (PDI = 0.366) and 187 nm (PDI = 0.388) for POPC-10mol%POPG-1mol%PE-PEG-biotin coated silica NPs and POPC-10mol%POPG-0.1mol%PE-PEG-biotin coated silica NPs, respectively. It is important to point out the fact that all the coated silica nanoparticles, that include PEG linkers, also have higher polydispersities than the coated particles without them. Nevertheless, an expected increase in hydrodynamic size of coated silica nanoparticles with PEG linkers should be roughly by 3.5 - 5 nm for 2 kDa PEG (without aggregation of particles) [93] compared to POPC or POPC-1mol%DOPE-biotin coated silica nanoparticles without PEG linkers.

The significance between POPC-0.1mol%PE-PEG-biotin and POPC-1mol%PE-PEG-biotin as well as the inclusion of 10mol%POPG in these coated NP structures in terms of z-average diameter was looked at by using two-tailed t-tests at the significance level of 0.05. It was observed that between 0.1mol%PE-PEG-biotin and 1mol%PE-PEG-biotin (t-critical value = 2.375107573, p-value = 0.05 - 0.10) there is no significant difference, however, between 10mol%POPG-POPC-0.1mol%PE-PEG-biotin and 10mol%POPG-POPC-1mol%PE-PEG-biotin (t-critical value = 4.45406305, p-value = 0.01 - 0.02) there was a significant difference in terms of z-average diameter. Also, in the example between POPC-1mol%PE-PEG-biotin and 10mol%POPG-POPC-1mol%PE-PEG-biotin (t-critical value = 12.17896299, p-value $< 0.001$), it was deducted that there is a significant difference in terms of z-average diameter, but there was no significant difference between POPC-0.1mol%PE-PEG-biotin and 10mol%POPG-POPC-0.1mol%PE-PEG-biotin (t-critical value = 2.773793346, p-value = 0.05 - 0.10) in terms of z-average diameter of the POPC-coated NPs.

Subfigures a) and b) in figures 3.25 and 3.27 are related through the fact that they do not include anionic lipids, hence, we observe higher polydispersity and stronger aggregation than

for their counterparts containing anionic lipids in their structure. In addition, their intensity size distributions are broader than the corresponding samples containing POPG anionic lipids. Furthermore, in plot a) fig. 3.25 three species of particles are observed - ones that are below 100 nm and other two occupying the size intervals of 100-400 nm and ≈ 200-1000 nm, which is distinctive from the other graphs in the figures. The z-average sizes are 351.1 nm (PDI = 0.448) and 272.4 nm (PDI = 0.444) for POPC-1mol%PE-PEG-biotin and POPC-0.1mol%PE-PEG-biotin coated silica NPs as well as 201.7 nm (PDI = 0.352) and 227.4 nm (PDI = 0.452) for POPC-2.5mol%PE-PEG-biotin and POPC-5mol%PE-PEG-biotin coated silica NPs, accordingly. Consequently, one can note that with increasing PEG ligands on the nanoparticle surface, the amount of aggregated nanoparticles increases as well. However, this dependence needs more investigation and, unfortunately, it will not be proceeded in this project.

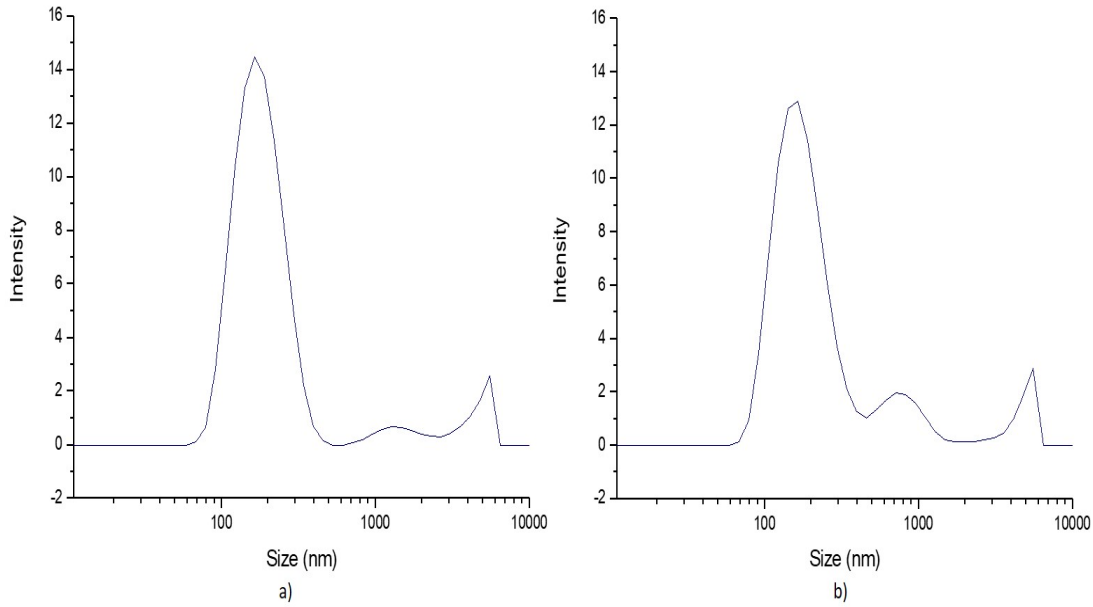


**Figure 3.27:** DLS intensity size distribution measurements on coated silica nanoparticles containing anionic lipids and PEG linkers. a) POPC-2.5mol%PE-PEG-biotin coated silica NPs in Tris 10x; z-average diameter = 201.7 nm b) POPC-5mol%PE-PEG-biotin coated silica NPs in Tris 10x; z-average diameter = 227.4 nm.[9]

Throughout the project the main ratio between surface areas of liposomes and silica nanoparticles in the coating procedures (during mixing appropriate volumes were chosen) were kept around the value of 90. Having a rather high volume of vesicles, attempts to reduce the volume, used for silica nanoparticle coating, were conducted. These experiments included coated silica nanoparticles with and without PEG linkers as well as the liposomes/silica NP ratio was diminished to 10 (figure 3.28).

[9] Sonicate NPs for 2 hours before addition; add 159.7 $\mu$L of liposomes (2 mg/mL), 740.3 $\mu$L of 1x TBS and 100 $\mu$L of NPs; 20 minutes vortex at 2000 rpm; centrifuge at 6000 rpm for 5 minutes; resuspend in 1x TBS and repeat centrifugation steps 3 times. With well activated NPs.

In the figure 3.28 it is noticeable that even though there was not a significant impact (small increase in polydispersity in the case of 10mol%POPG-POPC-1mol%biotin NPs from PDI = 0.273 to PDI = 0.284) on the coated silica nanoparticles without PEG linkers (subfigures a) and c)), the cases with PEG linkers (b) and d)) display a tremendous increase in aggregates compared to coated nanoparticles with PEG linkers, which were prepared via protocol where vesicle/NP ratio was ≈ 90. The z-average sizes are 179.8 nm (PDI = 0.341) for a), 307.8 nm (PDI = 0.559) for b), 178.5 nm (PDI = 0.284) and 358.6 nm (PDI = 0.613) for d) subfigures. Consequently, the final coating protocol was kept as it was established previously.[9]

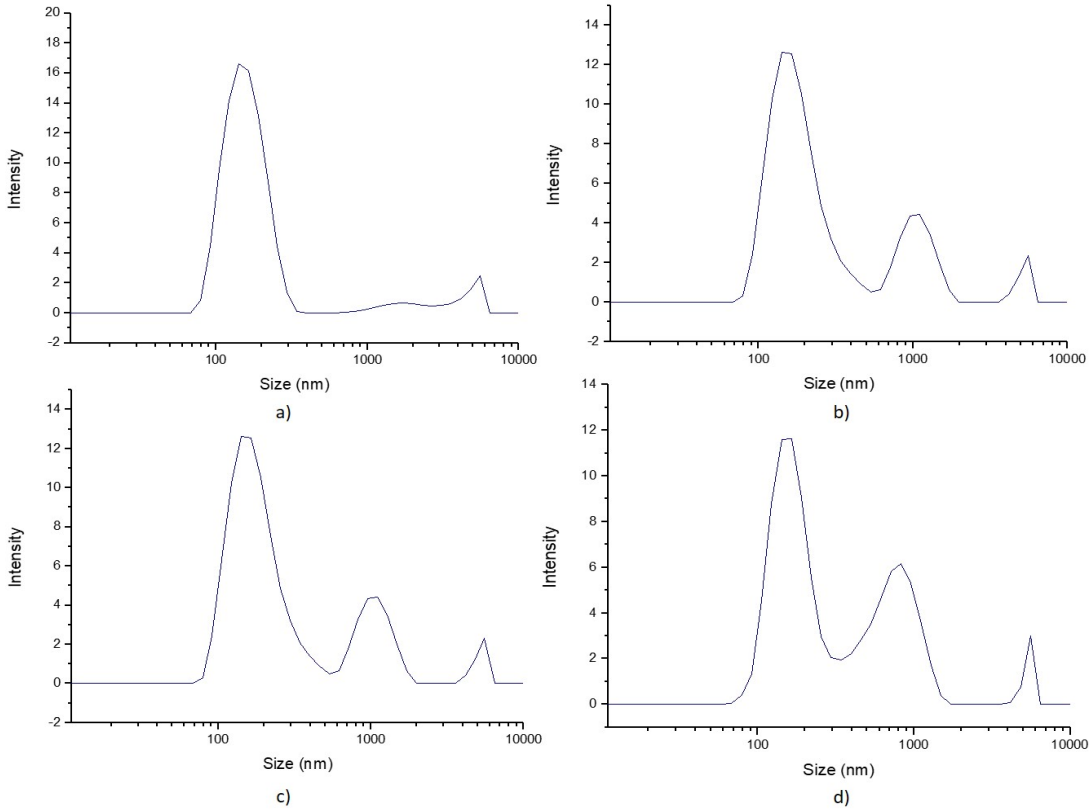


**Figure 3.28:** DLS intensity size distribution measurements on coated silica nanoparticles with 10 times liposome/NP surface area ratio. a) POPC-2mol%biotin NPs in Tris 10x; z-average diameter = 179.8 nm b) POPC-0.5mol%PE-PEG-biotin NPs in Tris 10x; z-average diameter = 307.8 nm c) 10mol%POPG-POPC-1mol%biotin NPs in Tris 10x; z-average diameter = 178.5 nm d) 10mol%POPG-POPC-1mol%PE-PEG-biotin NPs in Tris 10x; z-average diameter = 358.6 nm .[10]

[9] Sonicate NPs for 2 hours before addition; add 159.7 $\mu$L of liposomes (2 mg/mL), 740.3 $\mu$L of 1x TBS and 100 $\mu$L of NPs; 20 minutes vortex at 2000 rpm; centrifuge at 6000 rpm for 5 minutes; resuspend in 1x TBS and repeat centrifugation steps 3 times. With well activated NPs.

[10] Sonicate NPs for 2 hours before addition; Add appropriate volumes of vesicles, silica NPs and 1x TBS buffer to reach liposome/NP ratio ≈ 10; 20 minutes vortex at 2000 rpm; centrifuge at 6000 rpm for 5 minutes; resuspend in 1x TBS and repeat centrifugation steps 3 times. With well activated NPs.

In conclusion for this chapter, new smaller silica NPs (fig. 3.29) were synthesized and a few coating experiments were administered with already set up coating protocol[10]. The newly synthesized silica nanoparticles were not activated through the procedure 2.2.2 as they were thought to have enough hydroxy groups. In the picture 3.29 the intensity size distribution of these newly synthesized non-activated silica NPs is displayed. One can note that the z-average of these particles is 104.5 nm (PDI = 0.253), which is smaller than the particles used for coating procedures uptil now (Z-average 129.1 nm, PDI = 0.225). In addition, as the colloid dispersion was not activated with hydroxy groups and cleaned in that operation, dust and potential aggregates are visible. The smaller particles were included due to one of the project goals to experiment with the ligand density in relation to nanoparticle dimensions.

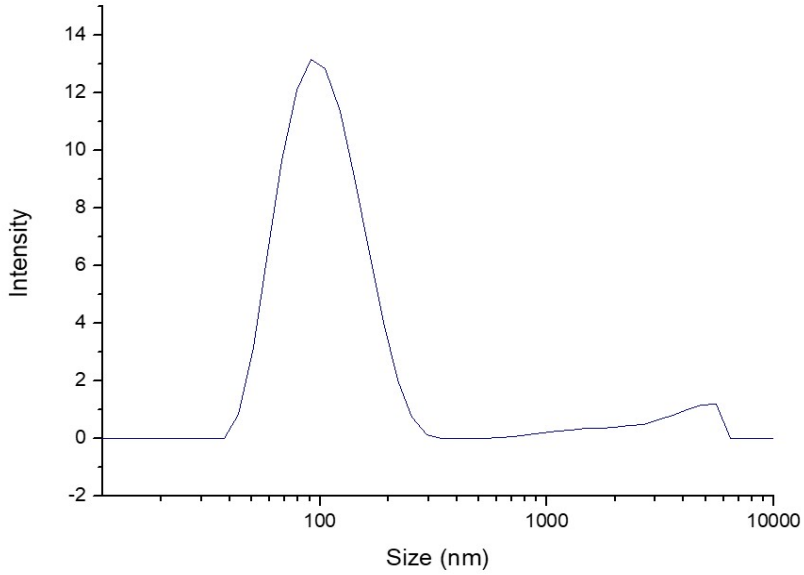


**Figure 3.29:** DLS intensity size distribution measurements on newly synthesized bare non-activated silica NPs in Tris 10x; z-average diameter = 104.5 nm.

It is also important to note that not a suffice amount of these experiments were conducted due to time restrictions on the project, however, a few may be observed in figure 3.30. The z-average sizes of these coated silica NPs are 232.5 nm (PDI = 0.381), 322.3 nm (PDI = 0.691) and 200.4 nm (PDI = 0.444) for POPC-2mol%biotin NPs, POPC-0.5mol%PE-PEG-biotin NPs and 10mol%POPG-POPC-1mol%biotin NPs, accordingly. In addition, it is observed that new optimization is needed for the coating procedure of the silica nanoparticles with different dimensions, because of the aggregation and high polydispersity in the system. However, due to time restraint for this project, these attempts were not conducted further.

[10] Sonicate NPs for 2 hours before addition; Add appropriate volumes of vesicles, silica NPs and 1x TBS buffer to reach liposome/NP ratio $\approx$ 10; 20 minutes vortex at 2000 rpm; centrifuge at 6000 rpm for 5 minutes; resuspend in 1x TBS and repeat centrifugation steps 3 times. With well activated NPs.

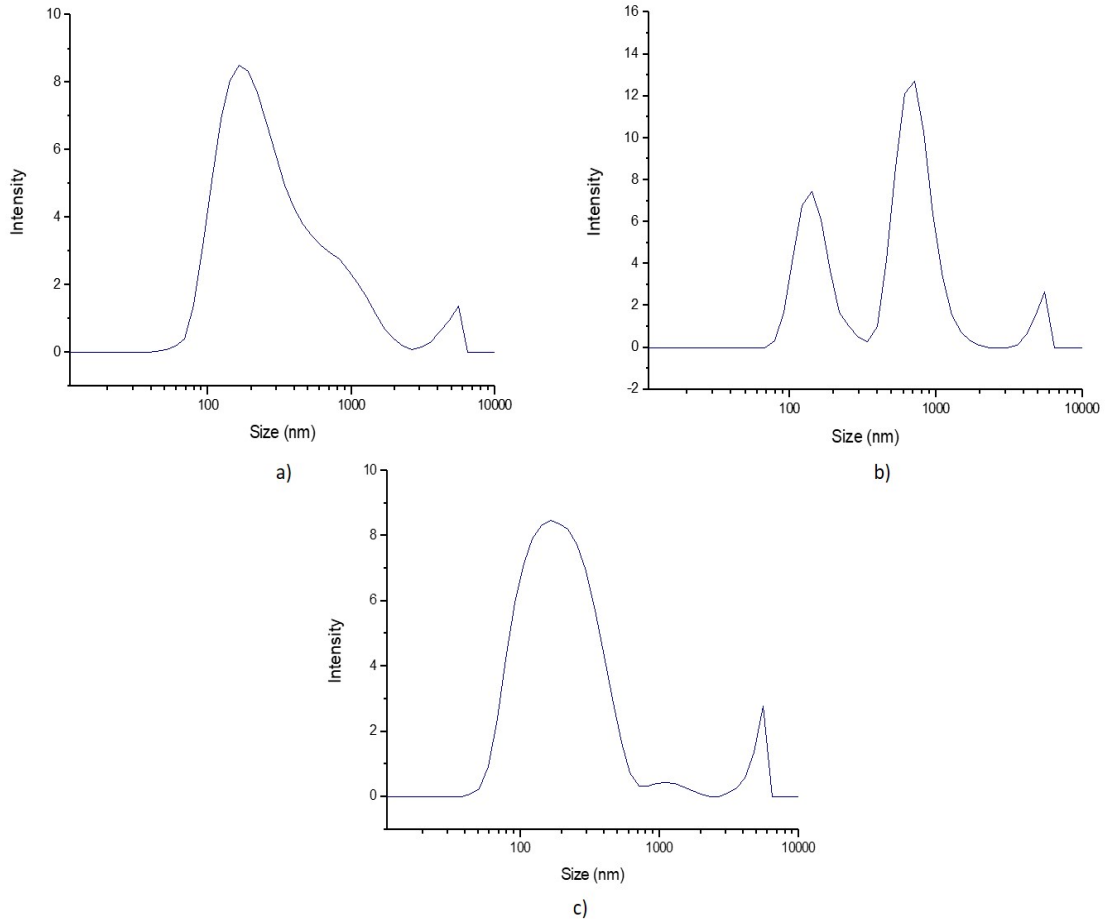


**Figure 3.30:** DLS intensity size distribution measurements on coated silica nanoparticles with 10 times liposome/NP surface area ratio and newly synthesized silica nanoparticles. a) POPC-2mol%biotin NPs in Tris 10x; z-average diameter = 232.5 nm b) POPC-0.5mol%PE-PEG-biotin NPs in Tris 10x; z-average diameter = 322.3 nm c) 10mol%POPG-POPC-1mol%biotin NPs in Tris 10x; z-average diameter = 200.4 nm.[10]

To sum up, the main optimization parameters that affected the coating protocol the most are shown in the figure 3.31. With these parameters, a protocol was established that results in rather monodisperse silica nanoparticles coated with single lipid bilayers of various compositions. In the next chapter, the interaction experiment results with these lipid bilayer coated silica nanoparticles and model cell interfaces will be presented and discussed.

[10] Sonicate NPs for 2 hours before addition; Add appropriate volumes of vesicles, silica NPs and 1x TBS buffer to reach liposome/NP ratio ≈ 10; 20 minutes vortex at 2000 rpm; centrifuge at 6000 rpm for 5 minutes; resuspend in 1x TBS and repeat centrifugation steps 3 times. With well activated NPs.

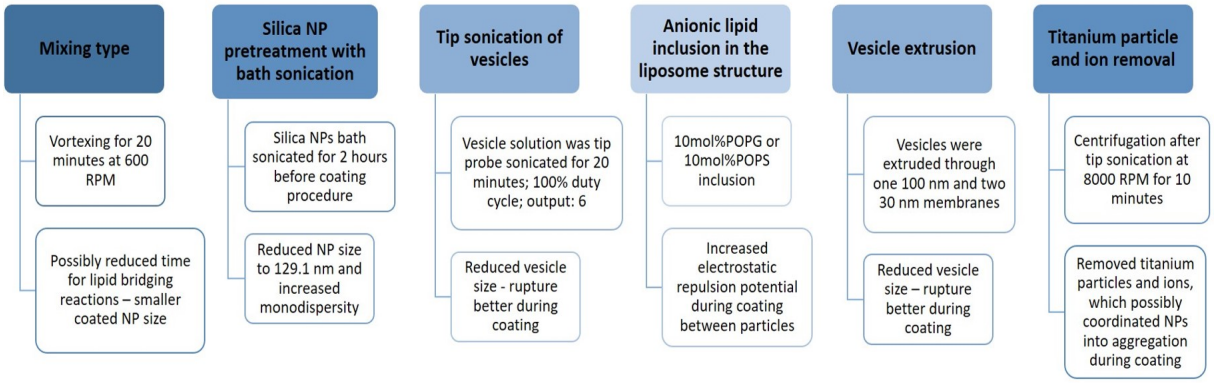


**Figure 3.31:** Main factors that influenced the preparation of an established silica nanoparticle (z-average size = 129.1 nm (PDI = 0.225)) coating protocol.

## 3.3 QCM-D interaction experiments

Firstly, before the QCM-D results, containing supported lipid bilayer interface alone, with streptavidin/neutravidin and/or interaction with bare or coated silica nanoparticles, and other assemblies are presented, it is important to mention that for most cases at least 1 more experiment was reproduced. Secondly, experiments that included bubbles during assemblies, thus, leading uncontrollable systems, were not included in the analysis.

The experiments include multivalent coated silica nanoparticles and the difference from the monovalent counterparts are displayed in fig. 3.32.

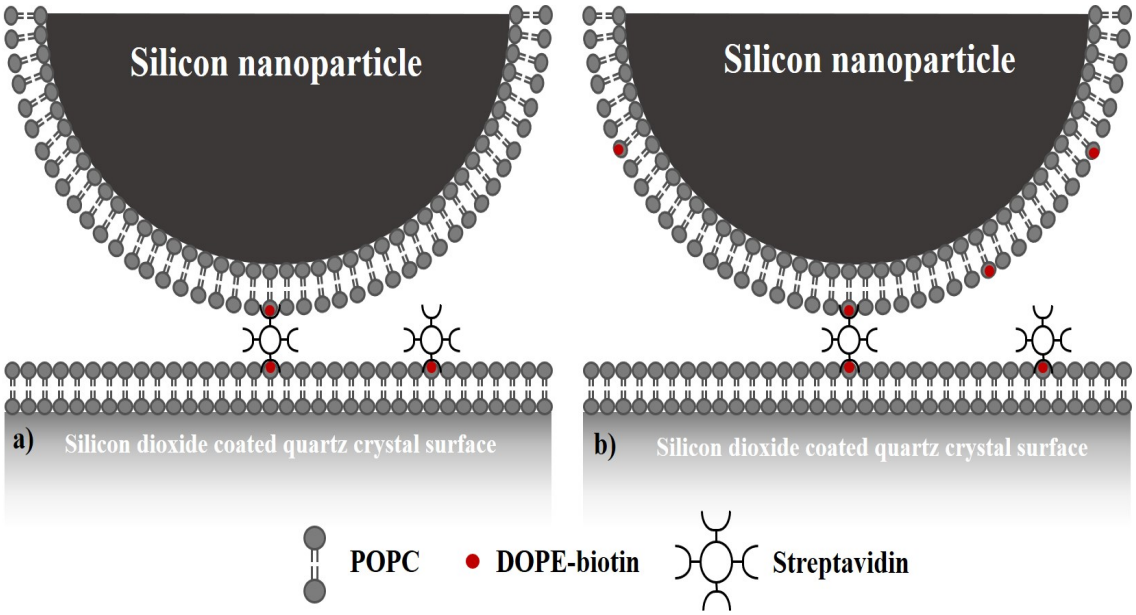


**Figure 3.32:** Graphic display of a) multivalent and b) monovalent coated nanoparticle interaction with a supported lipid bilayer through biotin - streptavidin connection. Take note that the dimensions are not to scale as bare silica NP z-average is $\approx$ 129 nm and supported lipid bilayer is estimated to be 5-7 nm thick [94]. Multivalent particles contain 10-2000 biotin functionalized headgroups on the surface whereas monovalent - 1-10.

In order to have a clearer understanding of how many biotin ligands there are on the coated nanoparticle, a rough estimation was made for 1mol%DOPE-biotin headgroups containing POPC-coated nanoparticles and is featured in the same picture. Also, a pre-treatment of employed crystal surfaces was conducted before each experiment (method 2.2.6) and the manner of the experiment as well as the concentrations of appropriate materials are explained in method section 2.2.7. The goal and motivation for forming an SLB is to mimic a cell membrane on the surface of the sensor crystal for the interaction measurements.

### 3.3.1 Supported lipid bilayer formation

The first assemblies of POPC and POPC-1mol%DOPE-biotin supported lipid bilayers on a silicon dioxide coated quartz crystal are displayed in fig. 3.33. However, the filtration of the liposome solution with 0.2 $\mu$m membranes led to problematic assemblies and this step was discarded later on. Even though, the typical lipid bilayer profile is observed in fig. 3.33 a), it is visible in subfigure

b) that the dissipation after the washing with the buffer step leads to values lower than zero, which imples that the assembly is not as expected. In addition, in subfigures c) and d) POPC-1mol%DOPE-biotin liposome assembly is observed, however, as shown in fig. 1.10, it resembles a case of liposomes not rupturing on the crystal's interface (as seen in the QCM-D introduction part, fig. 1.11) [52].

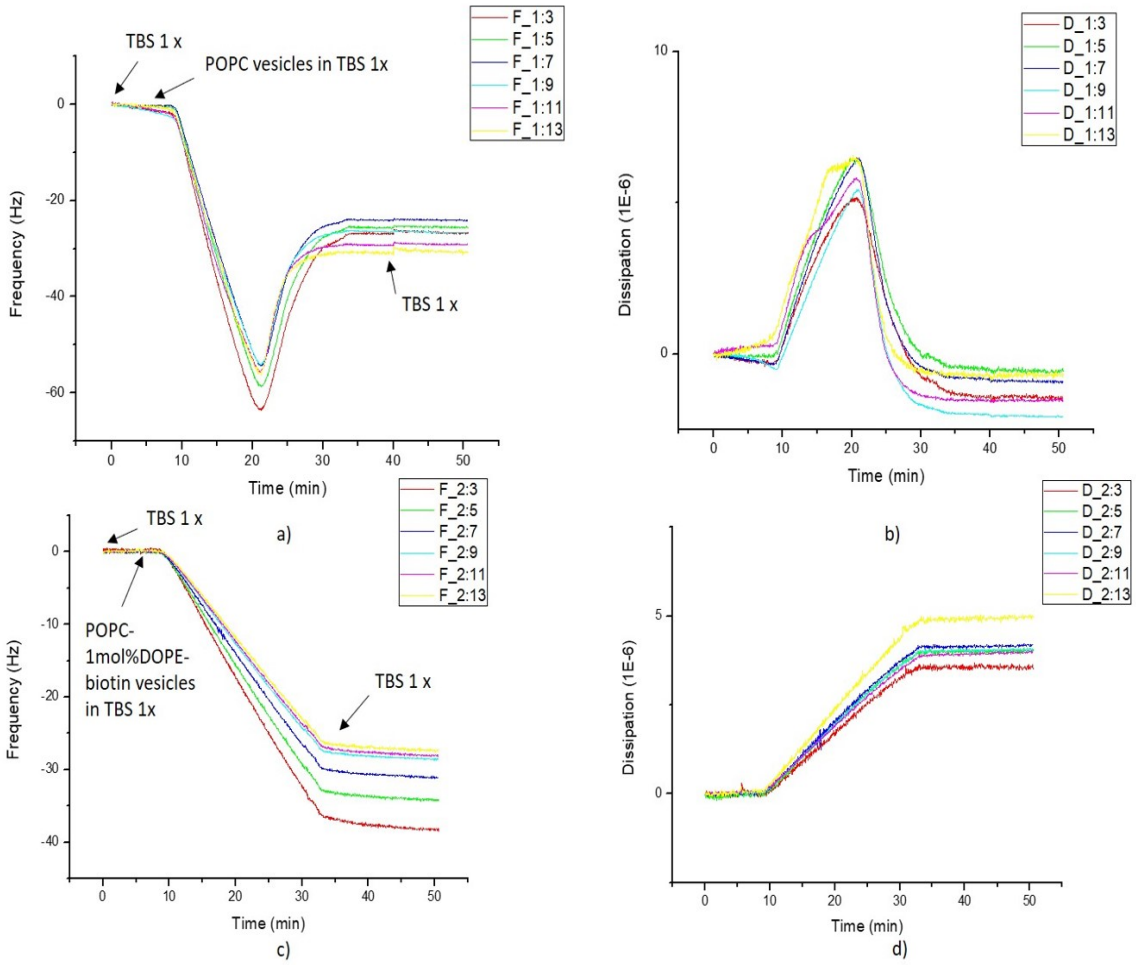


**Figure 3.33:** QCM-D experiment on supported lipid bilayer assembly (TBS 1x buffer). a) POPC supported lipid bilayer; b) POPC supported lipid bilayer dissipation profile; c) POPC-1mol%DOPE-biotin liposome assembly; d) POPC-1mol%DOPE-biotin liposome assembly dissipation profile (In the legends, dependendencies starting with letter "F" display frequency changes over time for different overtones (n = 3,5,7, etc. (in this case)) and with letter "D" the same for dissipation energy changes.

Consequently, unfiltered POPC and POPC-1mol%DOPE-biotin liposomes resulted in excellent supported lipid bilayer formations in accordance with the results of Reviakine et al. [52] due to the fact that the change is frequency after the assembly since the initial point is in the range of -20 - -30 Hz (fig. 3.34). In addition, the dissipaton after the assembly of the supported lipid bilayer is not below zero anymore, thus, indicating that the assembly was successful and the liposomes have ruptured on the crystal interface.

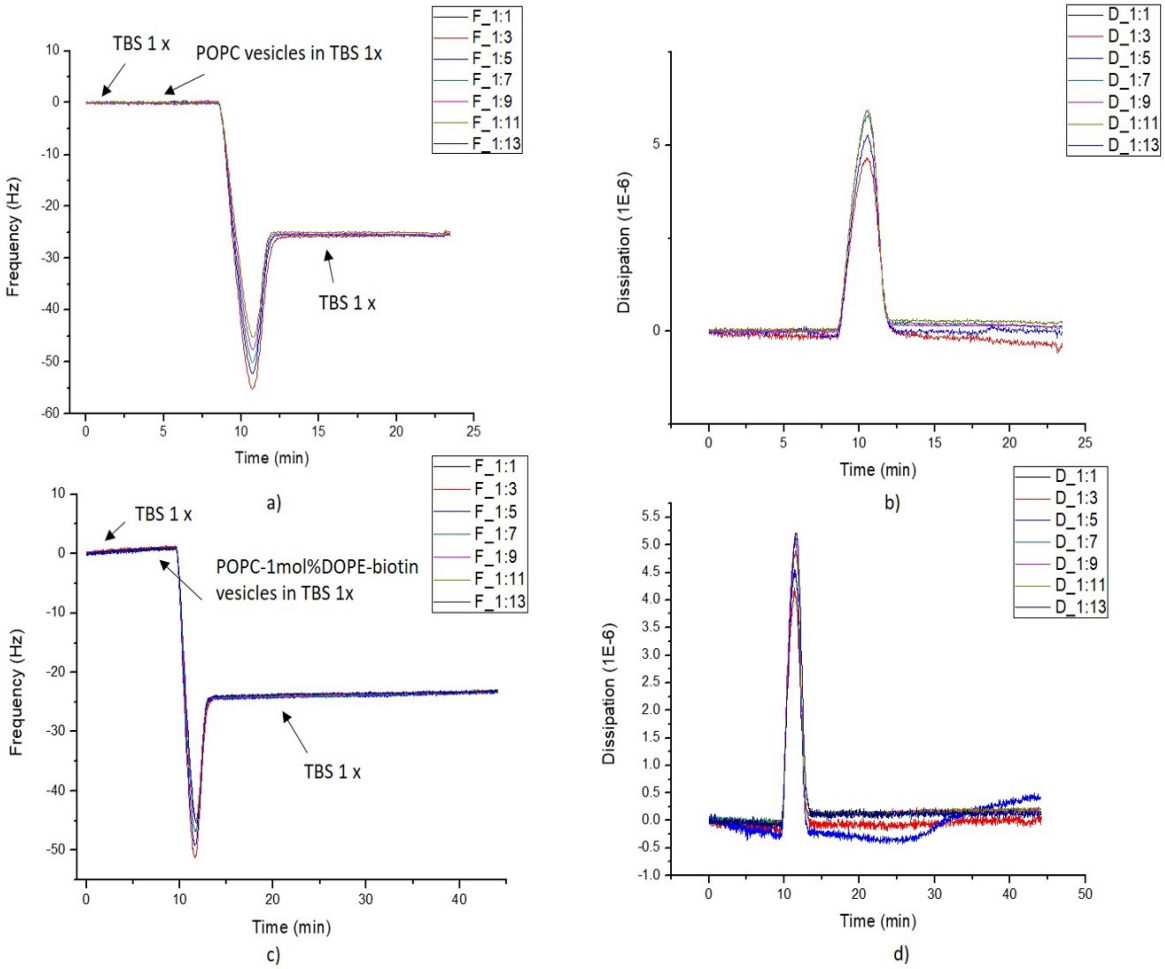


**Figure 3.34:** QCM-D experiment on supported lipid bilayer assembly (TBS 1x buffer). a) POPC supported lipid bilayer; b) POPC supported lipid bilayer dissipation profile; c) POPC-1mol%DOPE-biotin supported lipid bilayer; d) POPC-1mol%DOPE-biotin supported lipid bilayer dissipation profile.

### 3.3.2 Supported lipid bilayer interaction with streptavidin

After the supported lipid bilayers (SLBs) were successfully established on the silica sensor crystal surface, further experiments with streptavidin assembly on those layers have been handled (fig. 3.35). It is important to note that the expected change in frequency was 5 - 10 Hz after the attachment of streptavidin molecules to POPC-1mol%DOPE-biotin supported lipid bilayer due to necessity for 1/3 assembly coverage for later estimations. In subfigure a) POPC supported lipid bilayer interaction with streptavidin is observed. Due to no biotin ligands apparent in the POPC supported lipid bilayer, no streptavidin molecule attachment is seen even though in picture b) the system dissipates some energy, which can be related to washing steps with 1x TBS buffer during the experiment. In the case of supported lipid bilayer containing biotin ligands, streptavidin attachment is observed, however, the coverage of streptavidin has not reached 5-10 Hz (approximately 1/3 coverage of the bilayer) of frequency, which is the goal (to measure NP binding kinetics, where there is roughly one streptavidin molecule in the contact area between the NP and the supported lipid bilayer), as well as the dissipation profile almost does not differ from the case of SLB without biotin ligands. The observed change in frequency (fig. 3.35 b)) is $\approx$ 3.5

Hz (injection period: ≈ 30 - 70th minute; 3d overtone), therefore some further optimization was needed. In addition to that, as anionic lipids were included in the liposome production protocol, interaction experiments included SLBs and coated silica NPs with anionic (POPG and POPS; due to the closer proximity value for z-average of coated silica NPs) lipids as well (figures 3.38 and 3.39).

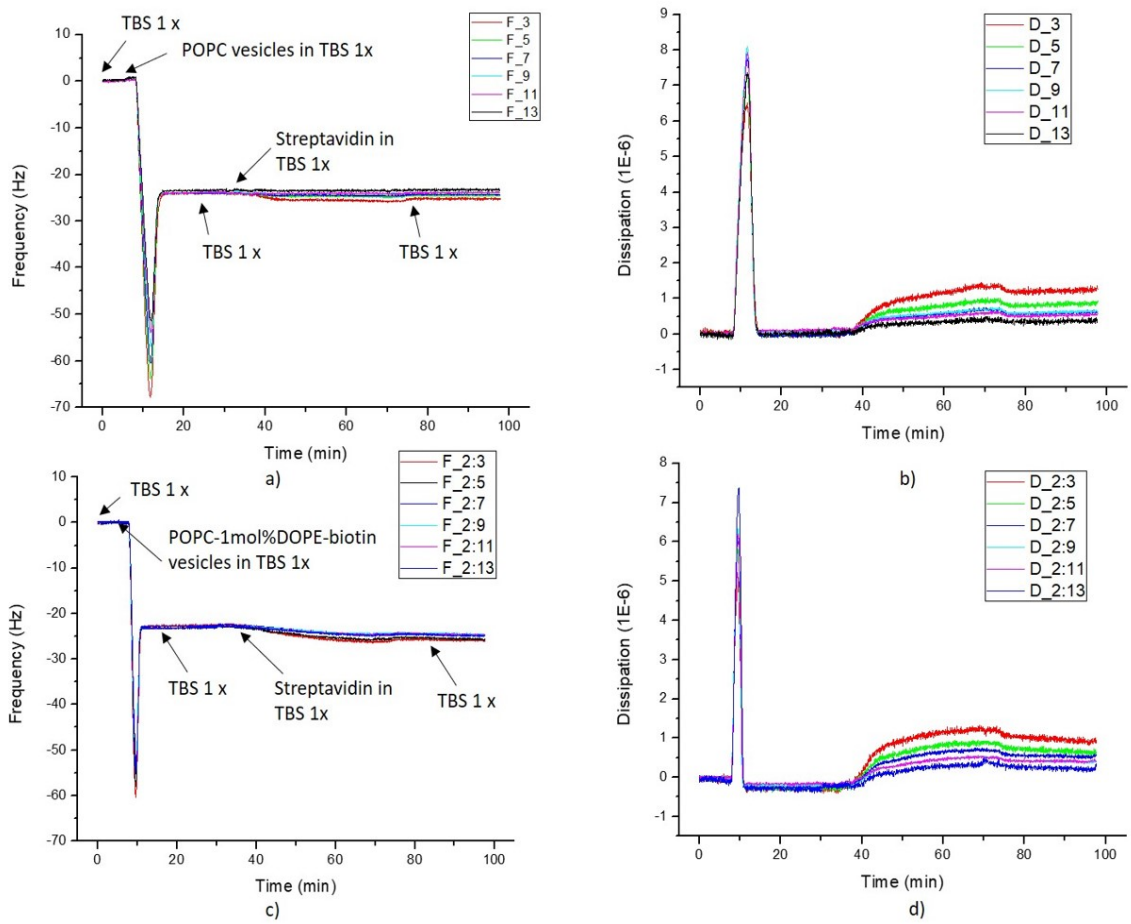


**Figure 3.35:** QCM-D experiments on supported lipid bilayer assemblies (TBS 1x buffer) with streptavidin (TBS 1x buffer). a) POPC supported lipid bilayer interaction with streptavidin; b) POPC supported lipid bilayer interaction with streptavidin dissipation profile; c) POPC-1mol%DOPE-biotin supported lipid bilayer interaction with streptavidin; d) POPC-1mol%DOPE-biotin supported lipid bilayer interaction with streptavidin dissipation profile.

### 3.3.3 Streptavidin covered supported lipid bilayer interaction with bare silica NPs

Furthermore, some control experiments were conducted with bare silica NPs before starting the interaction experiments with coated silica NPs. They are displayed in fig. 3.36 and implicate the interaction with POPC supported lipid bilayer (3.36 a)) and POPC-1mol%DOPE-biotin supported lipid bilayer (fig. 3.36 c)). An important fact to mention is that in these pictures the addition of bare silica NPs (in 10 x Tris) at around 95th minute results in a frequency shift, however, it should be regarded as change in buffer relation and not NP attachment as they are rather massive

(z - average = 129.1 nm) compared to the supported lipid bilayer and the ligands (biotin and streptavidin). Also, an error was made in this experiment as a washing step with 1x TBS was excluded after the injection of bare silica NPs.

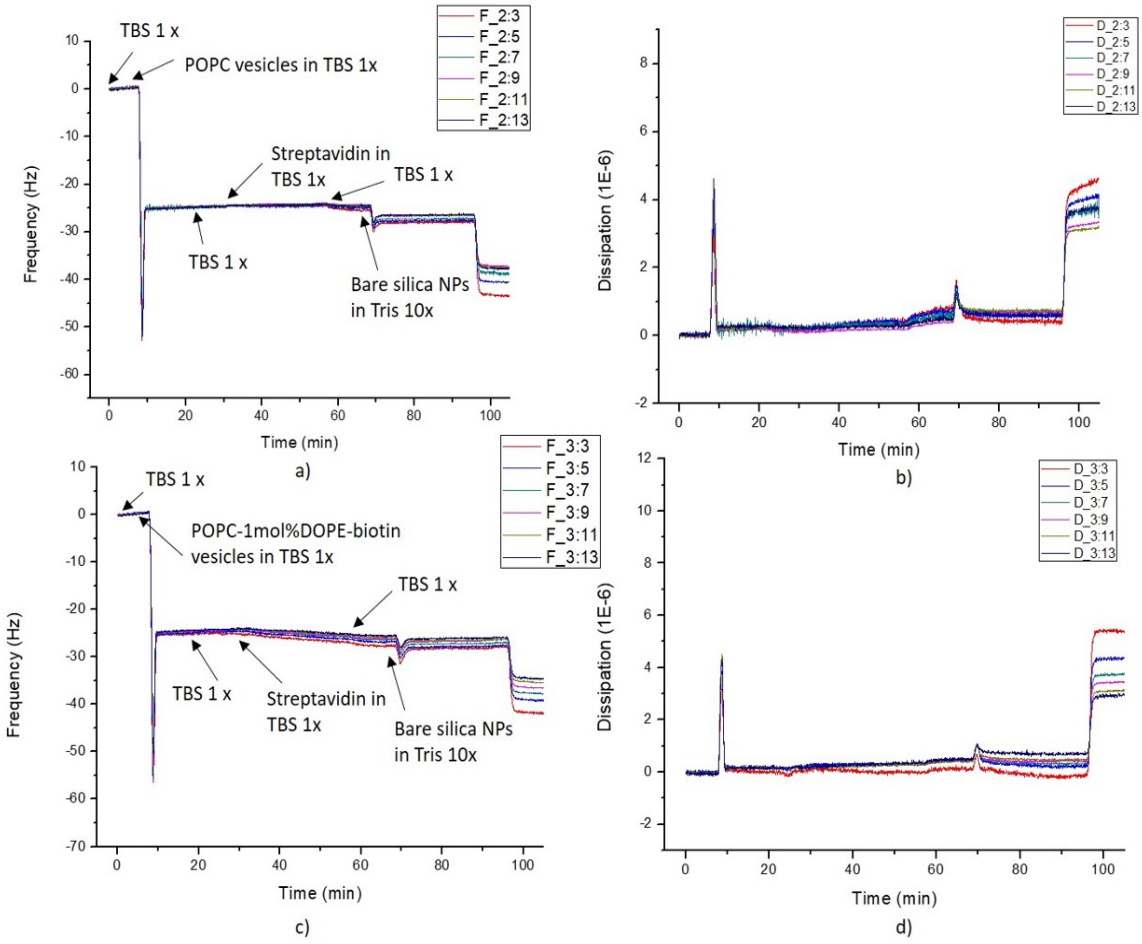


**Figure 3.36:** QCM-D experiments on supported lipid bilayer assemblies (TBS 1x buffer) with streptavidin (TBS 1x buffer) and bare silica NPs (Tris 10x buffer). a) POPC supported lipid bilayer interaction with streptavidin and bare silica NPs; b) POPC supported lipid bilayer interaction with streptavidin and bare silica NPs dissipation profile; c) POPC-1mol%DOPE-biotin supported lipid bilayer interaction with streptavidin and bare silica NPs; d) POPC-1mol%DOPE-biotin supported lipid bilayer interaction with streptavidin and bare silica NPs dissipation profile.

### 3.3.4 Interaction between streptavidin covered supported lipid bilayer and coated silica NPs

The interaction between a coated silica NP with a lipid bilayer and a SLB covered with streptavidin is displayed in fig. 3.37, which establishes an overview of how the interaction is supposed to occur.

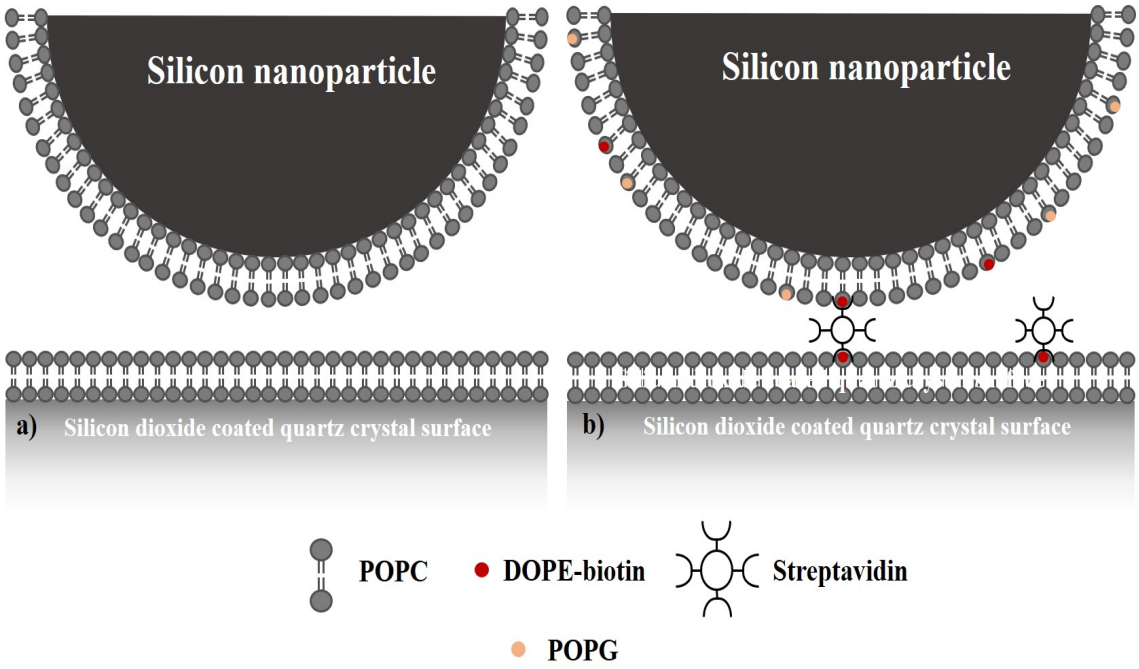


**Figure 3.37:** An illustration of a coated silica NP a) not containing and b) having POPG and biotin functionalized headgroups in it's structure a) not interacting or b) interacting through streptavidin with a SLB. Take note that the dimensions are not to scale as bare silica NP z-average is $\approx$ 129 nm and supported lipid bilayer is estimated to be 5-7 nm thick [94]. This experimental setup is observed in QCM-D real-time measurements in fig. 3.38.

From the plots 3.38 and 3.39 one may already have an educated guess that the supported lipid bilayers, containing biotin ligands in their structure, and have assembled a certain coverage of streptavidin on their surface, are not interacting with the injected appropriate coated silica nanoparticles. A possible explanation for the lack of adsorption of coated silica nanoparticles is insufficient coverage of streptavidin on the supported lipid bilayers. The apparent frequency shift in both pictures 3.38 and 3.39 in the time period of 80 - 100 minute are not due to some sort of molecule detaching from the assembled layer, but rather due to change in buffers. Since the initial liposome injection, liposome solution as well as the washing steps were in 1x TBS environment, however, the coated silica nanoparticles are dispersed in 10 x Tris buffer. Therefore, an additional washing step in 1x TBS after coated silica NP injection was done after as a reference whether the particles have actually attached or not. Nevertheless, no significant difference between nanoparticles coated with POPC-10mol%POPG-1mol%DOPE-biotin NPs or POPC-10mol%POPS-1mol%DOPE-biotin NPs, in terms of attachment of coated nanoparticles to streptavidin covered supported lipid bilayers (no change in frequency after the addition of coated appropriate silica nanoparticles), was observed.

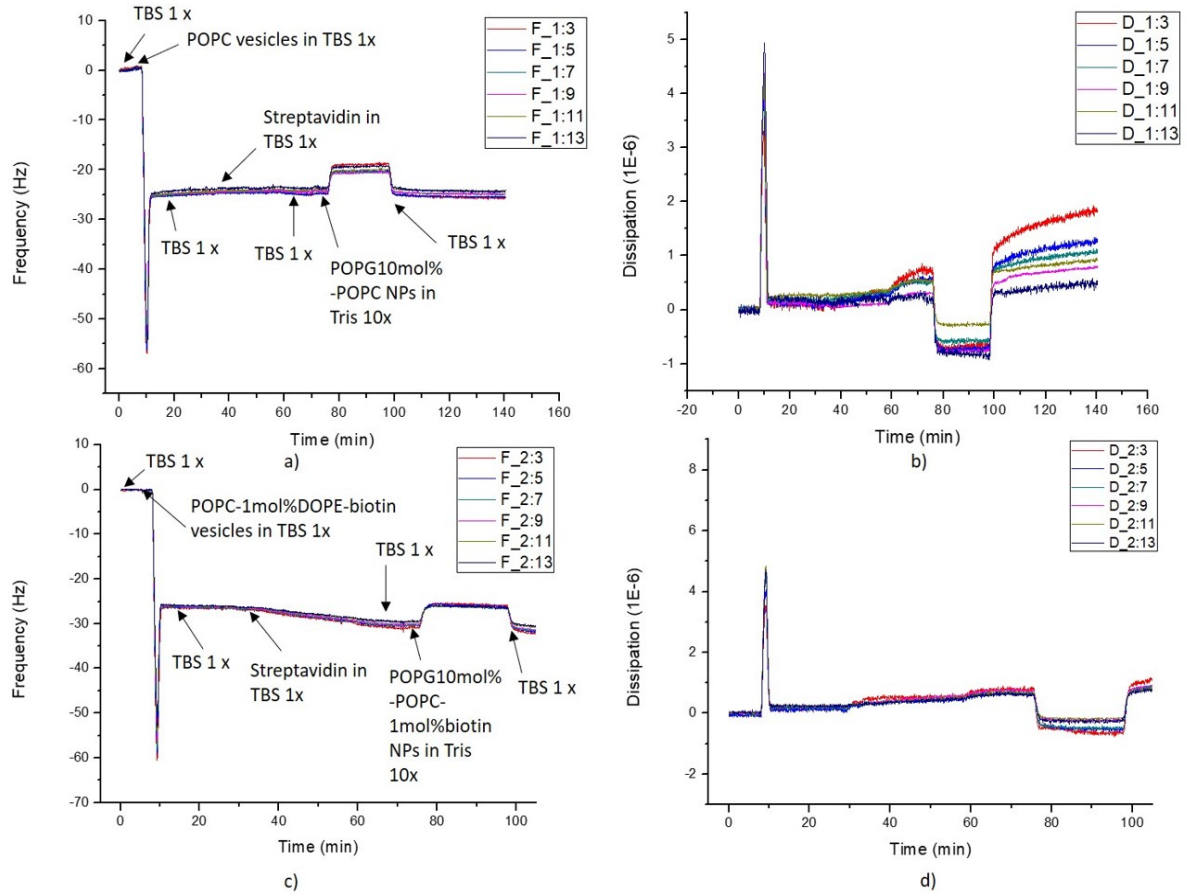


**Figure 3.38:** QCM-D experiments on supported lipid bilayer assemblies (TBS 1x buffer) with streptavidin (TBS 1x buffer) and coated anionic NPs (Tris 10x buffer). a) POPC supported lipid bilayer interaction with streptavidin and POPC-10mol%POPG NPs; b) POPC supported lipid bilayer interaction with streptavidin and POPC-10mol%POPG NPs dissipation profile; c) POPC-1mol%DOPE-biotin supported lipid bilayer interaction with streptavidin and POPC-10mol%POPG-1mol%DOPE-biotin NPs; d) POPC-1mol%DOPE-biotin supported lipid bilayer interaction with streptavidin and POPC-10mol%POPG-1mol%DOPE-biotin NPs dissipation profile.

In order to tackle the problem of coated silica nanoparticles with biotin functionalized headgroups not attaching to streptavidin covered supported lipid bilayer, several experiments with increasing streptavidin coverage were conducted. However, the maximum change in frequency after the addition of the protein could not exceed the 10 Hz, as established previously, this range corresponds to $\approx 1/3$ of streptavidin ligand coverage on the supported lipid bilayer.

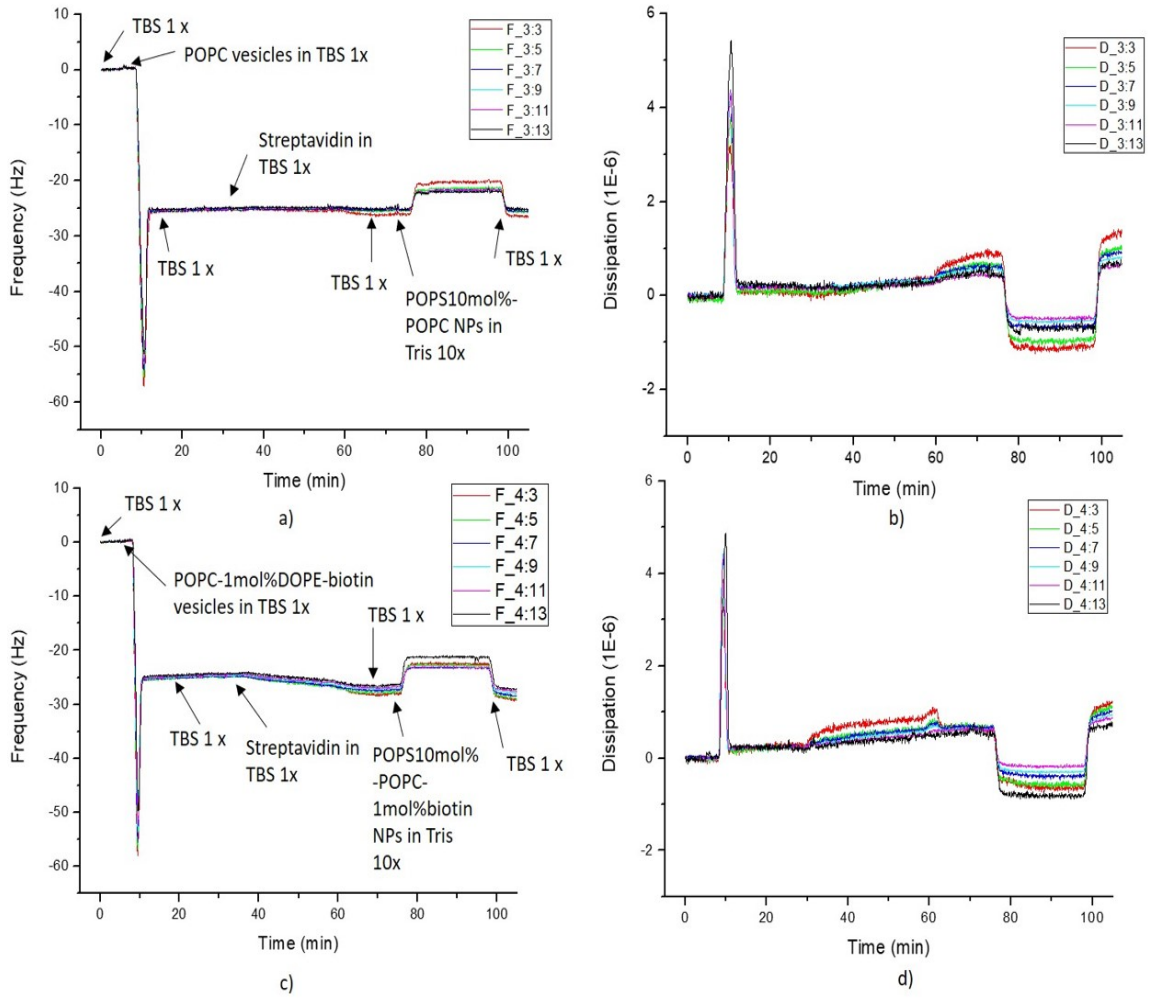


**Figure 3.39:** QCM-D experiments on supported lipid bilayer assemblies (TBS 1x buffer) with streptavidin (TBS 1x buffer) and coated anionic NPs (Tris 10x buffer). a) POPC supported lipid bilayer interaction with streptavidin and POPC-10mol%POPS NPs; b) POPC supported lipid bilayer interaction with streptavidin and POPC-10mol%POPS NPs dissipation profile; c) POPC-1mol%DOPE-biotin supported lipid bilayer interaction with streptavidin and POPC-10mol%POPS-1mol%DOPE-biotin NPs ; d) POPC-1mol%DOPE-biotin supported lipid bilayer interaction with streptavidin and POPC-10mol%POPS-1mol%DOPE-biotin NPs dissipation profile.

### 3.3.5 Increasing the streptavidin coverage on the supported lipid bilayers

The following experiments with increasing streptavidin coverage on the assembled supported lipid bilayer are displayed in pictures 3.40, 3.41. In figure 3.40 SLBs with POPC-1.5mol%DOPE-biotin and POPC-2mol%DOPE-biotin can be seen. When streptavidin is injected into the system, the appropriate shifts in frequency are achieved: 6.1 Hz and 9.3 Hz for POPC-1.5mol%DOPE-biotin and POPC-2mol%DOPE-biotin SLBs, respectively (estimated from the 3d overtone). The energy dissipation profiles display relatively rigid systems as for different overtones the dissipation results in almost the same values. However, in this case the SLB containing 2mol%DOPE-biotin was

chosen in the further experiments over the former one due to the fact it led to a greater streptavidin coverage in the necessary range (9.3 Hz > 6.1 Hz; necessary range = 5-10 Hz for ≈ 1/3 streptavidin coverage on the supported lipid bilayer).

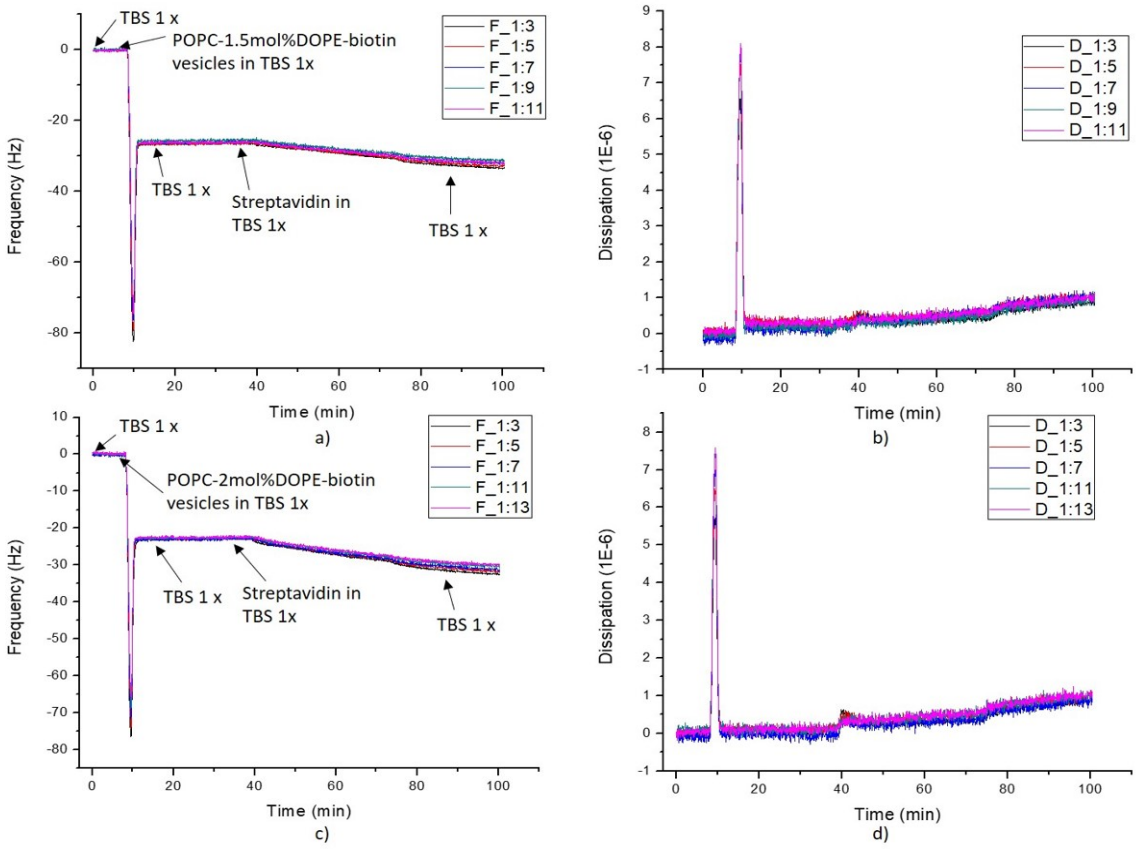


**Figure 3.40:** QCM-D experiments on supported lipid bilayer (TBS 1x buffer) assemblies with streptavidin (TBS 1x buffer). a) POPC-1.5mol%DOPE-biotin supported lipid bilayer interaction with streptavidin; b) POPC-1.5mol%DOPE-biotin supported lipid bilayer interaction with streptavidin dissipation profile; c) POPC-2mol%DOPE-biotin supported lipid bilayer interaction with streptavidin; d) POPC-2mol%DOPE-biotin supported lipid bilayer interaction with streptavidin dissipation profile.

The consecutive QCM-D experiments included SLBs POPC-2.5mol%DOPE-biotin and POPC-3.5mol%DOPE-biotin structures (fig. 3.41). As discussed in the previous experiment, upon injection of streptavidin, the shifts in frequency resulted in: 8.6 Hz and 12.2 Hz for POPC-2.5mol%DOPE-biotin and POPC-3.5mol%DOPE-biotin, accordingly (estimated from the 3d overtone). Due to the fact the given response from POPC-3.5mol%DOPE-biotin SLB in correspondance with attached streptavidin yielded a shift in frequency 12.2 Hz, which more than necessary frequency range possibly due to many streptavidin molecules adsorbing in respect to expected 10 Hz frequency shift, SLB with POPC-3.5mol%DOPE-biotin was not researched further. In addition, even though POPC-2.5mol%DOPE-biotin SLB with attached streptavidin led to 8.6 Hz frequency change, which fits into the required range of frequency, it was excluded as well later on due to the fact that compared to POPC-2mol%DOPE-biotin SLB, it yielded a smaller streptavidin coverage on the surface.

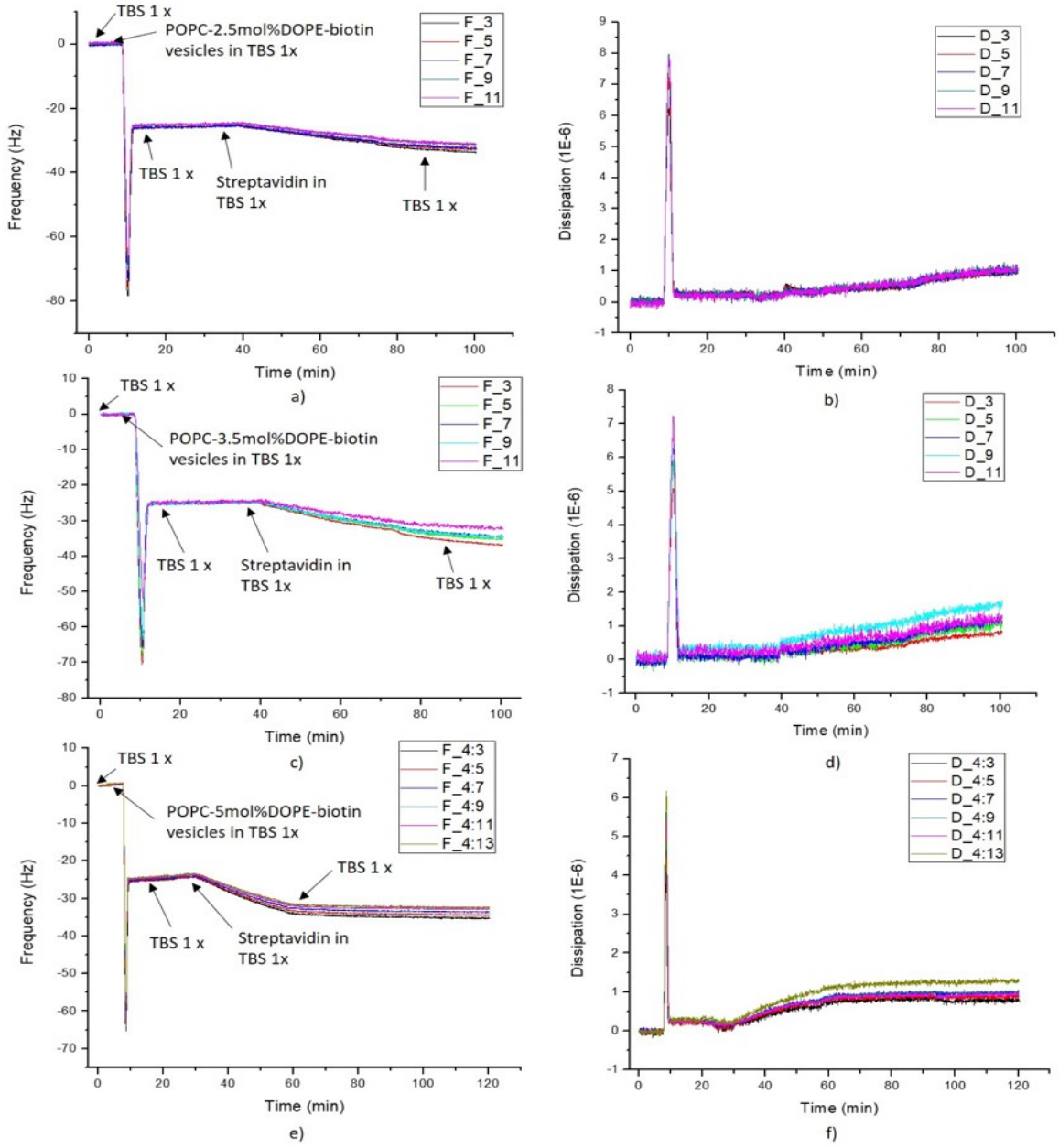


**Figure 3.41:** QCM-D experiments on supported lipid bilayer (TBS 1x buffer) assemblies with streptavidin (TBS 1x buffer). a) POPC-2.5mol%DOPE-biotin supported lipid bilayer interaction with streptavidin; b) POPC-2.5mol%DOPE-biotin supported lipid bilayer interaction with streptavidin dissipation profile; c) POPC-3.5mol%DOPE-biotin supported lipid bilayer interaction with streptavidin; d) POPC-3.5mol%DOPE-biotin supported lipid bilayer interaction with streptavidin dissipation profile; e) POPC-5mol%DOPE-biotin supported lipid bilayer interaction with streptavidin; f) POPC-5mol%DOPE-biotin supported lipid bilayer interaction with streptavidin dissipation profile

Furthermore, in order to see whether the increasing streptavidin amount on the SLB's surface has a linear proportionality to the surface coverage of stretavidin, an additional interaction test with POPC-5mol%DOPE-biotin SLB (fig. 3.41 e) and f)) was accomplished with QCM-

D. However, counter intuitively, the frequency shift after the addition of streptavidin, stemmed into 11.1 Hz (taken from the 3d overtone), which is a smaller value than previously mentioned POPC-3.5mol%DOPE-biotin supported lipid bilayer interaction with streptavidin (12.2 Hz). Consequently, supplementary research needs to be conducted to reach an appropriate explanation for this dependency. Also, it is important to mention, that all of the cases with different amount of biotin ligands resulted in the formation of rather rigid layers. Nevertheless, all in all, POPC-2mol%DOPE-biotin supported lipid bilayer structure was chosen as the foundation for upcoming interaction experiments with coated silica nanoparticles.

As appropriate coverage of streptavidin was reached, a test whether the coated silica particle non-binding to the assay is a problem of too low streptavidin coverage on the supported lipid bilayer. Hence, figure 3.42 illustrates this experiment with POPC-10mol%POPG and POPC-10mol%POPG- 1mol%DOPE-biotin coated silica NPs. However, as observed, no attachment of POPC-coated silica NPs with biotin functionalized headgroups is present, thus, an additional possible reason for non-binding can be a steric issue due to the fact that biotin headgroups on the POPC-coated silica nanoparticles are relatively small and probably result in unenvelopment event of supported lipid bilayer of the silica NPs during the interaction with the SLB.

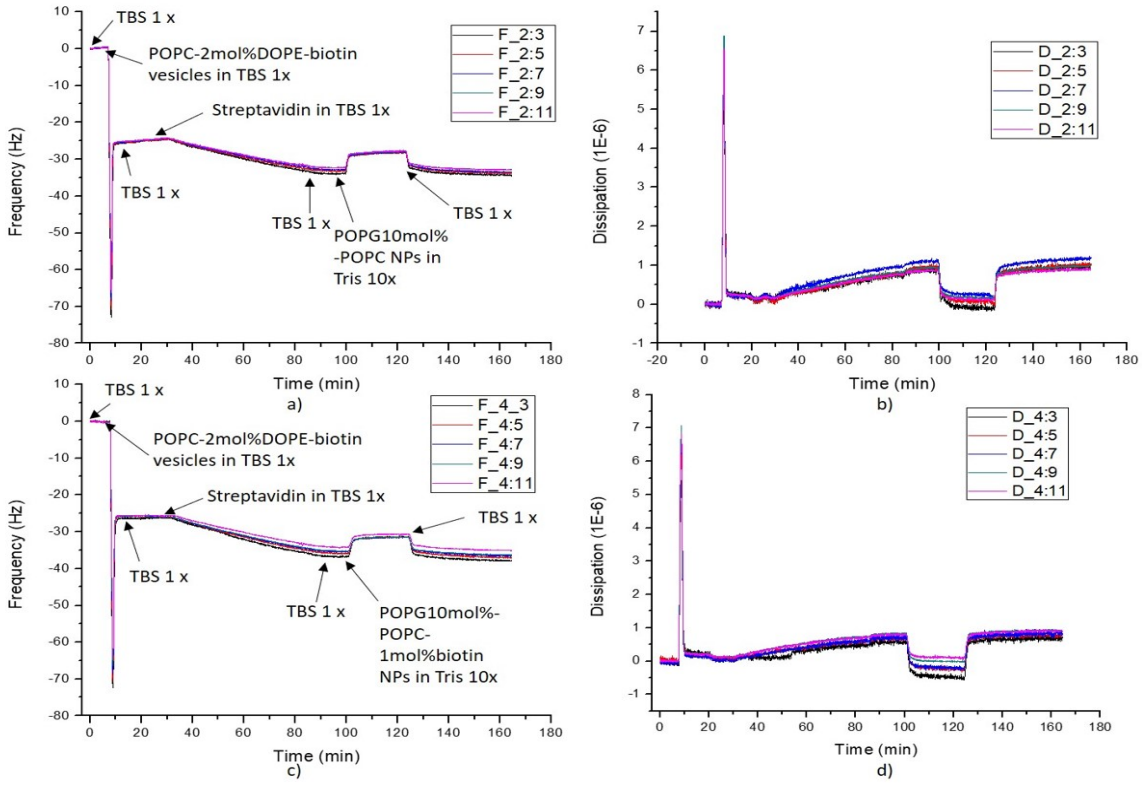


**Figure 3.42:** QCM-D experiments on supported lipid bilayer assemblies (TBS 1x buffer) with streptavidin (TBS 1x buffer) and coated silica NPs (Tris 10x buffer). a) POPC-2mol%DOPE-biotin supported lipid bilayer interaction with streptavidin and POPC-10mol%POPG coated NPs; b) POPC-2mol%DOPE-biotin supported lipid bilayer interaction with streptavidin and POPC-10mol%POPG coated NPs dissipation measurement; c) POPC-2mol%DOPE-biotin supported lipid bilayer interaction with streptavidin and POPC-10mol%POPG-1mol%DOPE-biotin coated NPs; d) POPC-2mol%DOPE-biotin supported lipid bilayer interaction with streptavidin and POPC-10mol%POPG-1mol%DOPE-biotin coated NPs dissipation measurement.

### 3.3.6 Neutravidin covered grafted polymer support (having PEG linkers) interactions with coated silica NPs containing or without PEG linkers

Further experiments were needed to test this theory of coated NP non-binding due to steric hindrance, therefore, two different setups were designed. Both of these setups contain polyethylene glycol (PEG) linkers, but differ in supported layers. One of the supported layer was chosen to be (Poly(L-Lysine)-g-Poly(ethylene-glycol)-biotin) or PLL-g-PEG-biotin, having PEG linkers on the substrate surface, and the other one POPC-2mol%DOPE-biotin, not having PEG linkers on the surface, but rather PEG linkers are incorporated on to the lipid bilayer coated silica NP's surface. In addition, some control experiments were conducted as well to see whether the binding of the coated NPs, if present, is influenced by the anionic lipids, integrated in the coated NP structure. These control experiments include both - coated silica NPs with anionic lipids and PEG linkers, and cases without anionic lipids, but with PEG linkers. Also, streptavidin was exchanged for neutravidin due to higher neutrality to non-specific reactions in the solution and highest specificity in comparison to avidin and streptavidin [95]. Furthermore, a model for setup having PLL-g-PEG-biotin as a support for coated NP with functionalized biotin headgroups interaction is seen in fig. 3.43.

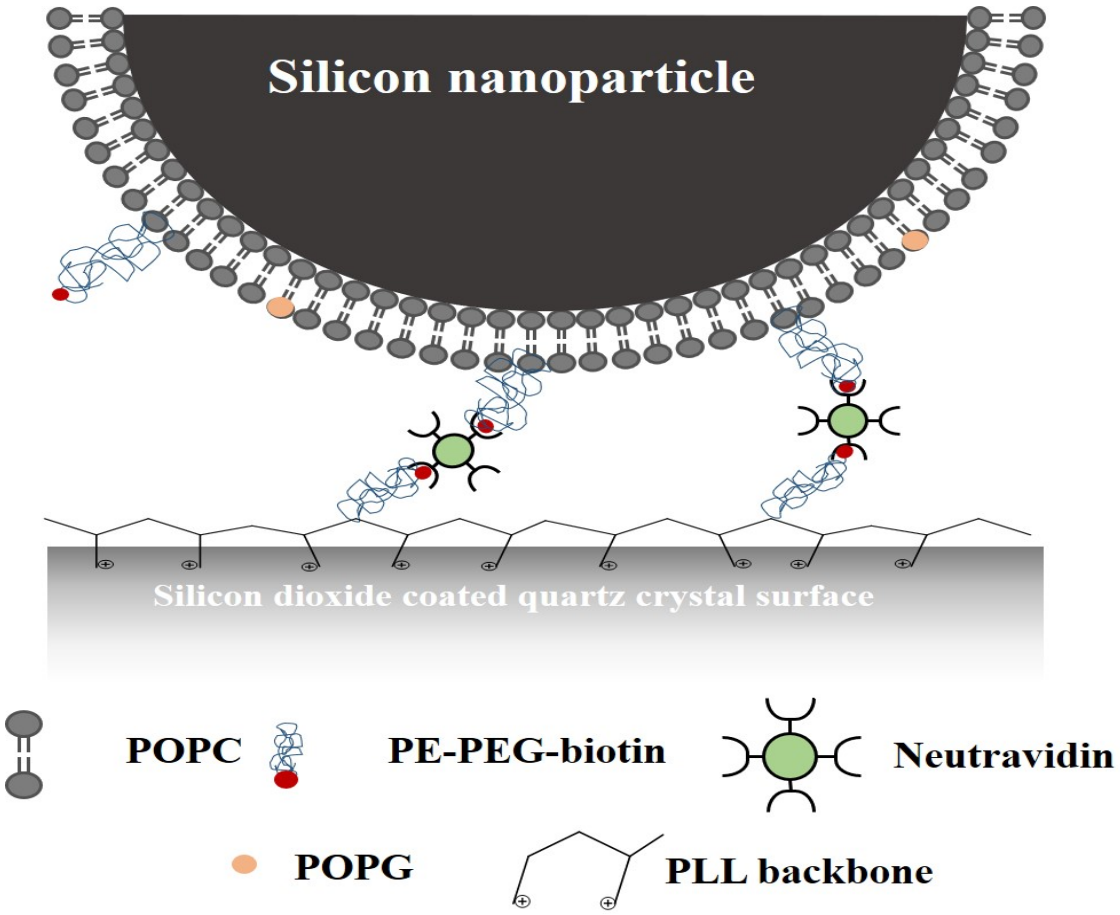


**Figure 3.43:** A display of a coated silica NP containing POPG and PEG-biotin functionalized headgroups in it's structure interacting with PLL-g-PEG-biotin covered with neutravidin. Take note that the dimensions are not to scale as bare silica NP z-average is $\approx$ 129 nm and supported lipid bilayer is estimated to be 5-7 nm thick [94].

The first experiment is presented in figure 3.44. In subfigure a) the test was run in this manner: injection of 1x TBS, 10 x Tris buffer (due to the fact that PLL-g-PEG-biotin polymer does not assemble that well on the silica surface in the presence of salts), PLL-g-PEG-biotin, wash with 1x TBS, addition of neutravidin, washing step with 1x TBS, POPC coated silica NPs and the washing step in the end with 1x TBS. The second test with coated silica NPs, including 10mol%POPG anionic lipids, is presented in subfigure b) and was carried out in the same manner as the experiment a). It is important to note that these two cases differ in terms of binding kinetics to the neutravidin covered PLL-g-PEG-biotin layer, which can be determined by the initial adsorption rates [96]:

$$r_d = -\frac{d\Delta f_n}{dt} \tag{3.1}$$

where $r_d$ is the adsorption rate on the $SiO_2$ surface of the quartz crystal sensor, $d\Delta f_n$ is the normalized change in frequency and dt is the difference in time of the measurement. It is important to note that the adsorption rates were calculated according to time periods, which seemed relevant for highest adsorption rates during single lipid bilayer coated silica nanoparticle binding to the neutravidin covered supported PLL-g-PEG-biotin layer. The estimations for these rates resulted in 0.00440 ng/s (first time point taken 108.644 min. and the second one = 145.087 min.; time points selected as educational guess for the highest adsorption rate in the time period of coated silica NP binding event) and 0.00398 ng/s (first time point taken 149.819 min. and the second one = 172.400 min.) in the cases of POPC coated silica and POPC-10mol%POPG coated silica NPs, respectively (taken from 3d overtone). In addition, in the case of POPC coated silica NPs, tangential function was added before the division term in equation 3.1 as exponential decay rather than linear behavior was observed. These values indicate, that single lipid bilayer coated silica NPs, that do not include anionic lipids, bind faster to the neutravidin covered supported polymer layer than their counterparts. The possible explanation for this event could be the induced electrostatic repulsion between coated silica nanoparticles, containing anionic lipids in their structure. Also, one can note that the assembly with POPC-10mol%POPG coated silica NPs is dissipating more energy than it's counterpart without the anionic lipid in it's structure.

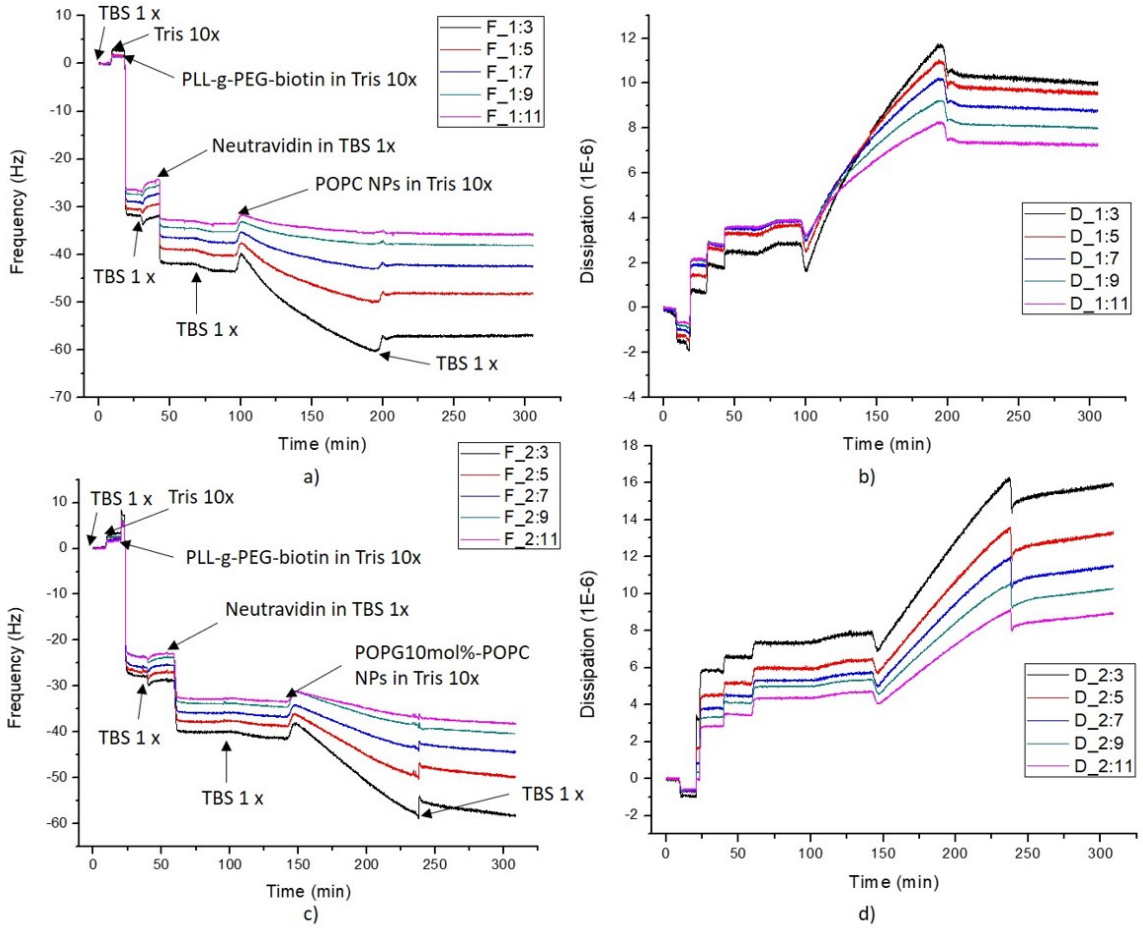


**Figure 3.44:** QCM-D experiments on grafted polymer layer assembly (Tris 10x buffer) with neutravidin (TBS 1x buffer) and coated silica NPs (Tris 10x buffer). a) PLL-g-PEG-biotin layer interaction with neutravidin and POPC coated NPs; b) PLL-g-PEG-biotin layer interaction with neutravidin and POPC coated NPs dissipation profile; c) PLL-g-PEG-biotin layer interaction with neutravidin and POPC-10mol%POPG coated NPs; d) PLL-g-PEG-biotin layer interaction with neutravidin and POPC-10mol%POPG coated NPs dissipation profile.

Other experiments with the same setup included single lipid bilayer coated silica nanoparticles with anionic lipids and different coverage of biotin in their structure (figure 3.45). By comparing two different structure coated silica NPs interaction experiments (fig. 3.45 a) and c)) binding kinetics, one can make a conclusion that with increasing ligand amount on the coated silica nanoparticle's surface, the adsorption rate increases as well. This is due to the fact that the adsorption rates resulted in 0.003718 ng/s (first time point = 156.269 min., second time point = 175.472 min.) and 0.00561 ng/s (first time point = 187.315 min., second time point = 202.086 min.) for POPC-10mol%POPG-1mol%DOPE-biotin coated NPs and POPC-10mol%POPG-5mol%DOPE-biotin coated NPs, accordingly (taken from 3d overtone). Of course, this conclusion might not be terminal due to the fact that only two experiments with two different biotin ligand densities on the coated silica NP surface were investigated and more data point could bring more evidence to this statement. In addition, the assemblies with POPC-10mol%POPG-1mol%DOPE-biotin coated NPs and POPC-10mol%POPG-5mol%DOPE-biotin coated NPs dissipate rather alike dissipation energies, except that POPC-10mol%POPG-5mol%DOPE-biotin coated NPs demonstrates higher

rigidness of the assembly compared to POPC-10mol%POPG-1mol%DOPE-biotin coated NPs due to closer proximity of the overtones in the dissipation profile.

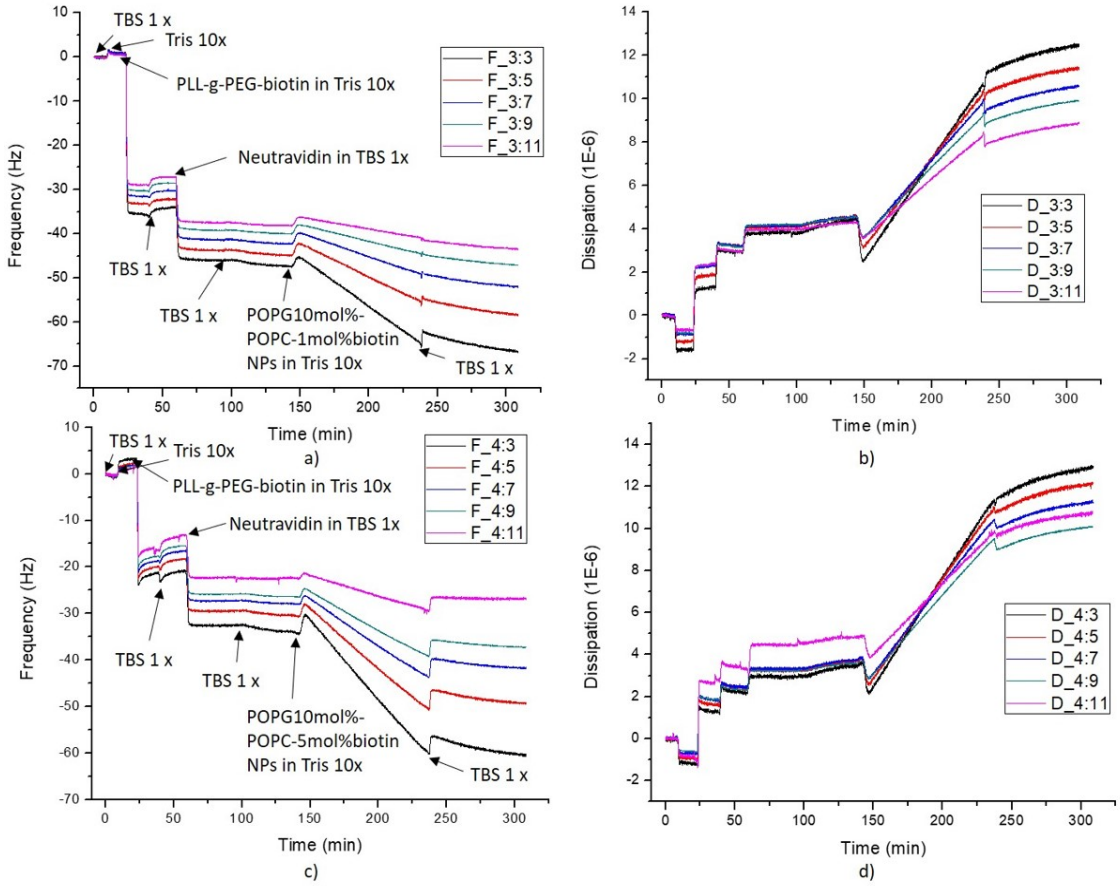


**Figure 3.45:** QCM-D experiments on grafted polymer layer assembly (Tris 10x buffer) with neutravidin (TBS 1x buffer) and coated silica NPs (Tris 10x buffer). a) PLL-g-PEG-biotin layer interaction with neutravidin and POPC-10mol%POPG-1mol%DOPE-biotin coated NPs; b) PLL-g-PEG-biotin layer interaction with neutravidin and POPC-10mol%POPG-1mol%DOPE-biotin coated NPs dissipation profile; c) PLL-g-PEG-biotin layer interaction with neutravidin and POPC-10mol%POPG-5mol%DOPE-biotin coated NPs; d) PLL-g-PEG-biotin layer interaction with neutravidin and POPC-10mol%POPG-5mol%DOPE-biotin coated NPs dissipation profile.

In correspondance to previously established QCM-D setup, additional control experiments were carried out with single lipid bilayer coated silica NPs containing PEG linkers in their structure. Firstly, experiments with coated silica nanoparticles containing PEG linkers, but without anionic lipids in their structure were attempted. The whole test was conducted in the same way as previously mentioned for the same PLL-g-PEG-biotin established supported layer. In figure 3.46, one can notice that both assemblies - POPC-0.1mol%PE-PEG-biotin coated NPs and POPC-1mol%PE-PEG-biotin coated NPs - dissipate relatively the same amount of energy at the end of the experiment (subfigures b) and d)). In addition, relating the frequency shifts at the same overtones, it is observable that supposedly a higher amount of POPC-1mol%PE-PEG-biotin coated NPs are attaching in comparison with POPC-0.1mol%PE-PEG-biotin coated NPs (subfigures a) and c)). Also, the adsorption rate for the higher PEG linker percentage including in their structure coates

silica NPs is bigger in resemblance with POPC-0.1mol%PE-PEG-biotin coated NPs; 0.00782 ng/s (first time point = 99.023 min., second time point = 112.315 min.) and 0.00800 ng/s (first time point = 107.016 min., second time point = 121.658 min.), respectively (taken from 3d overtone).

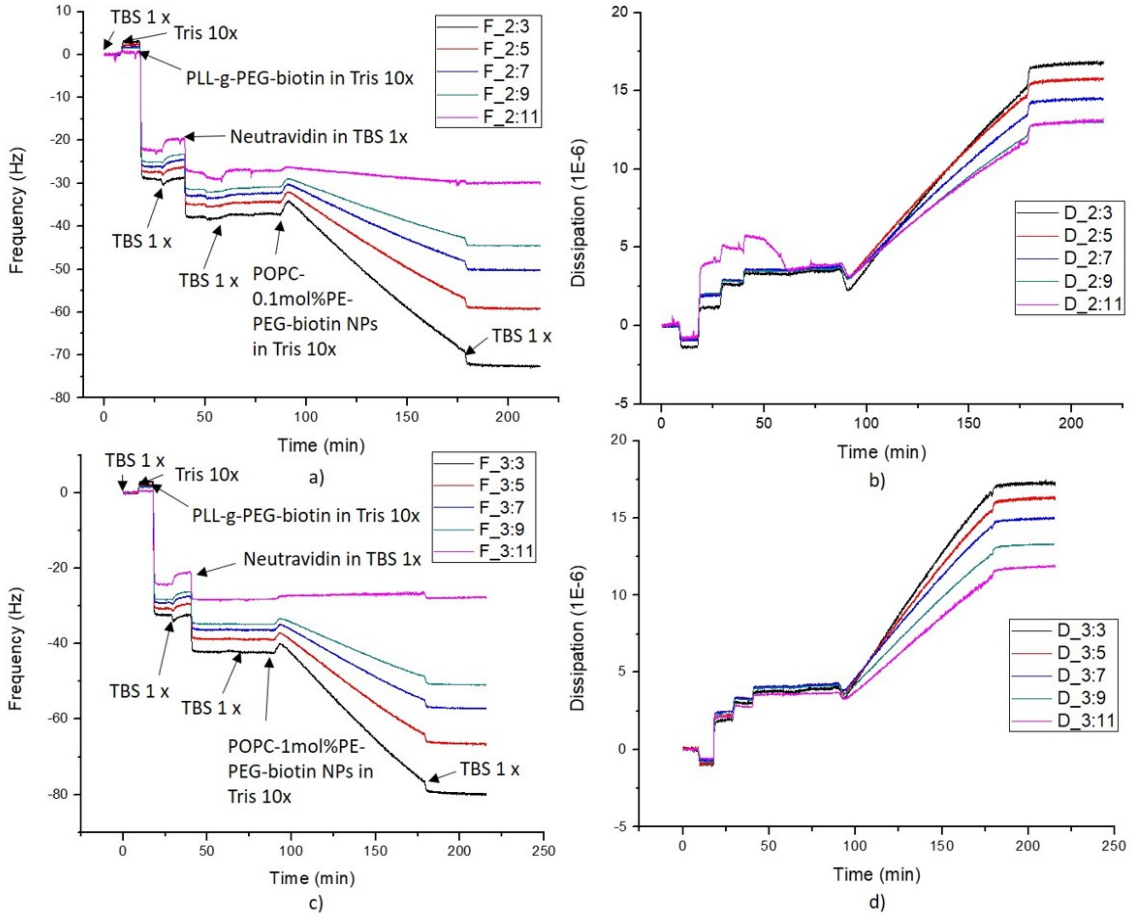


**Figure 3.46:** QCM-D experiments on grafted polymer layer assembly (Tris 10x buffer) with neutravidin (TBS 1x buffer) and coated silica NPs (Tris 10x buffer). a) PLL-g-PEG-biotin layer interaction with neutravidin and POPC-0.1mol%PE-PEG-biotin coated NPs; b) PLL-g-PEG-biotin layer interaction with neutravidin and POPC-0.1mol%PE-PEG-biotin coated NPs dissipation profile; c) PLL-g-PEG-biotin layer interaction with neutravidin and POPC-1mol%PE-PEG-biotin coated NPs; d) PLL-g-PEG-biotin layer interaction with neutravidin and POPC-1mol%PE-PEG-biotin coated NPs dissipation profile.

Furthermore, in respect with the same QCM-D setup and coated silica nanoparticles with PEG linkers, but not including anionic lipids in their structure, the coated silica NPs with anionic lipids and PEG linkers displayed (fig. 3.47) better binding to neutravidin covered PLL-g-PEG-biotin layer in terms of change in frequency (same overtones as in fig. 3.46). As in previously described cases without anionic lipids, POPC-10mol%POPG-0.1mol%PE-PEG-biotin coated NPs and POPC-10mol%POPG-1mol%PE-PEG-biotin coated NPs resulted in relatively analogous dissipation profiles (subfigures b) and d)). Also, it is important to mention, that the changes in frequencies during the coated silica NP binding are higher for POPC-10mol%POPG-1mol%PE-PEG-biotin coated NPs when compared to POPC-10mol%POPG-0.1mol%PE-PEG-biotin coated

NPs (for all overtones except 11th). In addition, the adsorption rates were estimated as 0.01213 ng/s (first time point = 103.134 min., second time point = 118.907 min.) and 0.01511 ng/s (first time point = 118.557 min., second time point = 131.688 min.) for POPC-10mol%POPG-0.1mol%PE-PEG-biotin coated NPs and POPC-10mol%POPG-1mol%PE-PEG-biotin coated NPs, accordingly (data taken from the 3d overtone). Thus, as observed in the previous case without the anionic lipids in the coated silica NP structure, with increasing PEG percentage in the coated NP, the adsorption rate is increasing as well leading to probable conclusion that the binding event is hastened by the amount of connection made between the coated silica NP with PEG linkers and and the neutravidin covered polymer layer.

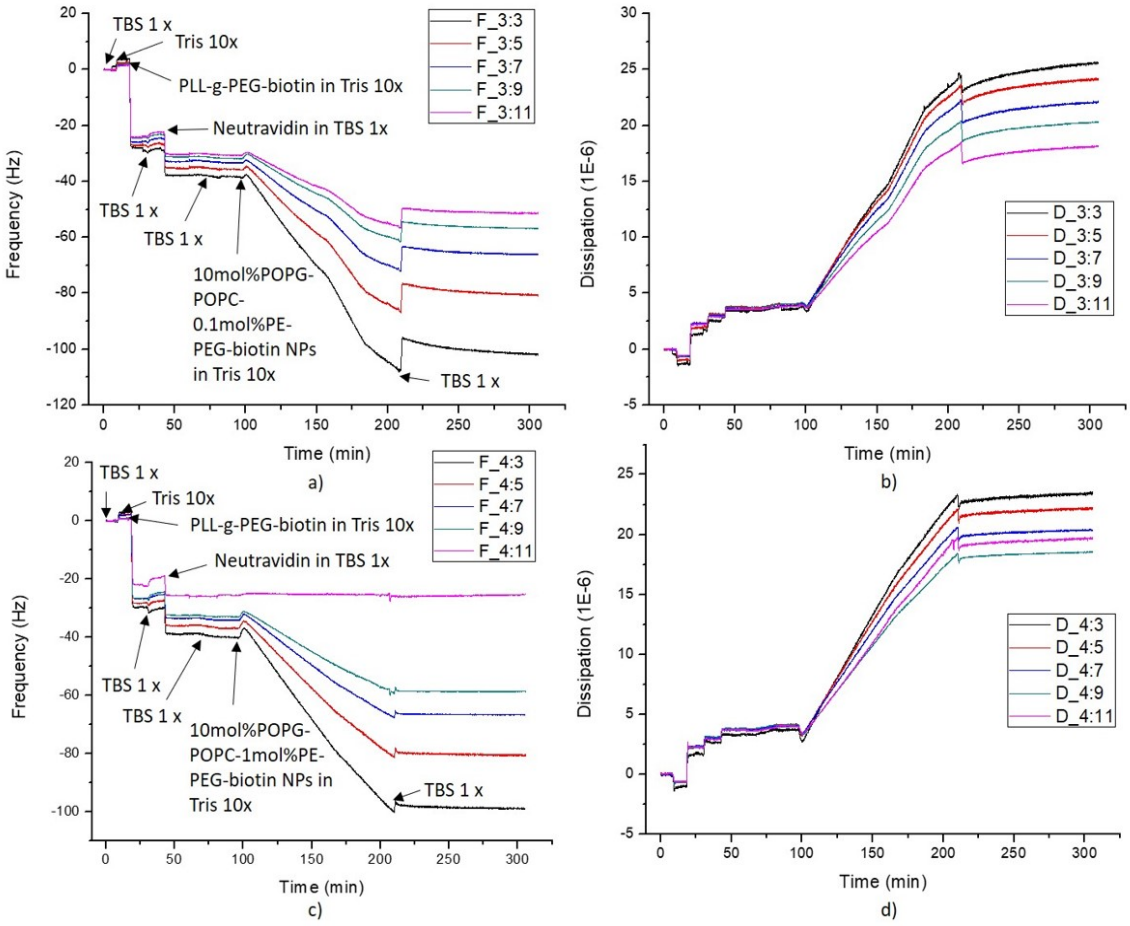


**Figure 3.47:** QCM-D experiments on grafted polymer layer assembly (Tris 10x buffer) with neutravidin (TBS 1x buffer) and coated silica NPs (Tris 10x buffer). a) PLL-g-PEG-biotin layer interaction with neutravidin and POPC-10mol%POPG-0.1mol%PE-PEG-biotin coated NPs; b) PLL-g-PEG-biotin layer interaction with neutravidin and POPC-10mol%POPG-0.1mol%PE-PEG-biotin coated NPs dissipation profile; c) PLL-g-PEG-biotin layer interaction with neutravidin and POPC-10mol%POPG-1mol%PE-PEG-biotin coated NPs; d) PLL-g-PEG-biotin layer interaction with neutravidin and POPC-10mol%POPG-1mol%PE-PEG-biotin coated NPs dissipation profile.

All in all, even though, the PLL-g-PEG-biotin setup has risen some ideas about how coated NPs interact with the supported layers, was disregarded as a fundamental base for other experiments due to the fact that electric double layer event takes place between the positively charged supported

PLL-g-PEG-biotin layer and the single lipid bilayer coated silica NPs with anionic lipids in their structure, thus, leading to rather unwanted additional interaction force.

### 3.3.7 Neutravidin covered supported lipid bilayer interactions with coated silica NPs containing or without PEG linkers

The final interaction experiments included POPC-2mol%DOPE-biotin SLB setup (fig. 3.48) with neutravidin and the same control experiments with different structure containing coated silica NPs with or without PEG linkers as in the case of PLL-g-PEG-biotin polymer layer setup.

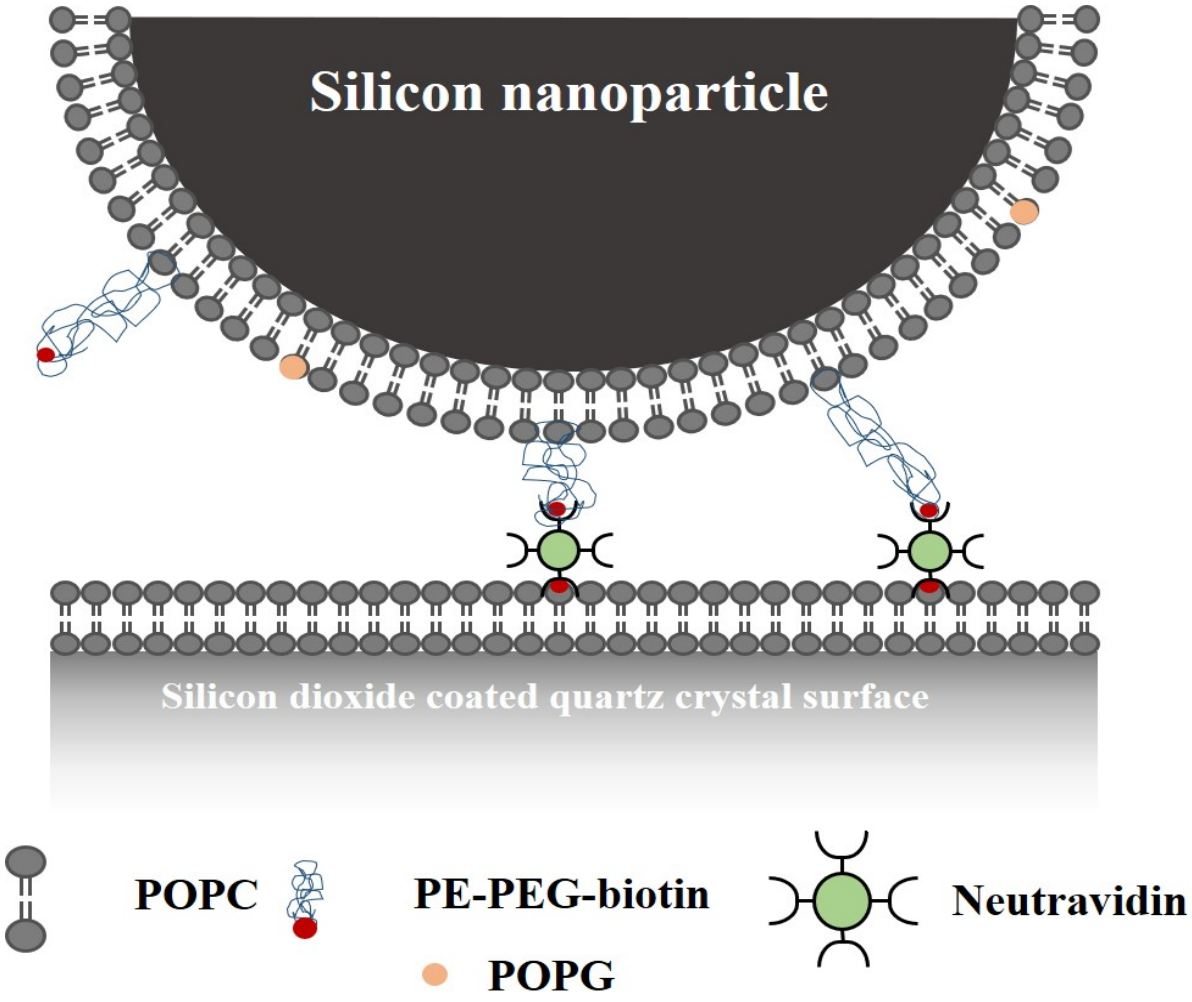


**Figure 3.48:** A display of a coated silica NP containing POPG and PEG-biotin functionalized headgroups in it's structure interacting with an SLB covered with neutravidin. Take note that the dimensions are not to scale as bare silica NP z-average is ≈ 129 nm and supported lipid bilayer is estimated to be 5-7 nm thick [94].

Firstly, the binding of POPC and POPC-10mol%POPG coated silica NPs was tested (as seen in fig. 3.49). Both subfigures a) and c) represent no attachment of POPC or POPC-10mol%POPG coated silica NPs to the neutravidin covered POPC-2mol%DOPE-biotin SLB, which was expected as the coated nanoparticles do not contain biotin ligands on their surface to bind to neutravidin molecules. Secondly, experiments including the same SLB setup and coated silica nanoparticles with PEG linkers, with and without anionic lipids and biotin ligands were conducted (fig. 3.50).

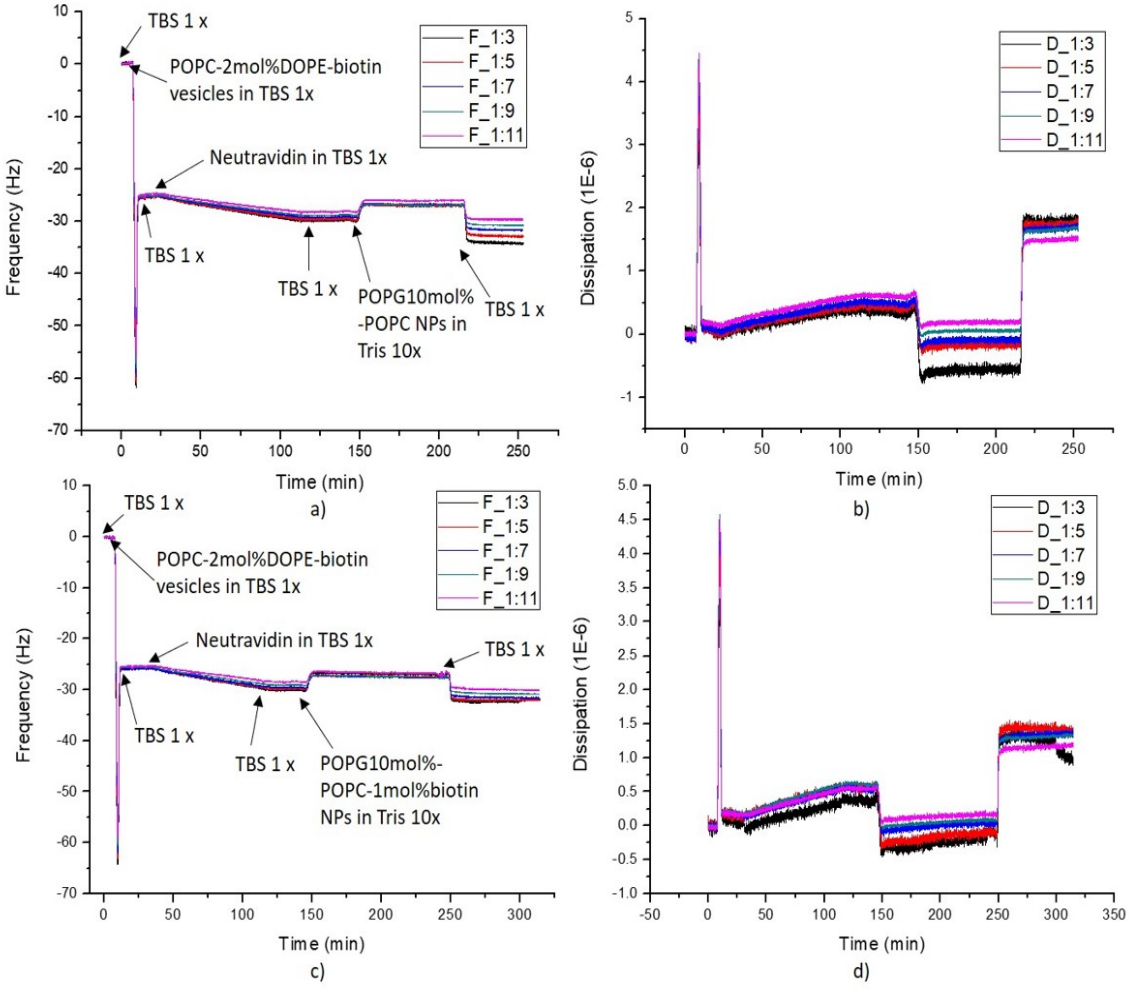


**Figure 3.49:** QCM-D experiments on supported lipid bilayer assemblies (TBS 1x buffer) with neutravidin (TBS 1x buffer) and coated silica NPs (Tris 10x buffer). a) POPC-2mol%DOPE-biotin supported lipid bilayer interaction with neutravidin and POPC coated NPs; b) POPC-2mol%DOPE-biotin supported lipid bilayer interaction with neutravidin and POPC coated NPs dissipation measurement; c) POPC-2mol%DOPE-biotin supported lipid bilayer interaction with neutravidin and POPC-10mol%POPG coated NPs; d) POPC-2mol%DOPE-biotin supported lipid bilayer interaction with neutravidin and POPC-10mol%POPG coated NPs dissipation measurement.

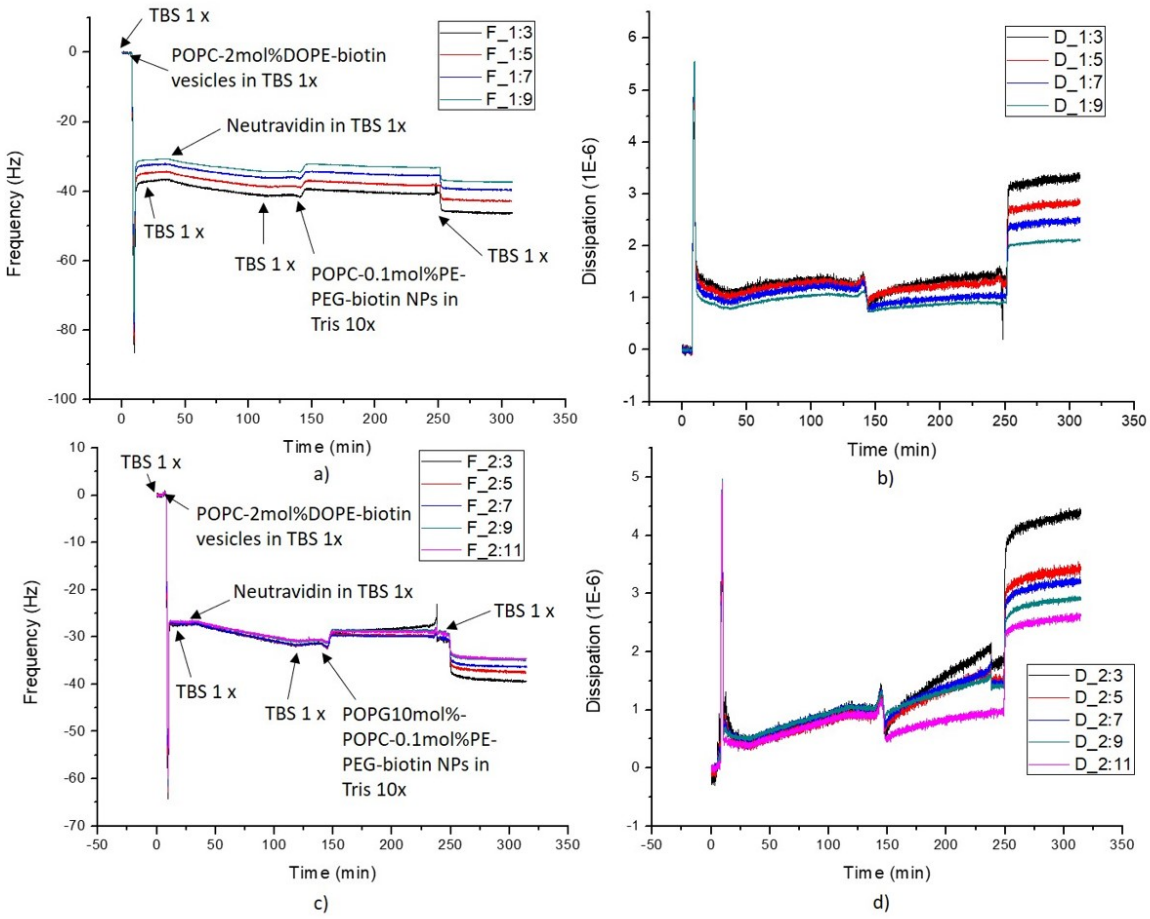


**Figure 3.50:** QCM-D experiments on supported lipid bilayer assemblies (TBS 1x buffer) with neutravidin (TBS 1x buffer) and coated silica NPs (Tris 10x buffer). a) POPC-2mol%DOPE-biotin supported lipid bilayer interaction with neutravidin and POPC-0.1mol%PE-PEG-biotin coated NPs; b) POPC-2mol%DOPE-biotin supported lipid bilayer interaction with neutravidin and POPC-0.1mol%PE-PEG-biotin coated NPs dissipation measurement; c) POPC-2mol%DOPE-biotin supported lipid bilayer interaction with neutravidin and POPC-10mol%POPG-0.1mol%PE-PEG-biotin coated NPs; d) POPC-2mol%DOPE-biotin supported lipid bilayer interaction with neutravidin and POPC-10mol%POPG-0.1mol%PE-PEG-biotin coated NPs dissipation measurement.

Even though, in these experiments (fig. 3.50) the dissipation profiles (b) and d)) for POPC-0.1mol%PE-PEG-biotin coated NPs and POPC-10mol%POPG-0.1mol%PE-PEG-biotin coated NPs, respectively, yield higher dissipation values for the corresponding overtones compared to the coated silica NPs without PEG-biotin ligands (fig. 3.49), no significant binding to the neutravidin covered SLB is observed. This raises a hypothesis that there might be a certain boundary for the molar concentration of PEG-biotin linkers, at which single lipid bilayer coated silica NPs do not bind or the amount of linker connections with the support are too weak to hold the coated NP attached. Hence, interaction experiments with increasing amount of PEG-biotin linkers were administered.

As observed in figure 3.51, the inclusion of higher molar per cent of PEG-biotin linkers on the coated silica NP surface, in this case 1mol% instead of 0.1mol%, results in the coated NP binding

to the neutravidin covered SLB.

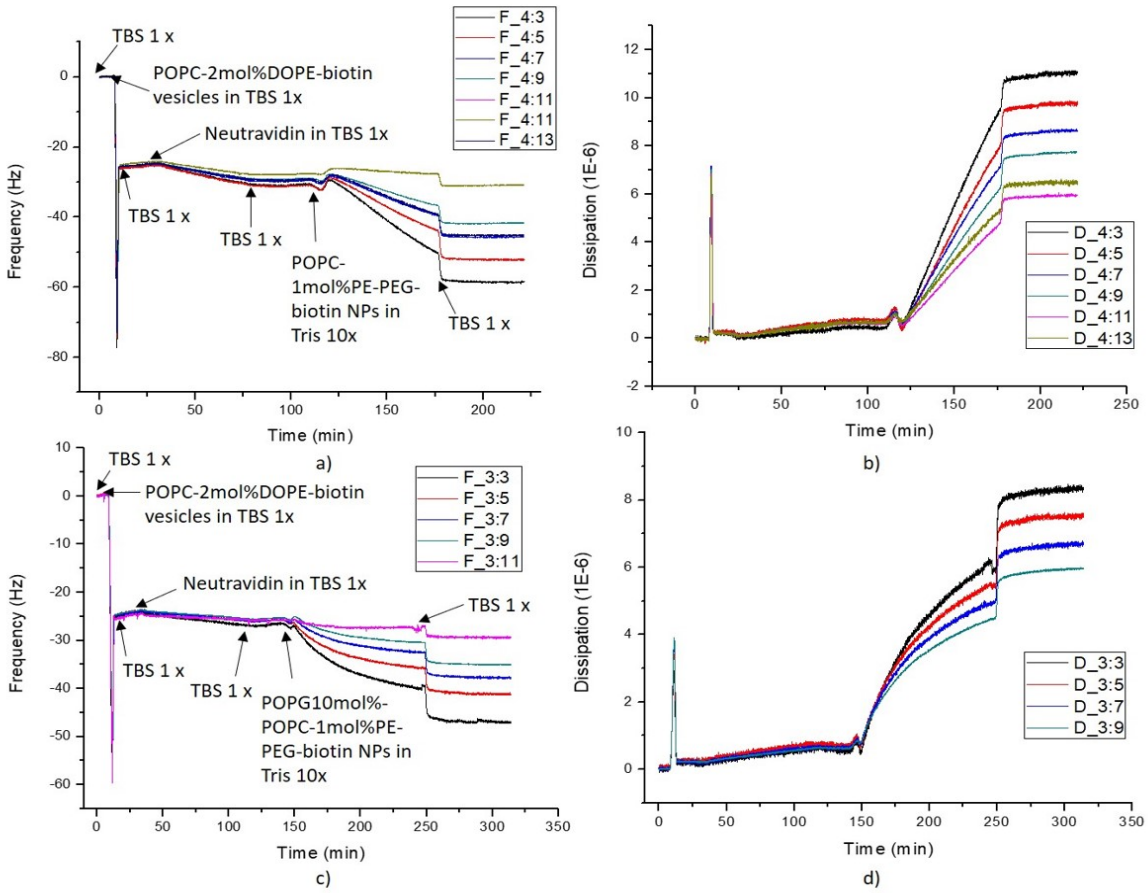


**Figure 3.51:** QCM-D experiments on supported lipid bilayer assemblies (TBS 1x buffer) with neutravidin (TBS 1x buffer) and coated silica NPs (Tris 10x buffer). a) POPC-2mol%DOPE-biotin supported lipid bilayer interaction with neutravidin and POPC-1mol%PE-PEG-biotin coated NPs; b) POPC-2mol%DOPE-biotin supported lipid bilayer interaction with neutravidin and POPC-1mol%PE-PEG-biotin coated NPs dissipation measurement; c) POPC-2mol%DOPE-biotin supported lipid bilayer interaction with neutravidin and POPC-10mol%POPG-1mol%PE-PEG-biotin coated NPs; d) POPC-2mol%DOPE-biotin supported lipid bilayer interaction with neutravidin and POPC-10mol%POPG-1mol%PE-PEG-biotin coated NPs dissipation measurement.

In addition, the adsorption rates were calculated and granted values of 0.00696 ng/s (first time point = 142.905 min., second time point = 152.865 min.) and 0.00485 ng/s (first time point = 151.800 min., second time point = 171.390 min.) for POPC-1mol%PE-PEG-biotin and POPC-10mol%POPG-1mol%PE-PEG-biotin coated NPs, accordingly, inclining that the inclusion of anionic POPG lipids on the coated silica NP surface decreases the binding rate (data taken from the 3d overtone). This might be explained by possible electronegative repulsion between the coated silica NPs while the attachment event is occurring. Thus, the next shown results will not include coated silica NPs with anionic lipids even though a certain degree of aggregation for such particles were observed before (figures 3.27 and 3.28 b)). In order to obtain more data for the boundary, in terms of PEG-biotin linker amount on the coated silica NP surface, at which coated silica NPs start binding to the neutravidin covered supported lipid bilayer, as well as for binding rate dependencies,

supplementary experiments were carried out with the same setup as discussed before, except for varying molar concentrations of PEG-biotin ligands on the coated silica NP surface (figure 3.52).

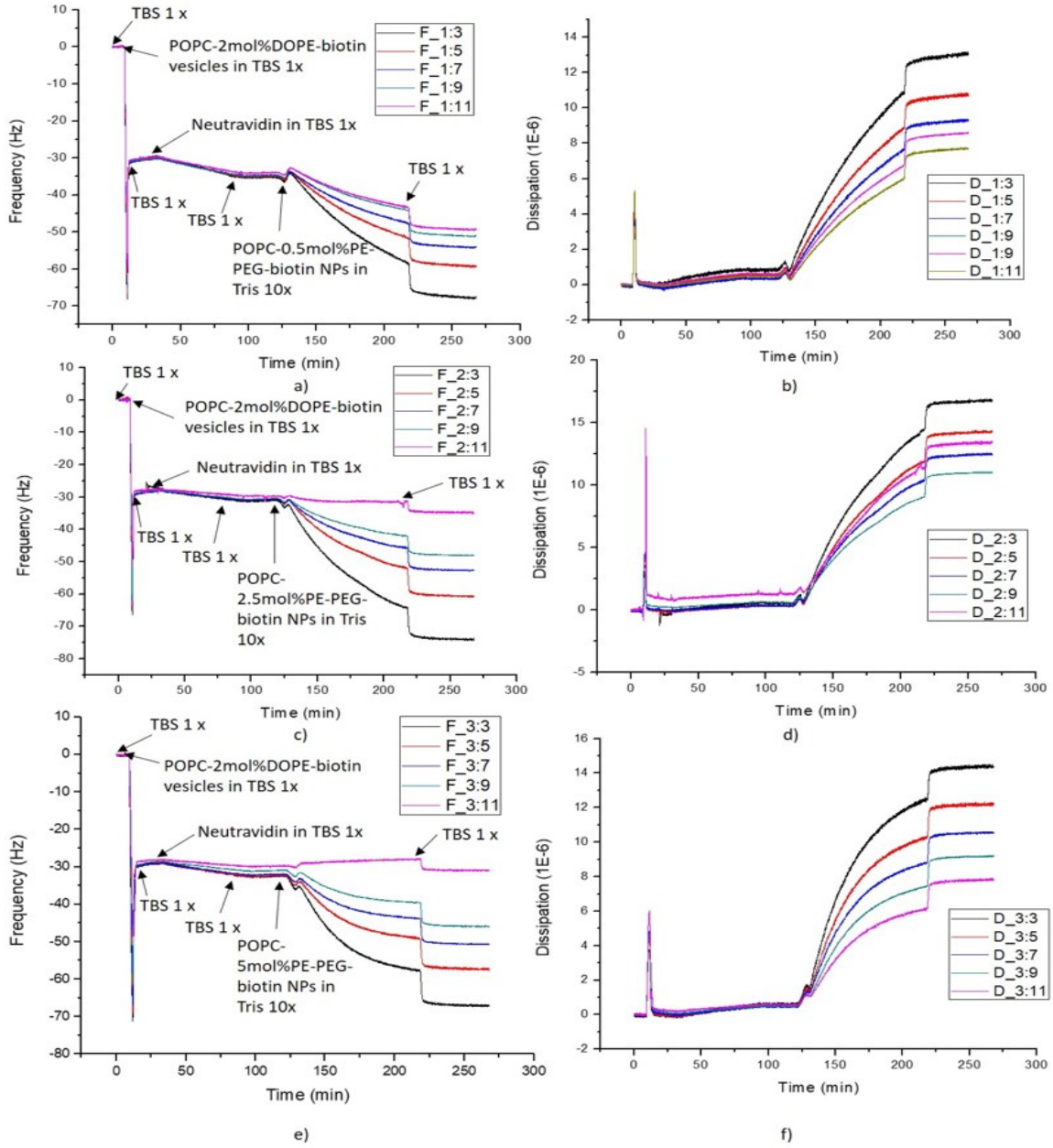


**Figure 3.52:** QCM-D experiments on supported lipid bilayer assemblies (TBS 1x buffer) with neutravidin (TBS 1x buffer) and coated silica NPs (Tris 10x buffer). a) POPC-2mol%DOPE-biotin supported lipid bilayer interaction with neutravidin and POPC-0.5mol%PE-PEG-biotin coated NPs; b) POPC-2mol%DOPE-biotin supported lipid bilayer interaction with neutravidin and POPC-0.5mol%PE-PEG-biotin coated NPs dissipation measurement; c) POPC-2mol%DOPE-biotin supported lipid bilayer interaction with neutravidin and POPC-2.5mol%PE-PEG-biotin coated NPs; d) POPC-2mol%DOPE-biotin supported lipid bilayer interaction with neutravidin and POPC-2.5mol%PE-PEG-biotin coated NPs dissipation measurement; e) POPC-2mol%DOPE-biotin supported lipid bilayer interaction with neutravidin and POPC-5mol%PE-PEG-biotin coated NPs; f) POPC-2mol%DOPE-biotin supported lipid bilayer interaction with neutravidin and POPC-5mol%PE-PEG-biotin coated NPs dissipation measurement.

As observed in fig. 3.52 a) the binding of POPC-0.5mol%PE-PEG-biotin coated NPs occurs, indicating that the possible boundary is in the range between POPC-0.1mol%PE-PEG-biotin (no binding) and POPC-0.5mol%PE-PEG-biotin coated NPs (binding witnessed). However, due to time restrictions for this project, different molar concentration in the range of 0.1-0.5mol%PE-PEG-biotin were not looked into further and would need more investigating in order to establish more accurate results. Nevertheless, the fig. 3.52 c) also displays the attachment of 2.5mol%PE-PEG-biotin coated NPs to the neutravidin covered supported lipid bilayer surface. Hence, the adsorption rates for both cases were estimated as 0.00604 ng/s (First time point = 139.002 min., second time point = 163.249 min.) and 0.007547 ng/s (First time point = 128.437 min., second time point = 139.890 min.), respectively. Also, by comparing the two dissipation profiles (figure 3.52 b) and d)), one can notice that the system with POPC-2.5mol%PE-PEG-biotin coated NPs dissipated more energy than the one with POPC-0.5mol%PE-PEG-biotin coated NPs (according to the same overtones). The last molar concentration of PEG-biotin ligands for the coated silica NPs was chosen to be 5mol% due to the fact that extra data point was needed to establish a dependency of such ligand molar concentration on the adsorption rate. The experiment is demonstrated in fig. 3.52 e) and f). Even though, the dissipation energy is lower (when comparing the same overtones) in this case compared to 2.5mol%PE-PEG-biotin coated NPs, the estimation for the adsorption rate was higher and yielded 0.0087697 ng/s (first time point = 131.987 min., second time point = 150.222 min.). Consequently, these last experiments with varying PE-PEG-biotin linker molar concentrations on the single lipid bilayer coated silica NP surfaces led to a conclusion that with increasing PE-PEG-biotin ligand density, coated silica NPs bind faster to the neutravidin covered supported lipid bilayer.

# 4. Conclusion

## 4.1 Liposome production

Through the project, an optimized protocol for necessary size and polydispersity liposomes has been produced. The key factors, influencing the vesicle manufacturing, were: changing the general assembly mode from solvent injection to rehydration, inclusion of tip sonication (with parameters: output 6 (probe), sonication time 20 minutes, 100% duty cycle), anionic lipids (either POPG or POPS) and extrusion through 100 and 30 nm membranes. Consequently, the size range for obtained liposomes were z - average $\approx$ 51 - 65 nm and PDI: $\approx$ 0.1 - 0.17, indicating that these vesicles are SUVs and rather monodisperse according to DLS intensity size distribution data.

## 4.2 Silica NP activation and stability

It was observed that bare silica NPs (z - average = 129.1 nm (DLS size intensity results; activated)) influence the silica NP coating procedure depending whether they are activated with hydroxy groups or not and how well they are cleaned with ethanol and water during the activation protocol. Also, they display relatively low stability in terms of aggregation and zeta potential. As seen, the z - average size of these particles tend to drift higher values (170 - 180 nm) within the time period of a week, hence, need to be bath sonicated for $\approx$ 2 hours before applying them in the coating procedure. Moreover, the zeta potential of these bare activated silica NPs (in 10 x Tris) changes as well within a period of one - three months from $\approx$ -43 mV to $\approx$ -49 mV.

## 4.3 Silica nanoparticle coating procedure

The initial silica NP coating protocol was optimized to achieve appropriate size and polydispersity of the particles (z - average $\approx$ 160 - 170 nm; PDI $\approx$ 0.24 - 0.27; DLS measurements) by varying these parameters: reducing the liposome size and polydispersity to the values mentioned beforehand (section 4.1); optimizing mixing type and vortexing speed, incubation time after the addition of all necessary ingredients, silica NP pretreatment with bath sonication for 2 hours and liposome/NP surface area ratio. Also, different salt concentrations during liposome production or coating procedure as well as addition of $Ca^{2+}$ ions during coating of the silica NPs had no significant effects in terms of their z-average diameter size and polydispersity. Nevertheless, the achieved coated colloid dispersions were used for interaction experiments with QCM-D machinery.

## 4.4 QCM-D interaction experiments

The single lipid bilayer coated silica NPs, with or without biotin ligands, interactions with either streptavidin/neutravidin covered supported lipid bilayer or PLL-g-PEG grafted polymer layer were investigated. It was seen that coated NPs either with or without anionic lipids and biotin functionalized headgroups in their structure do not bind to different coverage of streptavidin

attached to single lipid bilayers. Thus, an assumption was made to include PEG linkers in their structure, suggesting that the issue of non-binding was of sterical manner. The hypothesis was proven and the single lipid bilayer coated silica NPs, with and without anionic lipids, and containing at least 0.5mol% of PE-PEG-biotin ligands in their structure, attach to the neutravidin covered single lipid bilayer. In addition it was observed that with the increasing PE-PEG-biotin ligand density on the coated silica NP surface the initial adsorption rate on the neutravidin covered supported lipid bilayer increases as well. Furthermore, even though experiments with PLL-g-PEG grafted polymer setup were conducted, it should be kept in mind that they do not yield the necessary results as the single lipid bilayer coated silica NPs with anionic lipids in their structure most probably attach due to occurring electric double layer interaction in the addition to specific biotin-neutravidin interaction.

All in all, the outlook for this project includes investigation of the effect on the avidity of the targeted nanoparticle by ligand density in relation to particle dimensions (other than z - average = 129.1 nm) and ligand mobility, characterization and functionalization of iron oxide nanoparticles with single lipid membranes and investigate their interactions as for silicon oxide particles, test additional new optical sensing setups for kinetic measurements of nanoparticle binding events and move the research focus to lectin-type interactions.

# Bibliography


[1] A. Lundgren, B. Agnarsson, R. Zirbs, V. P. Zhdanov, E. Reimhult, and F. Höök. Nonspecific colloidal-type interaction explains size-dependent specific binding of membrane-targeted nanoparticles. *ACS Nano*, 10:9974–9982, 2016.

[2] M. Mammen, S. K. Choi, and G. M. Whitesides. Polyvalent interactions in biological systems: implications for design and use of multivalent ligands and inhibitors. *Angew. Chem., Int. Ed.*, 37:2754–2794, 1998.

[3] B. D. Chithrani, A. A. Ghazani, and W.C.W. Chan. Determining the size and shape dependence of gold nanoparticle uptake into mammalian cells. *Nano Lett.*, 6:662–668, 2006.

[4] W. Jiang, B.Y.S. Kim, J.T. Rutka, and W.C.W. Chan. Nanoparticle-mediated cellular response is size-dependent. *Nat. Nanotechnol.*, 3:145–150, 2008.

[5] E.A. Sykes, J. Chen, G. Zheng, and W.C.W. Chan. Investigating the impact of nanoparticle size on active and passive tumor targeting efficiency. *ACS Nano*, 8:5696–5706, 2014.

[6] X.X. Liu, N. Huang, H. Li, Q. Jin, and J. Ji. Surface and size effects on cell interaction of gold nanoparticles with both phagocytic and nonphagocytic cells. *Langmuir*, 29:9138–9148, 2013.

[7] Arnida, A. Malugin, and H. Ghandehari. Cellular uptake and toxicity of gold nanoparticles in prostate cancer cells: a comparative study of rods and spheres. *J.Appl.Toxicol.*, 30:212–217, 2013.

[8] S.L. Zhang, J. Li, G. Lykotrafitis, G. Bao, and S. Suresh. Size-dependent endocytosis of nanoparticles. *Adv.Matter*, 21:419–424, 2009.

[9] H.J. Gao, W.D. Shi, and L.B. Freund. Mechanics of receptor-mediated endocytosis. *Proc. Natl. Acad. Sci. U.S.A.*, 102:9469–9474, 2005.

[10] J. Rejman, V. Oberle, I.S. Zuhorn, and D. Hoekstra. Size-dependent internalization of particles via the pathways of clathrin-and caveolae-mediated endocytosis. *Biochem.J.*, 377:159–169, 2004.

[11] T. Mironava, M. Hadjiargyrou, M. Simon, V. Jurukovski, and M. H. Rafailovich. Gold nanoparticles cellular toxicity and recovery: effect of size, concentration and exposure time. *Nanotoxicology*, 4:120–137, 2010.

[12] M. Bally, A. Gunnarsson, L. Svensson, G. Larson, V.P. Zhdanov, and F. Höök. Interaction of single viruslike particles with vesicles containing glycosphingolipids. *Phys. Rev. Lett.*, 107:188103, 2011.

[13] J. Liu, G.E.R. Weller, B. Zern, P.S. Ayyaswamy, D.M. Eckmann, V.R. Muzykantov, and R. Radhakrishnan. Computational model for nanocarrier binding to endothelium validated using in vivo, in vitro, and atomic force microscopy experiments. *Proc. Natl. Acad. Sci. U.S.A.*, 107:16530–16535, 2010.

[14] J. Liu, N.J. Agrawal, A. Calderon, P.S. Ayyaswamy, D.M. Eckmann, and R. Radhakrishnan. Multivalent binding of nanocarrier to endothelial cells under shear flow. *Biophys. J.*, 101:319–326, 2011.

[15] T. Soukka, H. Harma, J. Paukkunen, and T. Lovgren. Utilization of kinetically enhanced monovalent binding affinity by immunoassays based on multivalent nanoparticle-antibody bioconjugates. *Anal. Chem.*, 73:2254–2260, 2001.

[16] S. Hong, P. R. Leroueil, I.J. Majoros, B. G. Orr, J.R. Jr. Baker, and M. M. B. Holl. The binding avidity of a nanoparticle-based multivalent targeted drug delivery platform. *Chem. Biol.*, 14:107–115, 2007.

[17] C. Tassa, J.L. Duffner, T.A. Lewis, R. Weissleder, S. L. Schreiber, A. N. Koehler, and S. Y. Shaw. Binding affinity and kinetic analysis of targeted small molecule-modified nanoparticles. *Bioconjugate Chem.*, 21:14–19, 2010.

[18] G. Pabst, N. Kučerka, Mu-Ping Nieh, and J. Katsaras. Liposomes, Lipid Bilayers and Model Membranes. *CRC Press, Taylor & Francis Group*, 2014.

[19] V. P. Torchilin. Recent advances with liposomes as pharmaceutical carriers. *Nature Reviews Drug Discovery*, 4(2):145–160, 2005.

[20] A. Akbarzadeh, R. Rezaei-Sadabady, S. Davaran, S. W. Joo, N. Zarghami, Y. Hanifehpour, M. Samiei, M. Kouhi, and K. Nejati-Koshki. Liposome: classification, preparation, and applications. *Nanoscale Research Letters*, 8(1):102, 2013.

[21] D. D. Lasic and D. Papahadjopoulos. Liposomes revisited. *Science (New York, N.Y.)*, 267(5202):1275–1276, 1995.

[22] M. L. Immordino, F. Dosio, and L. Cattel. Stealth liposomes: Review of the basic science, rationale, and clinical applications, existing and potential, 2006.

[23] A. Sharma and Uma S. Sharma. Liposomes in drug delivery: Progress and limitations, 1997.

[24] Hans-Jurgen Butt, G. Karlheinz, and M. Kappl. *Physics and Chemistry of Interfaces*, volume I. WILEY-VCH GmbH and Co. KGaA, 1995.

[25] L. Danilo and F. Martin. *Stealth Liposomes*, volume I. CRC Press, Inc, 1995.

[26] F. Olson, C.A.Hunt, F.C. Szoka, W.J. Vail, and D. Papahadjopoulos. Preparation of liposomes of defined size distribution by extrusion through polycarbonate membranes. *Biochimica et Biophysica Acta*, 557:9–23, 1979.

[27] A.K. Dua, J.S., Rana. A.C., Bhandari. Liposome : methods of preparation and applications. *International Journal of Pharmaceutical Studies and Research*, III(II):14–20, 2012.

[28] G. Trefalt and M. Borkovec. *Overview of DLVO Theory*. `www.colloid.ch/dlvo`. Accessed: 10-04-2018, 15:48.

[29] K.H. Jürgen Buschow, R.W. Cahn, M.C. Flemings, B. Ilschner, E.J. Kramer, S. Mahajan, and P. Veyssière. *Encyclopedia of Materials: Science and Technology*. Elsevier Science Ltd, 2001.

[30] W. Van Megen and I. Snook. Structure of dispersions of small, strongly interacting particles. *J.Chem.Soc.Faraday Trans.II*, 7:1095, 1979.

[31] E. J. Lane and H.T. Spurling. Forces between adsorbing walls: Monte Carlo calculations. *Chem.Phys.Lett.*, 67:107, 1979.

[32] P. Tarazona and L. Vicente. A model for density oscillations in liquids between solid walls. *Mol.Phys.*, 56:557, 1985.

[33] S.V. Mitlin and M.M. Sharma. Lattice-fluid model for solvation force oscillations in nonionic fluid films. *J. Colloid Interface Sci.*, 170:407, 1995.

[34] R.G. Horn. Surface forces and their action in ceramic materials. *J.Am.Ceram.Soc.*, 73:1117–1135, 1990.

[35] K.H. Christenson. Experimental measurements of solvation forces in nonpolar liquids. *J. Chem. Phys.*, 78:6906, 1983.

[36] J. Stetefeld, A.S. McKenna, and R.T. Patel. Dynamic light scattering: a practical guide and applications in biomedical sciences. *Biophys.Rev.*, 8:409–427, 2016.

[37] R. Pecora. Dynamic light scattering measurement of nanometer particles in liquids. *Journal of Nanoparticle Research*, 2:123–131, 2000.

[38] P. Zakharov and F. Scheffold. Advances in dynamic light scattering techniques. *Light Scattering Reviews*, 4:433–467, 2010.

[39] R. Simha. The influence of Brownian movement on the viscosity of solutions. *J. Phys. Chem*, 44(1):25–34, 1940.

[40] M. Kaszuba, D. McKnight, T.M. Connah, K.F. McNeil-Watson, and U. Nobbmann. Measuring sub nanometre sizes using dynamic light scattering. *J.Nanopart.Res.*, 10:823–829, 2008.

[41] P. Atkins and Julio De Paula. *Physical Chemistry (8 ed.)*. Oxford University Press, 2006.

[42] H. Ohshima and Makino. K. *Colloid and Interface Science in Pharmaceutical Research and Development*. Elsevier B.V., 2014.

[43] W. Shi, J. Wang, X. Fan, and H. Gao. Size and shape effects on diffusion and absorption of colloidal particles near a partially absorbing sphere: implications for uptake of nanoparticles in animal cells. *Phys. Rev*, 78:1–11, 2008.

[44] S. Bhattacharjee. DLS and zeta potential - What they are and what they are not? *Journal of Controlled Release*, 235:337–351, 2016.

[45] F.J. Ruiz-Cabello Montes, G. Trefalt, P. Maroni, and M. Borkovec. Electric double-layer potentials and surface regulation properties measured by colloidal-probe atomic force microscopy. *Phys.Rev.*, E90:012301, 2014.

[46] Z. Chen, Z. Wei, Y. Chen, and C. Dames. Anisotropic Debye model for the thermal boundary conductance. *Phys.Rev.*, B87:125426, 2013.

[47] F.J. Vidal-Iglesias, J. Solla-Gullón, A. Rodes, E. Herrero, and A. Aldas. Understanding the Nernst equation and other electrochemical concepts: an easy experimental approach for students. *J.Chem.Educ.*, 89:936–939, 2012.

[48] V. Uskokovič, Z. Castiglione, P. Cubas, L. Zhu, W. Li, and S. Habelitz. Zeta-potential and particle size analysis of human amelogenins. *J.Dent.Res.*, 89:149–153, 2010.

[49] A. Salis, M. Boström, L. Medda, F. Cugia, B. Barse, D.F. Parsons, B.W. Ninham, and M. Monduzzi. Measurements and theoretical interpretation of points of zero charge/potential of BSA protein. *Langmuir*, 27:11597–11604, 2011.

[50] J. Kirkwood, D. Hargreaves, S. O'Keefe, and J. Wilson. Using isoelectric point to determine the pH for initial protein crystalization trials. *Bioinformatics*, 31:1444–1451, 2015.

[51] E.W. Nägele. The transient zeta potential of hydrating cement. *Chem.Eng.Sci*, 44:1637–1645, 1989.

[52] I. Reviakine, D. Johannsmann, and Ralf P. Richter. Hearing What You Cannot See and Visualizing What You Hear. *Analytical chemistry*, 83:8838–8848, 2011.

[53] D. Johannsmann, I. Reviakine, and Ralf P. Richter. Dissipation in films of adsorbed nanospheres studied by quartz crystal microbalance (QCM). *Analytical Chemistry*, 81(19):8167–8176, 2009.

[54] M. C. Dixon. Quartz crystal microbalance with dissipation monitoring: Enabling real-time characterization of biological materials and their interactions, 2008.

[55] N. J. Cho, C. W. Frank, B. Kasemo, and F. Hook. Quartz crystal microbalance with dissipation monitoring of supported lipid bilayers on various substrates. *Nature Protocols*, 5(6):1096–1106, 2010.

[56] N. J. Cho, K. K. Kanazawa, J. S. Glenn, and C. W. Frank. Employing two different quartz crystal microbalance models to study changes in viscoelastic behavior upon transformation of lipid vesicles to a bilayer on a gold surface. *Analytical Chemistry*, 79(18):7027–7035, 2007.

[57] B. Seantier, C. Breffa, O. Felix, and G. Decher. Dissipation-enhanced quartz crystal microbalance studies on the experimental parameters controlling the formation of supported lipid bilayers. *Journal of Physical Chemistry B*, 109(46):21755–21765, 2005.

[58] D. Johannsmann. Viscoelastic, mechanical, and dielectric measurements on complex samples with the quartz crystal microbalance. *Physical Chemistry Chemical Physics*, 10:4516, 2008.

[59] C.A. Keller and B. Kasemo. Surface Specific Kinetics of Lipid Vesicle Adsorption Measured with a Quartz Crystal Microbalance. *Biophysical Journal*, 75:1397–1402, 1998.

[60] C.A. Keller, K. Glasmästar, V.P. Zhdanov, and B Kasemo. Formation of Supported Membranes from Vesicles. *American Physical Society, Physical Review Letters*, 84:5443, 2000.

[61] U. Seifert, K. Berndl, and R. Lipowsky. Shape transformations of vesicles: Phase diagram for spontaneous- curvature and bilayer-coupling models. *American Physical Society, Physical Review A*, 44:1182, 1991.

[62] R. P Richter, R. R. Escarpit, and P. Cedex. In V ited Feature Article Formation of Solid-Supported Lipid Bilayers : An Integrated View. *Langmuir*, 22(12):3497–3505, 2006.

[63] V.P. Zhdanov and B. Kasemo. Comments on Rupture of Adsorbed Vesicles. *Langmuir*, 17:3518–3521, 2001.

[64] P.R. Richter and A. Brisson. Following the Formation of Supported Lipid Bilayers on Mica: A Study Combining AFM, QCM-D, and Ellipsometry. *Biophys. J.*, 88:3422–3433, 2005.

[65] L.A. Bernard, A.M. Guedeau-Boudeville, L. Jullien, and M.J. de Meglio. Strong Adhesion of Giant Vesicles on Surfaces: Dynamics and Permeability. *Langmuir*, 16:6809–6820, 2000.

[66] P.M. Kasson and V.S. Pande. Molecular Dynamics Simulation of Lipid Reorientation at Bilayer Edges. *Biophys. J.*, 86:3744–3749, 2004.

[67] F.Y. Jiang, Y. Bouret, and J.H. Kindt. Determining the Gaussian Curvature Modulus of Lipid Membranes in Simulations. *Biophys. J.*, 87:182–192, 2004.

[68] P.R. Richter, A. Mukhopadhyay, and A. Brisson. Pathways of Lipid Vesicle Deposition on Solid Surfaces: A Combined QCM-D and AFM Study. *Biophys. J.*, 85:3035–3047, 2003.

[69] V.P. Zhdanov, C.A. Keller, K. Glasmastar, and B. Kasemo. Simulation of adsorption kinetics of lipid vesicles. *J. Chem. Phys.*, 112:900–909, 2000.

[70] E. Reimhult, F. Höök, and B. Kasemo. Intact Vesicle Adsorption and Supported Biomembrane Formation from Vesicles in Solution: Influence of Surface Chemistry, Vesicle Size, Temperature, and Osmotic Pressure. *Langmuir*, 19:1681–1691, 2003.

[71] A.J. Jackman, C.M. Kim, P.V. Zhdanov, and Nam-Joon Cho. Relationship between vesicle size and steric hindrance influences vesicle rupture on solid supports. *Phys. Chem. Chem. Phys.*, 18:3065–3072, 2016.

[72] J. Homola. Present and future of surface plasmon resonance biosensors. *J. Anal. Bioanal. Chem.*, 377:528–539, 2003.

[73] R.M.A. Azzam and N.M. Bashara. *Elipsometry and Polarized Light, 3d ed.* Elsevier Science BV, 1996.

[74] F. Hook, J. Voros, M. Rodahl, R. Kurrat, P. Boni, J.J. Ramsden, M. Textor, N.D. Spencer, P. Tengvall, J. Gold, and B. Kasemo. A comparative study of protein adsorption on titanium oxide surfaces using in situ elipsometry, optical waveguide lightmode spectroscopy, and quartz crystal microbalance/dissipation. *Colloid Surf. B.*, 24:155–170, 2002.

[75] W.P. Mason. *Piezoelectric Crystals and Their Application to Ultrasonics.* D. Van Nostrand Company, Inc., 1950.

[76] D. Johannsmann, K. Mathauer, G. Wegner, and W. Knoll. Viscoelastic properties of thin films probed with a quartz-crystal resonator. *Phys. Rev. B*, 46:7808–7815, 1992.

[77] H.L. Bandey, S.J. Martin, R.W. Cernosek, and A.R. Hillman. Modeling the Responses of Thickness-Shear Mode Resonators under Various Loading Conditions. *Anal. Chem.*, 71:2205–2214, 1999.

[78] R. Lucklum, C. Behling, R.W. Cernosek, and S.J. Martin. Determination of complex shear modulus with thickness shear mode resonators. *J. Phys. D: Appl. Phys.*, 30:346–356, 1997.

[79] J.D. Ferry. *Viscoelastic Properties of Polymers, 3rd ed.* Wiley Sons: New York, 1980.

[80] P. Oswald. *Rheophysics-The Deformation and Flow of Matter.* Cambridge University Press: Cambridge, 2009.

[81] O.S. Heavens. *Optical Properties of Thin Solid Films.* Butterworth: London, 1955.

[82] D. Johannsmann. Viscoelastic analysis of organic thin films on quartz resonators. *Macromol. Chem. Phys.*, 200:501–516, 1999.

[83] P. Bingen, G. Wang, N.F. Steinmetz, M. Rodahl, and R.P. Richter. Solvation Effects in the Quartz Crystal Microbalance with Dissipation Monitoring Response to Biomolecular Adsorption. A Phenomenological Approach. *Anal. Chem.*, 80:8800–8890, 2008.

[84] D. Johannsmann, L. Reviakine, and R.P. Richter. Effect of sample heterogeneity on the interpretation of QCM(-D) data: comparison of combined quartz crystal microbalance/atomic force microscopy measurements with finite element method modeling. *Anal. Chem.*, 80:8891–8899, 2008.

[85] G. Tarjus, P. Schaaf, and J. Talbot. Generalized random sequential adsorption. *J. Chem. Phys.*, 93:8360, 1990.

[86] I. Carton, A.R. Brisson, and R.P. Richter. Label-free detection of clustering of membrane-bound proteins. *Anal. Chem.*, 82:9275–9281, 2010.

[87] A.P. Borovikov. Measurement of viscosity of media by means of shear vibration of plane resonators. *Instrum. Exp. Tech.*, 19:223–224, 1976.

[88] Avantilipids. `https://avantilipids.com/`. Accessed: 2018-03-17, 16:03.

[89] O. Bixner and E. Reimhult. Controlled magnetosomes: Embedding of magnetic nanoparticles into membranes of monodisperse lipid vesicles. *J. of Col. and Int. Sc.*, 466:62–71, 2016.

[90] D.J. Castile and M.G.K. Taylor. Factors affecting the size distribution of liposomes produced by freeze–thaw extrusion. *J. Pharm.*, 188:87–95, 1999.

[91] A. Melcrová, S. Pokorna, S. Pullanchery, M. Kohagen, P. Jurkiewicz, M. Hof, P. Jungwirth, S.P. Cremer, and L. Cwiklik. The complex nature of calcium cation interactions with phospholipid bilayers. *Sci. Rep.*, 6:38035, 2016.

[92] W.B. Koenig, S. Krueger, J.W. Orts, F.C. Majkrzak, F.N. Berk, V.J. Silverton, and K. Gawrisch. Neutron Reflectivity and Atomic Force Microscopy Studies of a Lipid Bilayer in Water Adsorbed to the Surface of a Silicon Single Crystal. *Langmuir*, 12:1343–1350, 1996.

[93] D.M. Chavez and L.J. Schrimsher and S.A. Morar. *PEGylation of Proteins: A Structural Approach*. http://www.biopharminternational.com/pegylation-proteins-structural-approach?id=&pageID=1&sk=&date=. Accessed: 01-06-2018, 11:54.

[94] N. Kučerka, Mu-Ping Nieh, and J. Katsaras. Fluid phase lipid areas and bilayer thicknesses of commonly used phosphatidylcholines as a function of temperature. *BBA - biomembranes*, 1808:2761–2771, 2011.

[95] Thermofisher. https://www.thermofisher.com/order/catalog/product/31000. Accessed: 2018-05-04, 18:56.

[96] R.I. Quevedo, L.J.A. Olsson, J.R. Clark, G.C.J. Veinot, and N. Tufenkji. Interpreting Deposition Behavior of Polydisperse Surface-Modified Nanoparticles Using QCM-D and Sand-Packed Columns. *Env. Eng. Sc.*, 31:326–337, 2014.

# 5. Appendix

**Table 5.1:** Different methods for coated silica nanoparticle production, their size distributions, polydispersities and standard errors of mean. The table also includes DLS measurements on bare silica nanoparticles being activated or non-activated (method 2.2.2. for activation of the nanoparticles)

| Nr. | Sample; Subsection in method part; | Z-average, nm | PDI | St. error of mean, ±nm |
|---|---|---|---|---|
| 1 | Silica NPs in 10 mM Tris; Not activated. | 156.2 | 0.295 | 1.04 |
| 2 | Silica NPs in 10 mM Tris; Not sufficiently activated. | 146.3 | 0.166 | 1.79 |
| 3 | Silica NPs suspended in TBS 1:10. | 192.3 | 0.333 | 44.1 |
| 4 | Silica NPs in 10 mM Tris; Activated. | 129.1 | 0.225 | 0.67 |
| 5 | POPC-silica NPs; 2.2.4. 1); | 279.9 | 0.209 | 7.16 |
| 6 | POPC-1mol%biotin-silica NPs; 2.2.4. 1); | 334.8 | 0.426 | 70.81 |
| 7 | POPC-silica NPs; 2.2.4. 1) Bath sonic. 15 min.; | 249.4 | 0.276 | 10.63 |
| 8 | POPC-1mol%biotin-silica NPs; 2.2.4. 1) Bath sonic. 15 min.; | 300.5 | 0.31 | 41.07 |
| 9 | POPC-silica NPs; 2.2.4. 1)[1]; | 338.3 | 0.291 | 15.03 |
| 10 | POPC-1mol%biotin-silica NPs; 2.2.4. 1)[1]; | 308.2 | 0.321 | 52.59 |
| 11 | POPC-silica NPs; 2.2.4. 1)[2] | 741.1 | 0.654 | 155.99 |
| 12 | POPC-1mol%biotin-silica NPs; 2.2.4. 1)[2] | 279.8 | 0.38 | 14.77 |
| 13 | POPC-silica NPs; 2.2.4. 1)[3] 30 min. vortex, 30 min inc. | 241.2 | 5 | 2.89 |
| 14 | POPC-1mol%biotin-silica NPs; 2.2.4. 1)[3] 30 min. pipet., 30 min. inc. | 236.6 | 0.476 | 2.06 |
| 15 | POPC-silica NPs; 2.2.4. 1)[3] 20 min. pipetting. | 266.2 | 0.384 | 5.07 |
| 16 | POPC-silica NPs; 2.2.4. 1)[3] 20 min. vortex (2000 RPM) | 160.7 | 0.461 | 5 |
| 17 | POPC-silica NPs; 2.2.4. 1)[3] 20 min. vortex (2000 RPM); resuspend in miliqwater. | 202.1 | 0.264 | 2.31 |
| 18 | POPC-silica NPs; 2.2.4. 1)[3] 20 min. vortex (2000 RPM); resuspend in 10 mM Tris. | 204.6 | 0.228 | 1.51 |
| 19 | POPC-4mol%POPG-coated NPs;[4] | 273.6 | 0.256 | 6.67 |
| 20 | POPC-10mol%POPG-coated NPs;[4] | 185.9 | 0.237 | 2.43 |

| | | | | |
|---|---|---|---|---|
| 21 | POPC-4mol%POPG-coated NPs;[4] after 48 hours | 462.1 | 0.645 | 16.69 |
| 22 | POPC-10mol%POPG-coated NPs;[4] after 48 hours | 171 | 0.224 | 2.37 |
| 23 | POPC-25mol%POPG-coated NPs;[4] | 186.4 | 0.286 | 0.84 |
| 24 | POPC-25mol%POPG-coated NPs;[4] after 24 hours | 175.4 | 0.265 | 3.03 |
| 25 | POPC-10%POPG-coated NPs with 20 mM NaCl during coat.;[4] | 276.6 | 0.431 | 2.74 |
| 26 | POPC-10%POPG-1%biotin-coated NPs in 10 mM Tris;[4] | 180.3 | 0.242 | 2.32 |
| 27 | POPC-10%POPG-coated NPs with 200 mM NaCl during coating;[4] | 202.4 | 0.256 | 3.46 |
| 28 | POPC-10%POPG-coated NPs with 300 mM NaCl during coat.;[4] | 211.5 | 0.33 | 6.13 |
| 29 | POPC-4%POPS-coated NPs with Ca2+;[4] | 213.5 | 0.373 | 0.29 |
| 30 | POPC-10%POPS-coated NPs with Ca2+;[4] | 191.7 | 0.277 | 2.91 |
| 31 | POPC-4%POPS-coated NPs without Ca2+;[4] | 210.2 | 0.366 | 2 |
| 32 | POPC-10%POPS-coated NPs without Ca2+;[4] | 185.2 | 0.288 | 1.65 |
| 33 | POPC-10%POPS-1%biotin-coated NPs without Ca2+;[4] | 190.3 | 0.245 | 1.66 |
| 34 | 10%POPG-POPC NPs;[4], but vortex 1000 rpm | 169.3 | 0.275 | 4.91 |
| 35 | 10%POPG-POPC-1%biotin NPs;[4], but vortex 1000 rpm | 166.5 | 0.26 | 4.87 |
| 36 | 10%POPG-POPC-5%biotin NPs;[4], but vortex 1000 rpm | 172.5 | 0.25 | 4.16 |
| 37 | 10%POPG-POPC-1%biotin;[4], but vortex 600 rpm | 166.8 | 0.273 | 1.04 |
| 38 | POPC-coated-NPs;[4], but vortex 500 rpm | 232.8 | 0.402 | 21.05 |
| 39 | POPC-1%PE-PEG-biotin NPs;[4], but vortex 600 rpm | 351.1 | 0.448 | 13.35 |
| 40 | POPC-0.1%PE-PEG-biotin NPs;[4], but vortex 600 rpm | 272.4 | 0.444 | 30.34 |
| 41 | POPC-10%POPG-1%PE-PEG-biotin NPs;[4], but vortex 600 rpm | 227.6 | 0.366 | 7.51 |
| 42 | POPC-10%POPG-0.1%PE-PEG-biotin NPs;[4], but vortex 600 rpm | 187 | 0.338 | 5.14 |
| 43 | POPC-2.5%PE-PEG-biotin NPs;[4], but vortex 600 rpm | 201.7 | 0.352 | 0.61 |

| | | | | |
|---|---|---|---|---|
| 44 | POPC-5%PE-PEG-biotin NPs;[4], but vortex 600 rpm | 227.4 | 0.452 | 9.58 |
| 45 | POPC-2%biotin NPs 10 times ratio;[4] | 179.8 | 0.341 | 3.47 |
| 46 | POPC-0.5%PE-PEGbiotin NPs 10 times ratio;[4] | 307.8 | 0.559 | 23.61 |
| 47 | 10%POPG-POPC-1%biotin NPs 10 times ratio;[4] | 178.5 | 0.284 | 3.2 |
| 48 | 10%POPG-POPC-1%PE-PEG-biotin NPs 10 times ratio,[4] | 358.6 | 0.613 | 35.06 |
| 49 | Silica NPs in 10 mM Tris; Not activated. | 104.5 | 0.253 | 0.49 |
| 50 | POPC-2%biotin NPs 10 times ratio;[4] with new NPs | 232.5 | 0.381 | 3.6 |
| 51 | POPC-0.5%PE-PEGbiotin NPs 10 times ratio;[4] with new NPs | 322.3 | 0.691 | 6.63 |
| 52 | 10%POPG-POPC-1%biotin NPs 10 times ratio;[4] with new NPs | 200.4 | 0.444 | 1.59 |

[1] 30 minute incubation after mixing silica nanoparticles, vesicles and 1x TBS buffer together. Not activated NPs.

[2] Sonicate NPs for 30 minutes before addition; Add everything in the same order as in 2.2.4.1); shake overnight at 4 degrees celsium at 500 rpm; bath sonicate solution for 30 minutes; centrifuge at 500 rcf for 30 minutes; resuspend in 1x TBS and repeat centrifugation steps 3 times. With badly activated NPs.

[3] Sonicate NPs for 2 hours before addition; add 159.7 uL of liposomes (2 mg/mL), 740.3 uL of TBS and 100 uL of NPs; Apply appropriate mixing; centrifuge at 6000 rpm for 5 minutes; resuspend in 1x TBS and repeat centrifugation steps 3 times. With well activated NPs.

[4] Sonicate NPs for 2 hours before addition; add 159.7 uL of liposomes (2 mg/mL), 740.3 uL of TBS and 100 uL of NPs; vortex for 20 mins. (2000 RPM); centrifuge at 6000 rpm for 5 minutes; resuspend in 10x Tris and repeat centrifugation steps 3 times.